MICROSTRUCTURAL, BIOLOGICAL AND MECHANICAL INVESTIGATIONS OF HYDROXYAPATITE- β-TRICALCIUM PHOSPHATE COMPOSITES DOPED WITH STRONTIUM AND FLUORIDE

A THESIS SUBMITTED TO
THE GRADUATE SCHOOL OF NATURAL AND APPLIED SCIENCES
OF
MIDDLE EAST TECHNICAL UNIVERSITY

BY
ELMIRA POURREZA

IN PARTIAL FULLFILLMENT OF THE REQUIREMENTS
FOR
THE DEGREE OF MASTER OF SCIENCE
IN
ENGINEERING SCIENCES

AUGUST 2016

Approval of the thesis

MICROSTRUCTURAL, BIOLOGICAL AND MECHANICAL INVESTIGATIONS OF HYDROXYAPATITE- β-TRICALCIUM PHOSPHATE COMPOSITES DOPED WITH STRONTIUM AND FLUORIDE

Submitted by **Elmira Pourreza** in partial fulfillment of the requirements for the degree of **Master of Science in Engineering Sciences Department, Middle East Technical University** by,

Prof. Dr. Gülbin Dural Ünver _____
Dean, Graduate School of **Natural and Applied Sciences**

Prof. Dr. Murat Dicleli _____
Head of Department, **Engineering Sciences Dept.**

Prof. Dr. Zafer Evis _____
Supervisor, **Engineering Sciences Dept., METU**

Examining Committee Members:

Prof. Dr. Zafer Evis _____
Engineering Sciences Dept., METU

Assoc. Prof. Dr. Ayşen Tezcaner _____
Engineering Sciences Dept., METU

Assoc. Prof. Dr. Mustafa Tolga Yılmaz _____
Engineering Sciences Dept., METU

Assoc. Prof. Dr. Metin Dağdeviren _____
Industrial Engineering Dept., Gazi University

Assist. Prof. Dr. İhsan Toktaş _____
Mechanical Engineering Dept., Yıldırım Beyazıt University

Date: 15.08.2016

I hereby declare that all information in this document has been obtained and presented in accordance with academic rules and ethical conduct. I also declare that, as required by these rules and conduct, I have fully cited and referenced all material and results that are not original to this document.

Name, Surname: Elmira Pourreza

Signature:

ABSTRACT

MICROSTRUCTURAL, BIOLOGICAL AND MECHANICAL INVESTIGATIONS OF HYDROXYAPATITE- β-TRICALCIUM PHOSPHATE COMPOSITES DOPED WITH STRONTIUM AND FLUORIDE

Pourreza, Elmira

M. Sc., Department of Engineering Sciences

Supervisor: Prof. Dr. Zafer Evis

August 2016; 92 Pages

The aim of this study was to investigate the microstructure, mechanical and biological properties of biphasic hydroxyapatite-β-Tricalcium phosphate (HT) and HT substituted with constant fluoride (F^-) and varying strontium (Sr^{2+}) amounts. All the samples were synthesized via precipitation method and sintered at 1100°C for 1 h. It was observed that the relative density of the sintered strontium and fluoride doped HT slightly increased. For microstructural analysis, X-ray diffraction (XRD), scanning electron microscopy (SEM) and Fourier transform infrared spectroscopy (FTIR) examinations were performed. Remarkable amounts of β-TCP and CaO phases were detected in XRD analysis which could be due to the Ca/P ratio less than 1.67. Lattice parameters increased due to substitutions of ions. In SEM analysis, smaller grains were observed for HT doped with ions. In FTIR analysis, the characteristic bands of HA and β-TCP were exhibited. Increased Sr^{2+} ion contents resulted in increased microhardness values. The highest microhardness value was obtained for the HT doped with 5%Sr^{2+} and 1%F^-. In order to evaluate the cytocompatibility of doped HT, *in vitro* cytotoxicity tests were performed using Saos-2 cells. Higher initial cell attachment was observed on $Sr^{2+}$and F^- doped HT discs than observed on pure HT.

SEM analysis was conducted to examine the morphology of the cells on the surface of the samples. And it was observed that the surface of all discs was covered with cell layers showing perfect cell-material interaction.

HT doped with 5%Sr^{2+} and 1%F^{-} had the optimum structural, mechanical and biocompatibility properties and can be suggested as a good biomaterial for biomedical applications.

Keywords: Hydroxyapatite, Strontium, Fluoride, Mechanical properties, Biocompatibility.

ÖZ

STRONSİYUM VE FLOR İLAVE EDİLMİŞ HİDROKSİAPATİT-β-TRİKALSİYUM FOSFAT KOMPOZİTLERİN MİKROYAPI, BİYOLOJİK VE MEKANİK ÖZELLİKLERİNİN İNCELENMESİ

Pourreza, Elmira
Yüksek Lisans, Muhendislik Bilimleri Bölümü
Tez Yöneticisi: Prof. Dr. Zafer Evis

Ağustos 2016; 92 Sayfa

Bu çalışmanın amacı bi-fazik hidroksiapatit-β-trikalsiyum fosfat (HT) ve farklı miktarlarda flor (F^-) ve stronsiyum (Sr^{2+}) içeren HT'lerin mikroyapı, mekanik ve biyolojik özelliklerinin incelenmesidir. Tüm numuneler, çöktürme metoduyla sentezlenmiş ve 1100°C'de bir saat sinterlenmiştir. Sinterlenmiş stronsiyum ve flor içeren HT'lerin yoğunluk miktarı bir miktar artmıştır. Mikroyapı analizi için, X-ışını kırınımı (XRD), taramalı elektron mikroskobu (SEM) ve Fourier dönüşümlü kızıl ötesi spektroskopi (FTIR) incelemeleri yapılmıştır. X-ışını kırınımı çalışmasında yüksek miktarda β-TCP ve CaO fazlarının tespit edilmesi, malzemelerin Ca/P oranının 1.67 den daha az olması nedeniyle gercekleşmiştir. İyon eklenmesiyle kafes parametreleri büyümüştür. SEM incelemelerinde, iyon eklenmiş HT'lerde daha küçük tanecik boyutu gözlenmiştir. FTIR analizinde karakteristik HA ve β-TCP bantları gözlenmiştir. Sr^{2+} miktarlarının artışı mikrosertlik değerlerinin artmasına sebep olmuştur. En yüksek mikrosertlik değeri %5 Sr^{2+}, %1 F^- ilave edilmiş HT'de gözlenmiştir. İyon eklenmiş HT gruplarının biyouyumluluğunu değerlendirmek için, in vitro sitotoksisite testleri Saos-2 hücreleri kullanılarak yapılmıştır. Sr^{2+} ve F^- eklenmiş HT disklerinde, saf HT disklerine kıyasla, daha fazla başlangıç hücre

tutunması gözlenmiştir. Örnek yüzeyindeki hücre morfolojisini incelemek için taramalı elektron mikroskobu kullanılmıştır. Bütün disk örneklerinde, disk yüzeylerinin hücre katmanlarıyla kaplı olduğunun gözlenmesi, numune yüzeyinin kusursuz hücre-malzeme etkileşimine sahip olduğu göstermiştir.

%5 Sr^{2+} ve %1 F^{-} ile zenginleştirilen HT, optimum yapısal, mekanik ve biyouyumluluk özelliklerine sahip bir malzemedir ve biyomedikal uygulamalar için uygun bir biyomalzeme olarak önerilebilir.

.

Anahtar Kelimeler: Hidroksiapatit, Stronsiyum, Flor, Mekanik özellikler, Biyouyumluluk.

To my family and people who are reading this page

ACKNOWLEDGMENTS

It is my pleasure to acknowledge the roles of several individuals who were instrumental for completion of my M.S. study.

First of all, I would like to express my gratitude to my dear adviser, Prof. Dr. Zafer Evis, who encouraged me to pursue this project and thought me the art of rock engineering. I am truly grateful for his endless supports, suggestions and guidance during the research for my thesis.

I would also like to thank Assoc. Prof. Dr. Ayşen Tezcaner for providing indispensable advice, information, and support on different aspects of my thesis.

These acknowledgements would not be complete without mentioning my research lab colleagues: Dr. Ammar Z. Alshemary, Dr. Bengi Yilmaz, Dr. Aydin Tahmasebifar, and Reza Moonesirad. It was a great pleasure working with them and I appreciate their ideas, help and being there when I needed. And a special thank goes to my best friend, Maryam Hassanpour, who was always generous and kind to me through all these 10 years of our friendship.

Last but not least, my deepest appreciation belongs to my family. Words cannot express how grateful I am to my mother, father, mother-in law, and father-in-law for all of the sacrifices that they've made on my behalf. Their prayer for me was what sustained me thus far. I would also like to thank to my beloved sister Elham Pourreza and sister-in-law Fahimeh Q. Berenji for their generous support.

Saving the most important for last, I wish to give my heartfelt thanks to my beloved husband, Vahid G. Berenji, whose unconditional love, patience, and continual support of my academic endeavors over the past several years enabled me to complete this thesis.

TABLE OF CONTENTS

LIST OF TABLES

TABLES

LIST OF FIGURES

FIGURES

CHAPTER 1

INTRODUCTION

1.1. Apatite

"Apatites with a general chemical formula $X_{10}(YO_4)_6Z_2$ are widely distributed as accessory minerals in igneous rocks and in small quantities in most metamorphic rocks" (Elliott et al., 2002). They are regarded as a branch of chemical compounds with phosphoric bases with a similar hexagonal and structural shape. The fundamental raw material of biological origin is the phosphate rock (microcrystalline apatite), which is mainly composed of carbonated fluorapatite. As the basic material for phosphate fertilizer manufacture, this fundamental raw material is mostly consumed in the chemical industry for producing different commodities like detergents, dentifrices, plasticizers, rust removers and pharmaceuticals (Elliott et al., 2002; Elliott, 1994). Since the material's lattice is very permissive for ionic substitutions, vacancies and solid solutions, various ions can be substituted for its structure. Table 1.1 presents a summary of these ions.

Table 1.1. Various ionic substitutions to apatites with a chemical formula of $X_{10}(YO_4)_6Z_2$ (Leventouri, 2006).

X^{2+}	YO_4^{3-}	Z^-
Ca^{2+}, Ba^{2+}, Sr^{2+}, Pb^{2+}, Cd^{2+}, Mg^{2+}	PO_4^{3-}, AsO_4^{3-}, VO_4^{3-}	F^-, OH^-, Cl^-

The structure of apatite is flexible in case of coupled ionic substitutions, as seen in some minerals like pyromorphite ($Pb_5(PO_4)_3Cl$), vanadinite ($Pb_5(VO_4)_3Cl$) and mimetite ($Pb_5(AsO_4)_3Cl$). Normally, ionic substitutions occur between ions with same

negative or positive charge. In some cases, these substitutions occur between ions with different charges. In this case, unequal charges and the vacancies in the structure of the apatite compensate for each other. The mentioned vacancies cause non-stoichiometry in the structure of the molecule which results in complicated crystal chemistry (Vallet- Regí & González-Calbet, 2004).

In 1932, Mehmel published the basic apatite structure, which is a hexagonal shape with approximate lattice parameters a = 9.37Å and c = 6.88Å belonging to the P63/m space group (Mehmel, 1932). There are two crystallographically different Ca atoms and three O atoms. By overseeing the distinction between O atoms, the unit cell is composed of $Ca(1)_4Ca(2)_6(PO_4)_6F_2$ (Sakakura et al., 2010).

1.2. Bone

Bone is the fundamental tissue that forms the skeletal system, and our body consists of six different bone types: sutural, flat, long, short, irregular and sesamoid, all of which perform primary functions such as maintaining the shape of the body, protecting the soft tissues, transmitting the forces during movement and acting as calcium storage in body (Rho et al.,1998). The bone composition is 65 wt% mineral, 35 wt% organic matrix, cells and water. Bone minerals are located among collagen fibers in the form of small crystals in needles and plates and rod shapes. Bone mineral is impure hydroxyapatite (HA) whose impurities are carbonate, citrate, magnesium, fluoride, strontium etc. Moreover, organic matrix is composed of 90% collagen and 10% of various non-collagenous proteins which are osteocalcin, osteonectin, osteopontin and bone sialoprotein (Rho et al.,1998).

1.2.1. Structure and Mechanical Properties of Bone

Bone can be considered as a natural composite material consisting of organic and inorganic components (Wang & Feng, 2005). Type I collagen and some noncollageneous matrix proteins mainly form the organic part of the bone, and HA ($Ca_{10}(PO_4)_6(OH)_2$) whose basic constituents are calcium and phosphate mainly form the inorganic part. Various elements also exist in trace amounts in the structure of HA (Fratzl et al., 2004).

Bone has a hierarchical structure that varies from macroscopic to nanoscale levels (Ji & Gao, 2004). These levels and structures are: the macrostructure, which is composed of 2 types of bones, namely compact (cortical) and trabecular (cancellous or spongy) bone; the microstructure (from 10 to 500 μm), containing Haversian systems, osteons, single trabeculae; the sub-microstructure (1–10 μm), consisting of lamellae; the nanostructure (from a few hundred nanometers to 1 μm), containing fibrillar collagen and embedded mineral; and the sub-nanostructure (below a few hundred nanometers), with molecular structure of constituent elements, such as mineral, collagen, and non-collagenous organic proteins (Wang & Feng, 2005). These structures are illustrated in Figure 1.1.

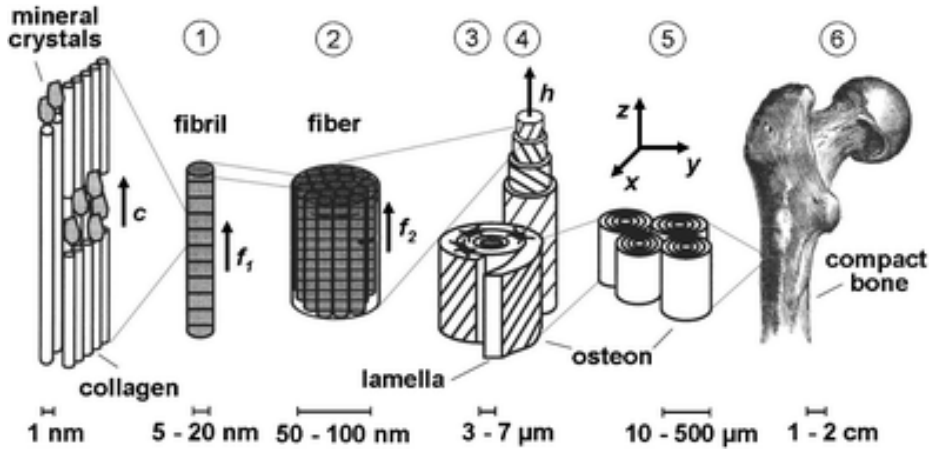

Figure 1.1. Hierarchical structure of compact bone : (1) fibril—collagen molecules laid down in parallel and reinforced with bone mineral, (2) fiber—an assembly of fibrils, (3) lamella—fibers laid in parallel on a plane sheet, (4) osteon—an assembly of twisted lamellae, (5) an assembly of osteons sum up to a compact bone, (6) geometry of the mid-frontal section of a femur bone (Marlow et al., 2007).

There are two different types of bones in terms of their physical properties: compact and spongy. Various characteristics of the compact and spongy bone are compared in Table 1.2. (Martin, 2003).

Table 1.2. Comparison of compact and spongy bone (Martin, 2003)

Properties	Compact bone	Spongy bone
Skeletal mass	80%	20%
Bone surface	33%	67%
Surface/ volume ratio (mm^2/mm^3)	20	2.5
Soft tissue content	~10 %	~75 %
Turnover period	Long	Short
Function	Biomechanical, supportive and protective	Supportive and mineral homeostasis

1.2.1.1. Mechanical Properties of Compact (Cortical) Bone

When stress is applied from a limited range of directions, it results in the formation of compact bone and making it thicker. Likewise, all of the osteons in the compact bone are ordered in the same directions and the structure becomes strong in that direction. However, when stress is applied perpendicularly to the alignment of osteons, the structure is weak and can be easily bent in that direction (Martin, 2003). When compression force is applied in the direction of osteon alignment, the tension is experienced on the lateral side due to body weight on the medial side of the bone. Therefore, high stress applied on both sides of the bone stimulates the compact bone formation (Currey, 2002). Figure1.2 shows the distribution of forces on a long bone, in which the femur, or thigh bone, has a diaphysis (shaft) with walls of compact bone and epiphyses filled with spongy bone. The body weight is transferred to the femur at the hip joint. Because the hip joint is off center relative to the axis of the shaft, the body weight is distributed along the bone such that the medial (inner) portion of the shaft is compressed and the lateral (outer) portion is stretched (Martini & Nath, 2009).

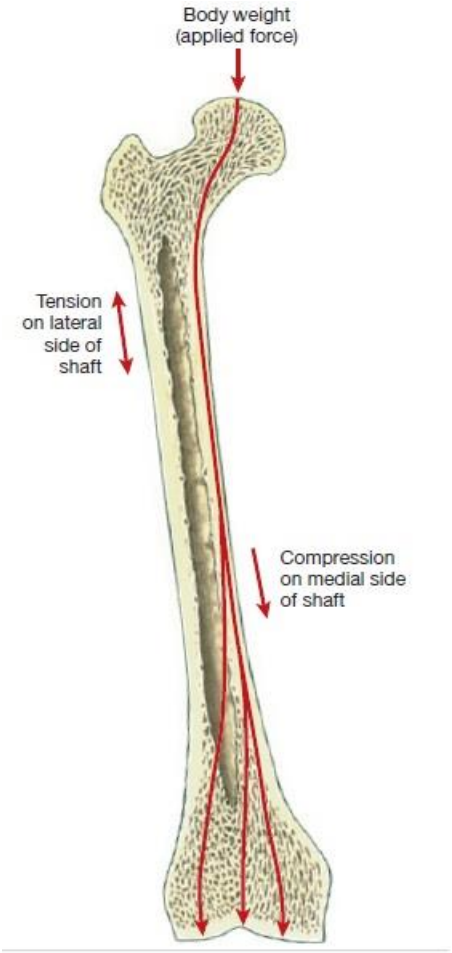

Figure 1.2. The distribution of forces on a long bone (Martini & Nath, 2009).

1.2.1.2. Mechanical Properties of Spongy Bone

Understanding mechanical properties of spongy bone is not easy despite the investigations done in low stressed areas as well as the areas being under stress from many directions. Due to the fact that spongy bone is lighter than compact bone, it causes the reduction in the weight of the skeleton and helps muscles indirectly. Moreover, this type of bone is less stiff and much weaker than compact bone (Martini & Nath, 2009).

Another important property affecting the mechanical features of the spongy bone is porosity. This type of bone is highly porous, inhomogeneous and anisotropic, a condition which led to differences in the measured elasticity (elastic modulus values ranging from 1 to 20 GPa) (Cowin & Telega, 2003). Next feature is its ability of energy

absorption (Martin, 2003). Some of the mechanical properties of human compact and spongy bones are given in Table 1.3.

Table 1.3. Mechanical properties of human compact and spongy bones in a range of values (Marks & Odgren, 2002).

Bone	**Compact**	**Spongy**
Axial Modulus of Elasticity (GPa)	14 – 27	0.011 – 3.12
Tangential Modulus of Elasticity (GPa)	7 – 17	0.023 – 1.5
Radial Modulus of Elasticity (GPa)	7 – 16	0.024 – 1.5
Density (ρ) (g/cm^3)	1.545 – 2.118	0.055 – 0.0744
Ultimate Tensile Strength (σ_{UTS}) (MPa)	150	0.11 – 11

1.2.2. Cells, Organic and Inorganic Parts of the Bone

1.2.2.1. Bone Cells

Bone cells make up a low percentage of the bone composition but this percentage is very crucial in forming and maintaining the bone matrix. There are four different types of bone cells: osteoblasts, osteocytes, osteoclasts and bone lining cells two of which are engaged in the resorption process and other two play a role in the formation of the bone (Martini & Nath, 2009).

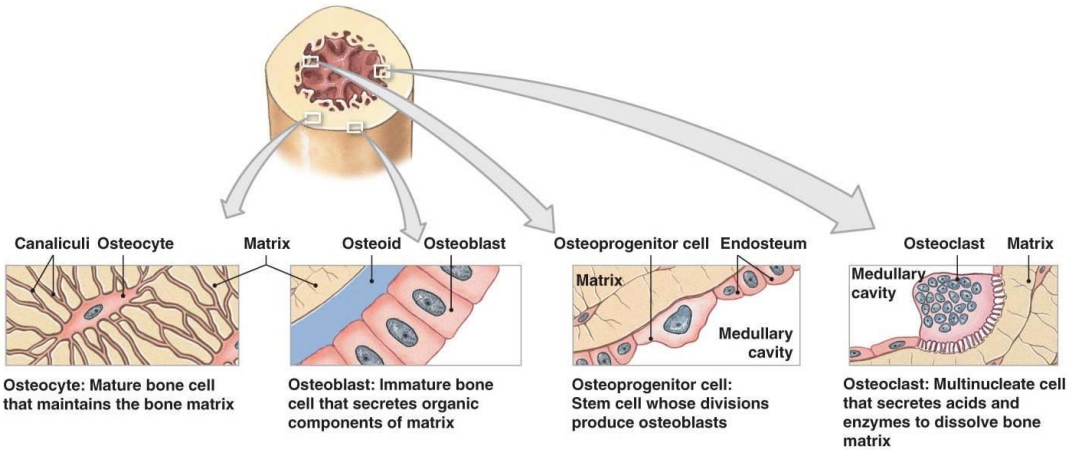

Figure 1.3. Diagram for the bone cells (Martini & Nath, 2009).

The first type of bone cells is osteocytes, which is the most abundant type of cells having two main functions. The first function of these cells is maintaining the protein and mineral contents of the surrounding matrix by secreting chemicals that dissolve the matrix (Currey, 2012). This causes the minerals to be released and then formation of a new matrix. This also creates the possibility of embedding HA crystals in this new matrix. Repairing damaged bone is the second function of these cells (Currey, 2012) since it is possible to convert osteocytes easily into less specialized type of cells such as osteoblasts. This also plays an active role in the synthesis of new matrix (Martin, 2003).

The second type of bone cells is osteoblasts. These cells are responsible for the production of a new bone matrix called osteoid by synthesis and releasing proteins and other organic components, a process called osteogenesis (Currey, 2012). They stimulate the deposition of calcium salts and consequently the transformation of osteoid to bone by increasing the concentration of calcium salts above their solubility limits, (Martin, 2003)

Third type of bone cells is osteoclasts, the cells responsible for osteolysis process (Martin, 2003), including matrix decomposition by acids and proteolytic enzymes. The dissolution of the matrix makes the stored minerals be released. Here, it is important to keep the balance between osteoblasts and osteoclasts because of their opposing activities.

The last type of bone cells is bone lining cells, coming from osteoblasts which have become flattened. They have flat organelles so they can easily cover the bone without interfering with other cells functions. The lining cells are relatively inactive forms of osteoblasts that cover all available surfaces of the bone and are responsible for the immediate release of calcium in the bone if calcium in the blood is too low (Currey, 2012).

1.2.2.2. Organic Content of the Bone

Collagen type I with 90% and amorphous ground substance are the constituents of bone while the second constituent was primarily composed of glycoproteins and glycosaminoglycans with 10% (Clarke, 2008).

The non-collagenous proteins take role in the initiation and control of mineralization and reconstruction, as well as binding of collagen and mineral together, especially in the case of glycoproteins (Clarke, 2008). These types of proteins in bone can be classified into five main groups: glycoproteins, glycosaminoglycans, gamma-carboxyl glutamic acid, RGD-containing glycoproteins and serum proteins (Clarke, 2008).

1.2.2.3. Inorganic Content of the Bone

Inorganic phase of the bone consists of amorphous hydroxyapatite with the formula of $Ca_{10}(PO_4)_6(OH)_2$, but with a more specialized structure. Bone mineral with the crystal size of about 20×40×200 $Å^3$ can also be categorized into calcium deficient apatite and hydroxide deficient apatite (Marieb & Hoehn, 2013). This small size provides the opportunity of replacing the bone mineral crystal with various ions, which, in turn, can be classified into anions and cations. These cations in the bone structure are Mg^{2+}, Sr^{2+}, Fe^{2+}, Pb^{2+}, Na^+, K^+ while the anions are CO_3^{2-}, F^-, HPO_4^{2-} and $H_2PO_4^-$. The constituents of the mineral part are summarized in Table 1.4 with their amounts in wt% range for healthy adult bone ash (Clarke, 2008; Martini & Nath, 2009).

Dahllite crystals are the synthetic structure, the closest to the bone mineral structure, and these crystals are carbonated HA with the general formula of $Ca_5(PO_4$,

$CO_3)_3OH$. Despite the similarity, the shape of the bone crystals was confirmed to be plate-like by atomic force microscopy (AFM) while that of the carbonated HA was an hexagonal structure (Martini & Nath, 2009). The similarity of octacalcium phosphate to the apatitic structure and plate-like shaped crystals resulted in its conversion to the bone mineral (Martini & Nath, 2009). Octacalcium phosphate differs from the bone mineral since octacalcium phosphate has a hydrated layer in one axis, which grows slowly during the crystal formation, and results in the formation of a structure similar to the apatitic one (Weiner & Traub, 1992).

Although the bone mineral formation is not a well-understood process, it is clear that brushite is formed, redissolved, and amorphous calcium phosphate formation is consecutively seen. Then, the produced amorphous calcium phosphate changes into octacalcium phosphate, and later, octacalcium phosphate is converted into HA, the most insoluble phase among calcium phosphates (Weiner & Traub, 1992). The chemical composition of healthy adult bone ash is listed in Table 1.4.

Table 1.4. The chemical composition of healthy adult bone ash (Clarke, 2008; Martini & Nath, 2009)

Ions	**Range of amount (wt%)**
Calcium	32.6-39.5
Phosphorus	13.1-18.0
Water	10
Carbonate	3.2-13.0
Magnesium	0.32-0.78
Sodium	0.26-0.82
Chloride	0.13
Pyrophosphate	0.07
Citrate	0.04-2.67
Potassium	0.03
Fluoride	0.020-0.207

1.2.3. Presence of Ions in Bone

Hydroxyapatite (HA) as the main component of the mineral part of bone can be doped with various elements, and these dopant elements affect the mechanical properties of the bone (Best et al., 2008).

It was reported that Al^{3+} ions enter hard tissues along with Ca^{2+} ions in order to act as an inhibitor of the formation of HA *in vitro* (Exley, 2008). For instance, it was observed that increase in the Al amount in blood plasma led to a significant drop in bone mineral density and bone mineral content of premature infants (low term infants), but this was not applicable to full term infants. Actually, it is claimed that amount of Al affects the initiation and progression of bone mineralization in premature infants. However, Al accelerates the formation of osteoid (Exley, 2008).

Boron (B) is another metallic ion essential for mammalians, and its amount affects the amount of absorbed vitamin D and as a result it may influence the bone metabolism (Devirian & Volpe, 2003). There is also another research that showed B's role in postmenopausal osteoporosis (Cui et al., 2004).

Next is cadmium (Cd) with high toxicity and carcinogenicity. Researches showed that Cd diminishes calcium absorption, increases calcium loss from bone, and decreases mineralization ability of bone. Thus, Cd prevents the self-assembly in the extracellular matrix of bone and decreases collagen production (Bhattacharyya, 2009).

In addition, Mg^{2+} ion deficiency affects all stages of skeletal metabolism resulting in the cessation of bone growth and the decrease of osteoblastic and osteoclastic activities, and therefore, causes osteopenia and bone fragility (Rude et al., 2009). The Mg^{2+} ion content of the natural apatite is around 6 mol%, but Mg^{2+} content of the bone changes with aging. Furthermore, the Mg^{2+} ion is present in high concentrations in the cartilage and bone tissues during the initial phases of osteogenesis, and it is likely to disappear as the bone tissue becomes mature (Laurencin et al., 2011).

Strontium (Sr^{2+}), as another ion, shows a metabolic behavior similar to calcium (Dahl et al., 2001). It was reported that Sr^{2+} has beneficial effects on bone such as increasing the replication of preosteoblastic cells and bone formation in cell calvarial cultures.

In addition, Sr ranelate (a Sr salt) decreases the amount of bone resorption while it increases the bone strength because of the increase in the bone formation and the decline in the resorption (Dahl et al., 2001). Therefore, Sr^{2+} increases the number of osteoblasts and decreases the number of osteoclasts (Dahl et al., 2001).

It was illustrated that three mechanisms determine the uptake and release of bone seeking elements. These three mechanisms are listed below (Dahl et al., 2001):

- Adsorption with an important role in bone metabolism leading to an increase in mineral volume.
- Resorption
- Surface exchange and diffuse exchange.

It was also reported that Sr^{2+} is taken up into bone by two different mechanisms:

- an initial rapid mode depending on osteoblastic activity (ionic exchange)
- a slower mechanism involving the incorporation of Sr^{2+} into the crystal lattice of the bone mineral (Dahl et al., 2001).

Fluoride is a trace element that impacts the bone mineralization during bone formation. Mousny et al. proved that the effect of fluoride depends on the dose of fluoride, and genetic is an important feature in the effect of fluoride in bone mineralization (Mousny et al., 2008). They reported that F^{-} stimulates osteoblastic activity and postpones mineralization of new bone (Mousny et al., 2008). They also showed that fluoride treatment has no influence on bone microarchitecture though it increases the osteoid formation and declines mineralization heterogeneity (Mousny et al., 2008). Also, fluoride ions influence the bone mechanical properties due to the alterations in mineral organic interfacial bonding (Mousny et al., 2008).

Zinc (Zn), the first element in group 12 of periodic table, is another ion with an important role in the preservation of bone mass through stimulating osteoblastic bone formation and inhibiting osteoclastic bone resorption (Wang et al., 2007). Considering the effects of Zn on osteogenic and adipogenic differentiation of bone marrow stromal cells and the adipogenic isolated mouse primary bone marrow stromal cells and osteoblasts they stated that there was no effect on cell growth because of the Zn supplements although in individual concentrations it can affect it. Zn^{2+} ion limits the osteogenic and adipogenic differentiation of marrow stromal cells and depresses

adipogenic differentiation at lower concentration for osteoblasts. This effect can change into promotion or decrease as the concentration of Zn increases.

1.3. Bioceramics

There is a great deal of applications of bioceramics because of their benefits they offer the orthopedic applications (Best et al., 2008). Some of these bioceramics such as alumina and zirconia have remarkable mechanical features; some others like calcium phosphates are preferable owing to their similarity to the bone mineral. Based on the interaction between the host and the implant, Best et al., (2008) categorized bioceramics into bioinert or bioactive while bioactive ceramics can be further classified as resorbable or non-resorbable.

1.4. Calcium Phosphate

In biomedical applications, calcium phosphates are preferable due to their similarity to the mineral part of the bone and their high bioactivity in the body. There are different forms of calcium phosphates, each with unique material property. These properties are also influenced by the Ca/P ratios from different aspects (Best et al., 2008). For example, Ca/P ratio of HA lower than 1.58 results in the appearance of α or β-Tricalcium phosphate (TCP) phase after processing. However, with Ca/P ratio higher than 1.67, there is a chance for the appearance of calcium oxide (CaO) phase along with HA. In general, the biological properties of the material can be influenced by the presence of secondary phases, and TCP with the Ca/P ratio of 1.5 has a higher resorption rate than that of HA (Best et al., 2008). Ca/P ratios of some calcium phosphates are shown in Table 1.5.

Table 1.5. Ca/P ratios of some calcium phosphates (Kalita et al., 2007).

Phase	Ca/P ratio
Hydroxyapatite (HA)	1.67
α-Tricalcium phosphate (α-TCP)	1.5
β-Tricalcium phosphate (β-TCP)	1.5
Tetracalcium Phosphate (TTCP)	2

There are different types of calcium phosphates used for different biomedical applications due to differing bioactivity or resorption rates, although they have poor mechanical properties (Kalita et al., 2007). However, it is possible to improve these mechanical properties in calcium phosphates, and these methods of improvement will be discussed in the following chapters. Among calcium phosphates, HA is widely used because of its bioactivity and stability in physiological environment.

1.4.1. Monocalcium Phosphates

Monocalcium phosphate is the compound consisting of one calcium ion and Ca/P ratio of 0.5, and they appear in two types according to the CaO-P_2O_5-H_2O phase diagram: (1) monohydrate ($Ca(H_2PO_4)_2 \cdot H_2O$) and (2) anhydrous salt ($Ca(H_2PO_4)_2$) in acid with a pH range of 0.0-2.0). It also has a triclinic space group, P1 with primitive unit cell parameters a=5.6261, b=11.889 and c=6.4731 Å with α=98.633°, β=118.262° and γ=83.344° (Dorozhkin & Epple, 2002). For each unit cell, there are two formula units. Another important calcium phosphate is monocalcium phosphate monohydrate, a starting material of hydrothermal synthesis of monetite and hydroxylapatite. Its suspension creates hydroxylapatite needle shaped crystals and monetite whiskers through treating hydrothermal under the conditions of 160°C and 1 MPa and 200°C and 2 MPa, respectively (Jinawath et al., 2001).

The reported density of monocalcium phosphate monohydrate is 2.231 g/cm^3 (Dorozhkin & Epple, 2002), which is used in phosphorus containing fertilizer

production industry, dry baking powders, food, tooth pastes, and some beverages as nutrient, acidulant and mineral supplement (Dorozhkin, 2012); in medicine, as a component of self-hardening calcium orthophosphate cements. As it is very soluble and acidic, it is not possible to find monocalcium phosphate monohydrate in biological calcifications.

In contrast to the other calcium phosphates monocalcium phosphate solubility changes according to the changes in temperature and its solubility also increases with increase in the temperature. It means it is necessary to apply sulfuric acid treatment in order to get phosphorus for the agricultural fertilizers from the phosphate rock, and to produce more soluble monocalcium phosphate (Dorozhkin & Epple, 2002).

1.4.2. Dicalcium Phosphates

Dicalcium phosphate, another compound in the calcium phosphate family, has two positive ion sites occupied by one calcium ion and one hydrogen ion, and Ca/P ratio of 1.0 (Dorozhkin, 2012). Dicalcium phosphate compounds are very important in terms of bone mineralization, and therefore they are used in bone and teeth as dental cement and restorative material. Additionally, they are used as protonic conductors for fuel cell applications (Tortet et al., 1997). Dicalcium phosphates also have two forms: (1) dicalcium phosphate dehydrate or brushite ($CaHPO_4 \cdot 2H_2O$) and (2) dicalcium phosphate anhydrous or monetite ($CaHPO_4$).

1.4.3. Tricalcium Phosphates (TCP)

TCP with a Ca/P ratio equal to 1.5 has two main types: α-TCP and β-TCP with the chemical formula of α-$Ca_3(PO_4)_2$ and β-$Ca_3(PO_4)_2$, respectively. It is possible that each transforms into the other one when there is a change in the temperature. For instance, β-TCP changes into α- TCP at 1125°C (Kockan & Evis, 2010).

With a monoclinic crystalline structure, α-TCP has a P21/a space group with lattice parameters of a=12.877 Å, b= 27.280 Å, c=15.219 Å and β= 126.20° (Carrodeguas & De Aza, 2011). Moreover, with a rhombohedral structure, β-TCP has a space group of R3c with a unit cell parameters of a= 10.439 Å and c=37.375 Å (Vallet-Regí & González-Calbet, 2004).

1.4.4. Tetracalcium Phosphates

Tetracalcium phosphates have four calcium atoms, and a Ca/P ratio of 2, (Dorozhkin, 2012). They have the formula of ($Ca_4(PO_4)_2O$), and the monoclinic structure with a primitive unit cell P21 space group and with unit cell parameters of a=7.023, b=11.986 and c=9.473 Å with β=90.90° (Dorozhkin, 2012; Moseke & Gbureck, 2010). Tetracalcium phosphates also have four formula units per unit cell with the density of 3.051 g/cm^3 (Moseke & Gbureck, 2010). Unlike hydroxylapatite, tetracalcium phosphates are more soluble in the aqueous media, so it cannot be produced by precipitation reaction. Therefore, tetracalcium phosphate can be only produced through the method of the solid-state reactions at temperatures above 1300°C. As it is not stable in aqueous conditions because of its high solubility, tetracalcium phosphate transforms into hydroxylapatite and calcium oxide quickly. That's to say, there is no tetracalcium phosphate in physiological systems (Kalita et al., 2007).

These phosphates are also used in the production of self-setting bone cements by mixing with monetite or brushite. The produced mixture changes into hydroxylapatite in the presence of water in the medium in bone cement. This mixture as bone cement can also be used as the composite of tetracalcium phosphate and collagen, and graft in bone and cartilage tissue. Another benefit of using this materials is the small amount of time it takes to replace bone and better fixation after surgery by preventing loosening and micromotion (Kalita et al., 2007). Moreover, it is used to "control the properties of metals by being a product of the reaction between phosphorus, oxygen and lime in the iron manufacturing."

1.5. Hydroxyapatite

HA is widely used as a substituent of implant materials for hard tissues like bone and teeth, its biocompatibility and bioactive properties have made HA a perfect material to enhance peri-implant bone tissue formation (Mackie et al., 1972). It has the most stable phase above a pH of 4.3, so it is very useful for biomedical applications, such as matrices for controlled drug release and also as coatings on orthopedic implants (Bose et al., 2009; Kalita et al., 2007). On the other hand, HA has some disadvantages

in mechanical properties. like low strength, hardness and fracture toughness, which limit the application of HA to the non-load bearing areas in the body (Bose et al., 2009). The molecular formula of HA is $Ca_{10}(PO_4)_6(OH)_2$ with a Ca/P ratio of 1.67. However, this ratio changes by doping some ions into HA structure and this results in non-stoichiometric HA.

Having a well-documented biocompatibility, HA with good osteoconductive property is rapidly integrated into the human body. However, it is not possible to use HA in bulk form for load bearing applications such as orthopedics as it has poor mechanical properties.

1.5.1. Crystal Structure of Hydroxyapatite

HA has an hexagonal structure which belongs to the space group $P6_3/m$, characterized by a six fold c-axis perpendicular to three a-axes (a1, a2, a3,) 120° angles to each other (Legeros et al., 2003). In addition, the unit cell of HA is composed of Ca^{2+}, PO_4^{3-} and OH^- groups packed in a certain orientation as shown in Figure 1.4.

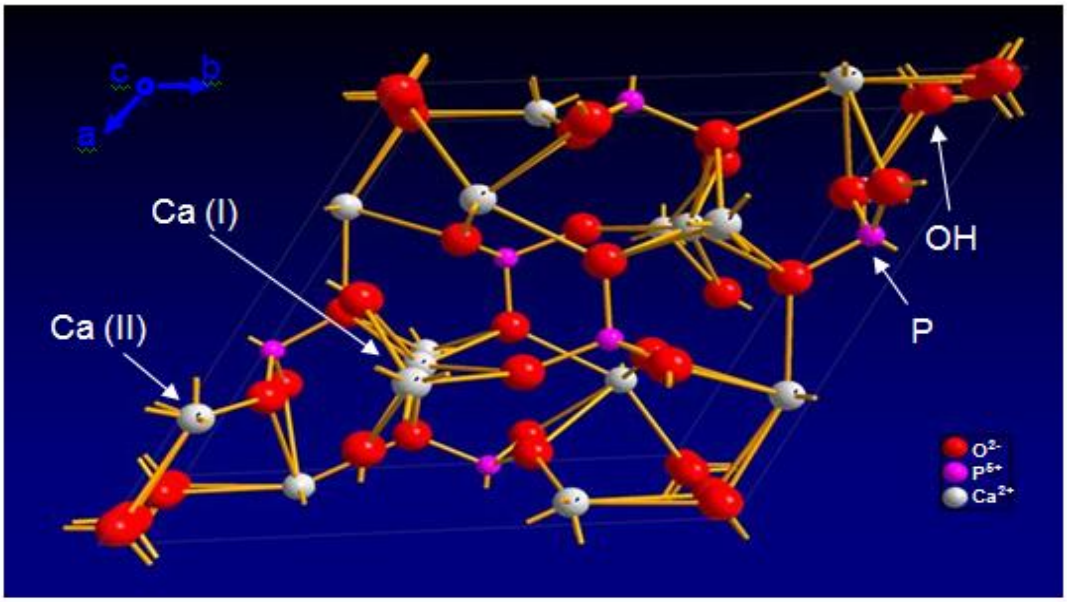

Figure 1.4. Graphical representation of crystal structure of HA (Rivera-Muñoz, 2000)

1.5.2. Monoclinic Structure

Monoclinic HA crystal structure possesses P21/b space group with the unit cell parameters of a = 9.421 Å, b = 2a = 18.842, c = 6.881 Å, and γ=120° (Ma & Liu, 2009). This crystal structure in monoclinic HA looks like hexagonal HA, except the directions of OH groups. This structure results in high thermodynamical stability and ordered structure in monoclinic HA, which also has more stoichiometric structure than hexagonal HA because of the difficulty in substituting ions created by OH orientation.

1.5.3. Mechanical Properties of Hydroxyapatite

HA is brittle and has low ductility because of its low fracture toughness (<1 MPa · $m^{1/2}$). Moreover, there is the possibility of a fracture happening at the bone and material surface due to the high elastic modulus of HA (~120 GPa) and great stress concentration. The mechanical properties of HA are also influenced by the factors such as the compression pressure and sintering conditions (He et al., 2008; Meyers et al., 2008). Besides, it was reported that there is a direct relationship between the sintering temperature and density, grain size, compressive strength and elastic modulus. For instance, with an increase in sintering temperature up to 1250°C, there is an increase in the fracture toughness of HA. However, with an increase in sintering temperature higher than 1250°C, there is a decrease in toughness value of HA. Synthesis method of HA has also an effect on mechanical properties since these methods have impact on the grain size of HA (He et al., 2008; Meyers et al., 2008).

1.5.4. Biological Properties of Hydroxyapatite

As a stable material with a similar structure to bone mineral, HA can be used at physiological pH, temperature and composition (Kalita et al., 2007). It can accelerate bone growth on the material (Fernández et al., 1999). Furthermore, it is preferable for implants as it can be resorbed by the bone after assisting bone repair (Best et al., 2008). In order to achieve this property, a mixture of HA with TCP can be used because it dissolves quickly in comparison to HA. In an implant, this feature is a desirable property (Best et al., 2008).

For the bioactivity of HA, cell behaviors, such as adhesion, proliferation, and morphology are important factors. Webster et al. studied the morphology and resorption activity of osteoclast-like cells on conventional and nanophase HA and alumina (Webster et al., 2001). In this study, they determined the cellular activity of the osteoclast-like cells based on the synthesis of tartrate resistant acid phosphatase (TRAP) and the resorption pits formed on material surfaces by the cells. It was observed that TRAP synthesis was the highest on nanophase materials, and the highest TRAP activity was observed on nanophase HA for all time periods. Resorption pits formation on both conventional and nanophase HA was similar to that observed on the bone reference material although there was a higher resoption activity on nanophase HA. This study also showed that there was higher osteoclast-like cell function on nanophase HA compared to conventional HA. This feature can be described through the increased roughness, higher surface wettability and the improved solubility of nanophase HA (Webster et al., 2001). Another study investigated the osteoblast functions like proliferation, alkaline phosphatase synthesis and extracellular matrix calcium concentration on various nanophase ceramics including HA (Webster et al., 2001). All cellular activities were higher on nanophase HA with longer cell culture periods in comparison to the conventional HA. These two studies showed that there is the possibility of improving biological properties by nanophase HA use through enhancing osteoclast and osteoblast cell activity on the material. Another method of improving biological properties of HA is through doping it with different elements. This concept is discussed in detail in the following sections.

1.5.5. Synthesis Methods of Hydroxyapatite

To produce HA, there are several methods including solution precipitation and co-precipitation, solid-state reactions, sol-gel technique, emulsion and microemulsion technique, hydrothermal reactions, hydrolysis and solution mediated reactions. Based production method, it is possible to produce HA with different mechanical, structural and biological properties. Cox reviewed various methods of synthesis of HA in detail (Table 1.7).

Table 1.6. Summary of each synthesis method with a brief description and other features (Cox, 2012).

HA Synthesis Method	Method Description	Processing Time (</> 24h)	Reaction Temperature (°C)	Particle Size (µm)	Scalability	Comments
Wet-chemical Precipitation	Calcium and phosphate solutions combined under controlled reaction parameters resulting in nucleation an crystal growth	>	Room temperature – 85	> 0.1	High	•Most common method •Three step procedure; requires calcinations and sintering after processing •Difficulties with reproducibility due to lack of precise control
Hydro- and Solvo-thermal	Reaction takes place in aqueous solution in a closed system under conditions of high temperature and pressure	<	150 – 400	> 0.05	Low	•Homogeneous crystal shapes and sizes •Single step process to form crystallised HA •Cost dependent on particle morphology
Solid State Reactions	HA formed via solid-state diffusion of ions from solid reactants Requires thermal treatment to initiate reaction	>	1050 – 1250	> 2.0	Medium	•Most traditional method •Involves long ball milling, drying, compression, and sintering steps •May need to repeat process steps to improve quality and reduce particle size •Slow and difficult to achieve a complete reaction; mixed phase product
Sol-gel	'Sol' solution is formed that evolves into a 'gel' system via hydrolysis and polycondensation	>	37 - 85	> 0.001	Low	•Molecular mixing improves chemical homogeneity •Difficult to form single phase •Involves more than 3 processing steps •HA exhibits inferior crystallinity and thermal stability
Self-propagating combustion synthesis (SPCS)	Particles formed from aqueous solution via spontaneous combustion of a fuel and oxidiser at elevated temperatures	<	170 – 500	> 0.45	Expected to be low	•Reaction time <20mins •Uncontrollable high temperature reaction front may lead to mixed phases •Particle morphology dependent on fuel used
Emulsion and Microemulsion	Droplets of immiscible liquids react in a heterogeneous mixture	>	Room temperature – 50	> 1.0 (emulsion) > 0.005 (micro)	Low – Medium	•Porous particles can be formed •High temperature calcination and sintering steps required •Highly dependent on oil and surfactants used

1.5.5.1. Precipitation method

One of the most widespread approaches is conventional wet chemical precipitation method because of its simplicity, ready availability and use of relatively inexpensive raw materials. The operating cost is also minimal due to the combination with low reaction temperatures use (Cox, 2012). In 2007, Mobasherpour et al. synthesized HA powder from the calcium nitrate hydrated and di-ammonium hydrogen phosphate solution with the precipitation method and heat treatment of HA powders. They also used the Fourier transform infrared spectroscopy (FTIR), the X-ray diffraction (XRD) and simultaneous thermal analysis (STA) to study the structural evolution, and used transmission electron microscopy (TEM) and scanning electron microscopy (SEM) to estimate the particle size of the powder and observe the morphology and agglomeration state of the powder. Accordingly, it is possible to synthesize nanocrystalline HA from raw materials by the precipitation technique. In addition, there was a gradual increase in the size of HA grain when temperature was increased from 100°C to 1200°C, and there was no transformation from HA hexagonal-dipyramidal phase to the other calcium phosphates phases up to 1200°C (Mobasherpour et al., 2007).

1.5.5.2. Solid State Reactions

There are not many reports of the solid-state synthesis of HA although this is relatively a traditional method. This method depends on the solid diffusion of ions amongst powder raw materials and therefore needs a processing with a relatively inefficient high temperature (< 1250°C) to start the reaction. Although the method is relatively simple, there are a number of processes involved. First of all, starting materials must be ball milled for approximately 16h, so the presence of homogeneity and sufficiently small particle sizes were ensured. The next process is to add calcium and phosphate sources to additives (e.g. silicon dioxide, alumina, and hydrofluoric acid), a binder (e.g. PVA) and an organic vehicle (e.g. acetone) to create a slurry before milling. Afterwards, this produced slurry must be dried (Pramanik et al., 2007). This produced powder, in return, can be used to produce pellets by applying pressures up to 135MPa using either hot or cold press.

Lastly, it is necessary to perform sintering up to 1250°C to crystallize the product. However, Pramanik et al. (2007) suggested another phase in order to refine the crystal structure, and reduce the grain (7-8 μm) and crystal size (50-70 nm) by recrushing the sintered samples and then by further compaction and sintering at 1250°C. Although there are different reports representing the production of HA in a single phase through this method, it is highly possible to have α-TCP ($Ca_3(PO_4)_2$) in the final product since high temperatures are required to initiate the reaction. They also proposed that there is the possibility of the transformation of the α-TCP phase to β-TCP during sintering; this process is going to occur at 1063°C (Pramanik et al., 2007). The dissolution and mechanical properties of the material will be changed in case of any incorporation of different calcium phosphate phases in the final product. Due to this feature, its performance is adversely unpredictable.

1.5.5.3. Sol-Gel Dip Method

Recently, one of the favorable methods is sol-gel technique because of the inherent associated advantages of this method: homogeneous molecular mixing, low processing temperatures (<400°C), and the ability to generate nano-sized particles. However, one disadvantage of this method is its high cost of the reactants, which can be compensated by the energy saving gained from the low temperatures. Unlike other methods with low temperatures, this technique also has very limited scalability due to the sensitivity of the process. First, a dispersion of solid particles, called 'sol' or colloids, is formed in a liquid. Then, precursor materials – metal alkoxides (e.g. tetraethoxysilane to introduce silicon) and metal salts (e.g. calcium nitrate to add calcium; ammonium phosphate to add phosphorus) – should be mechanically mixed in a solvent at a pH that inhibits precipitation. Meanwhile, hydrolysis and polycondensation reactions happen to connect these monomer units to each other and create M-O-M bonds within the sol resulting in the increase of the viscosity.This process is termed gelation, whose result is the production of a 'gel', defined as a diphasic system including a solid and interstitial liquid phase. It should be considered that it is difficult to form a gel without flocculation.

Later, a drying process can be used to remove the liquid phase, the process which is normally coincides with a significant amount of shrinkage and densification. As there is the possibility of a fracture in a target 3-D monolith structure, it is essential to age the gel before drying. Moreover, when the aim is to produce "a fine sol-gel powder for further processing as granulate or shaped product," there is also the possibility of the crack occurrence. Finally, there is a necessity of employing a material specific sintering protocol, the step which can be very time-consuming (Cox, 2012).

1.5.5.4. Emulsion/Micro-emulsion Techniques

"Emulsions are heterogeneous mixtures of at least one immiscible liquid dispersed in another in the form of droplets" (Zhang & Cooper, 2005). There are two different methods to define these systems: water-in-oil (W/O) or oil-in water (O/W); the first stated phase is the dispersed one, during which O/W systems are generally used to synthesize HA. This technique can be named emulsion or microemulsion regarding the size of the aqueous drops, i.e. the size of the reaction domains. The collision of two different droplets containing the reactants, in this process causes a reaction. These two techniques, microemulsion and emulsion, result in the production of nano- and micro-sized particles of HA, respectively and microemulsion technique results in the reduction of particle agglomeration of HA (Koumoulidis et al., 2003).

This synthesis process is specifically used to form porous spherical HA granules for drug delivery (Lee et al., 2011). Granules of 50 – 2000 μm in size have been formed up to 1250°C with porosity up to 58.5% and no substantial trace of impurities via emulsion routes. However, it was reported that these pores were poorly interconnected. This feature might stop cell growth, vascularisation, and diffusion of nutrients *in vivo*. Furthermore, this research used these HA particles produced via microemulsion routes with spherical morphology and small particle sizes (>22 nm) for plasma spraying because of their superior powder flow characteristics (Koumoulidis et al., 2003).

1.5.5.5. Pulsed Laser Deposition

In 2007, Koch et al. investigated the pulsed laser deposition method, and reviewed recent developments including pulsed laser deposition of HA thin films in

medicine and dentistry. They also described the structural, mechanical, and biological properties of HA thin films and discussed the future directions of this method (Koch et al., 2007).

1.5.6. Doping of Ions into HA

1.5.6.1. Doping of F^- Ions into HA

Fluorine (F^-), the key supplement for protection and better growth of teeth and bones (Rodríguez-Lorenzo et al., 2003), can be found in enamel layer, blood plasma, saliva, and the mammalian hard tissue in small amounts (≈0.1 wt%) (Boanini et al., 2010a). Fluoride doping is often used to improve the thermal stability and biological properties of HA in addition to cation dopants, and the fluoride substitution in HA had a great impact on the physical and biological characteristics of HA. Having a very crucial role in suppressing dental caries, fluoride in saliva and blood plasma is necessary for dental and skeletal development (Kim et al., 2003). Moreover, it was able to stimulate proliferation and differentiation of bone cells (Aaseth et al., 2004).

Moreover, it is necessary to use fluoride in the osteoporosis treatment (Aaseth et al., 2004). In order to substitute F^- in the crystal lattice of HA, there are numerous techniques including wet precipitation, neutralization, sol–gel and solid-state path. One advantage of the incorporation of F^- ions into the HA structure is increasing its biocompatibility, chemical stability and mechanical behavior (Gross & Rodríguez-Lorenzo, 2004a), and next advantage is the help it provides in the control of tooth decay. In particular, F^- doped HA ($Ca_{10}(PO_4)_6(OH)F$) promotes cell proliferation and attachment, whereas the fluoroapatite (FA) ($Ca_{10}(PO_4)_6F_2$) works as an anti-cancer agent (Öchsner et al., 2013).

During doping of HA with fluoride, F^- ion competes with OH^- ion, decreases the solubility of HA, and increases HA density after sintering. This increase, in turn, causes twofold or four fold improvement in strength and hardness in comparison to pure HA (Kim et al., 2003).

However, this is not always the case and high concentration of fluoride ions may stop the cell proliferation by releasing Ca^{2+} ions in HA as its solubility decreases (Cheng et al., 2005). Moreover, it is reported that high concentrations of fluoride

results in abnormal tissue growth (McCormack et al., 1993). It was reported that high amount of fluoride additions into HA causes some poor mechanical properties, but at the same time it also results with the improvement of the mechanical properties of HA, such as hardness, fracture toughness, elastic modulus and brittleness at lower fluoride doping levels (Gross & Rodríguez-Lorenzo, 2004b). As a result, it is essential to control the F^- content of HA since excessive amounts of F^- ions may have negative effects on the bone including osteomalacia or decreasing osteo-conductivity although it has favorable impacts on the bone formation and its ability to improve mechanical properties of HA (Eslami et al., 2010; Fathi & Mohammadi Zahrani, 2009).

Another improved feature caused by addition of F^- is crystallinity, so its addition is very helpful in osteoporosis therapy (Kim et al., 2003; Rauschmann et al., 2005). This doped HA also increases collagen synthesis and alkaline phosphatase activity by indirectly affecting the cell proliferation. The biocompatibility also rises in comparison to those with pure HA thought there is no evidence of significant change in cell attachment (Inoue et al., 2004; Zhu et al., 2008).

In another study, wet chemical technique was used to produce nano HA, FHA and FA in order to test the obtained materials mechanically and biologically (Eslami et al., 2010). In XRD analysis, the formation of secondary phases was not perceived in any of the samples sintered at temperature up to 1200°C. The replacement of OH^- ions by F^- ions was confirmed by the results obtained from FTIR analysis; by increasing the F^- doping, the lattice parameters were observed to decrease according to TEM analysis. Furthermore, it was observed in vitro experiments of this study that the increased F^- content of HA was able to impact cell behavior in two ways: the cell attachment on HA surface increases by the presence of high F^- content, but the decrease in Ca^{2+} ion release caused by the increase in F^- content inhibits cell proliferation.

In another study, biological effects of F^- release from FHA produced was investigated (Qu & Wei, 2006a). FHA samples with varying F^- were produced via pH-cycling method. Cell attachment on FHA discs was tested. It was reported that high F containing discs were found to have lower contact angles, thus lower protein adsorption. This was explained by the removal of OH^- ions which provided binding

sites for protein adsorption. However, in cell culture studies, although a similar result was obtained for the first 2 hours of cell attachment, later observations showed that, with increasing time of cell culturing, higher cell attachment was observed on FHA discs compared to HA discs. These results suggested that, with increasing cell culture time more F^- ions were released into the cell culture medium, which promoted cell attachment. In cell proliferation studies, increased F^- was also found to stimulate cell proliferation.

In another study, mechanical properties of hydroxyfluorapatites – hydroxyapatites in which hydroxyl groups were replaced by F^- ions at F levels of 0%, 20%, 40%, 60%, 80% and 100% were investigated (Gross & Rodríguez-Lorenzo, 2004b). Hardness, elastic modulus, fracture toughness and brittleness of the samples were measured by micro indentation. In hardness measurements, no change was observed until 80% F doped HA, after which a rapid increase was observed. A linear increase was observed in elastic modulus with increasing F^- content. Fracture toughness was improved by F^- doping up to an incorporation of 60%, after which a decrease in fracture toughness was observed. The lowest brittleness value was observed for the 60% F^- containing samples and this value also increased after 60% doping with F^- (Legeros et al., 2003). This study showed that, up to a certain level of F^- incorporation favors mechanical properties if HA while high F^- levels cause adverse results in terms of mechanical behavior. Thus, for optimum mechanical properties F^- content of doped HAs should not exceed a certain value. These studies investigating doping of HA with F^- ion showed that, F^- ion incorporation could improve both mechanical and biological properties of HA as long as optimum levels of doping are achieved.

When the effects of F^- ion substitutions are observed, it was seen that as the amount of F^- ion substitution increased, lattice parameter "a" gradually decreased while fluctuating changes were observed in the decrement pattern of lattice parameter "c". Since OH^- ions lie along the "c" axis at the center of Ca (II) triangles, F^- ion substitutions for OH^- ions take place along the "c" axis (Legeros et al., 2003). Thus, no severe changes were observed in the "c" axis of the crystal structure. The decrement in lattice parameter "a" with increasing F^- content may be attributed to the higher

electronegativity of the F^- ions compared to OH^- ions that they substitute for (Lee et al., 2005). The increased electronegativity difference between Ca^{2+} and F^- ions results in greater attraction between them, thus the decrease in the distance between these two ions leads to a decrease in the length of "a" axis.

So, by adding a certain amount of F to an appetite, a slight increase in the lattice parameters were observed with the substitution of F^- ion, although F ion substitution was expected to result in shrinkage. This might be due to the partial replacement of OH^- ions by F^- ions since further decrease in lattice parameters were observed by increasing F^- ion content (Toker et al., 2011).

The results of another study also showed that, addition of impurities like Y^{3+} and F^- did not cause severe fluctuations in XRD patterns. Previous reports also reported that the grain sizes of HA doped with fluoride ions increased with increasing degree of fluoridation (Basar et al., 2010). Another study showed that, incorporation of F^- into HA resulted in a slight shift of XRD peaks to the higher 2Θ value. The shift was more evident in the (300) reflection, which shifted from the 2Θ value of 33.118° in HA to 33.338° in FHA, indicating the decrease in lattice parameters due to the successful substitution of smaller sized F^- ion, compared to OH^- (Wei et al., 2003). Furthermore, a very slight increase in the degree of crystallinity was also observed upon F^- substitution (Alshemary et al, 2015).

1.5.6.2. Doping of Sr^{2+} Ions into HA

Strontium (Sr) is one of the metallic elements found in bones and teeth. Sr appears to be one of the most effective substances for the treatment of osteoporosis and other bone-related conditions (Kim et al., 2004). The structure of the strontium ion (Sr^{2+}) is similar to that of Ca^{2+} ion in view of comparable atomic radii (Li et al., 2007b). Sr can substitute for Ca^{2+} in many of the physical processes of the body, including muscular contraction and blood clotting (Pors Nielsen, 2004). It also can replace Ca^{2+} in HA, and hence in bone, without much difficulty. It is reported that the stable Sr is non-toxic in specific amount in our body for prolonged periods (Fu & Chen, 2008).

Incorporating Sr^{2+} into the HA lattice structure has become of significant interest due to the fact that Sr^{2+} has a biological role in bone, where it decreases the

activity of osteoclasts and increases the activity of osteoblasts (Bonnelye et al., 2008; Matsunaga & Murata, 2009). Incorporating Sr^{2+} ions into the HA structure involves the removal of Ca^{2+} ions to allow Sr^{2+} ion incorporation into the Ca sites. There are ten Ca sites in the HA lattice, the larger M (I) sites and smaller M (II) sites (Bigi et al., 2007; O'Donnell et al., 2008), and occupation by the larger Sr ions can affect lattice dimensions, crystallinity, and increase apatite solubility (Bigi et al., 2007). It is probable that dihydroxylation and subsequently decomposition may occur at lower temperatures during sintering. In the case of a strontium–hydroxyapatite (Sr–HA) material, the solubility characteristics could be important in facilitating the slow release of Sr^{2+} into the implant area; increasing osteoblast activity. Thus, although HA is more stable and has intrinsic bioactive properties, Sr–HA is a more soluble material but its increased bioactivity, due to Sr^{2+} release, makes it more desirable *in vivo*. In addition to Sr^{2+} ion release, increased Ca^{2+} ion release from Sr–HA is believed to activate Ca channels and thus stimulate cell response (Coulombe et al., 2004).

According to an investigation done by Curran et al, the incorporation of Sr^{2+} for calcium (Ca) in HA allows the formation of a pure but nonstoichiometric hydroxyapatite (ns-HA) with low (Sr + Ca)/P ratio and increased lattice dimensions and also decreased mean crystallite size. Following sintering at 1200°C, degradation of HA occurs at different extents to form TCP phases depending on the level of Sr^{2+} substituted for Ca and the sintering regime used. There was a decrease in the overall amount of TCP formation when 5% Sr^{2+} was substituted for Ca but the amount of TCP increased when 10% Sr^{2+} was substituted for Ca. β-TCP stabilization occurred and eliminated the formation of α-TCP effectively. Moreover, increased densification occurred in the samples but to a lesser extent. The undoped samples had a higher grain size than the doped samples (Curran et al., 2011).

Improvement of the mechanical properties of HA can be achieved by the incorporation of metal. In addition, incorporation of strontium ion into HA crystal structures has been proved effective to enhance biochemical properties of bone implant. In a recent research, strontium-doped HA powder was developed via a sol-gel method to produce extraordinarily fine strontium-doped HA (Sr-doped HA) powder. XRD measurement had shown that the powder contained HA phase only for

all doping concentration except for 2%, showing that Sr^{2+} atoms have suppressed the appearance of beta TCP as the secondary phase.

Morphological evaluation by FESEM measurement showed that the particles of the Sr-doped HA agglomerates were globular in shape with an average size of 1-2 micron in diameter while the primary particles had a diameter of 30-150 nm in average (Mardziah et al., 2009).

There are many works on strontium doped HA that have been done by other researchers. They have employed different route for synthesis in order to produce Sr-doped HA. Various morphology, stoichiometry and level of crystallinity can be achieved depending on the technique and methods used for the synthesis process (Saint-Jean et al., 2005). Kim and his co-workers have fabricated strontium substituted calcium phosphate ceramics using a precipitation method (Kim et al., 2004). Saint-Jean et al. have employed the hydrolysis method (Saint-Jean et al., 2005), Fu and Chen have synthesized Sr-doped HA using the solution reaction method (Fu & Chen, 2008) while Kim and his co-worker used the hydrothermal method (Kim & Park, 2005).

In another research, Mardziah and his coworkers study prepared Sr-doped HA powder using a sol gel method. This method is preferred because it produces high purity and better homogeneity ceramics with good crystallinity. Another benefit is that the mixing level of the solution retained in the final product often on the molecular scale. The effects of Sr^{2+} doping concentrations and calcination temperatures on the phase behavior of Sr-doped HA were examined and discussed. As a conclusion, Sr-doped HA fine powders have been successfully synthesized using sol-gel method. The effects of Sr^{2+} doping concentration and calcination temperature on its phase behavior were investigated. The formation of α-TCP phase as the secondary phase only occurred at the lowest dopant concentration, it happened even at 2 mol%, after calcination at temperatures of 900°C and above. Higher Sr^{2+} concentrations contributed to the stabilization of HA phase thus the disappearance of α-TCP phase and to low crystallinity of HA. Individual particles of Sr^{2+} doped HA are globular in shape with an average size of 30-150 nm in diameter. An increase in the concentration of doped Sr^{2+} made the agglomerated particles smaller due to strontium's crystal growth retarding effect, which suppresses the enlargement of HA, crystals. A significant

expansion in the lattice has been proven from calculation of the lattice parameters indicating the substitution of bigger radius Sr^{2+} into Ca^{2+} ion in HA crystal (Mardziah et al., 2009).

1.5.7. Co-doping of Various Ions into HA

Co-doping of HA is a common way to alter the mechanical and biological properties of HA (Evis et al., 2010; Kannan et al., 2006). In a study, F^- and Cl^- co-substitution in HA was investigated. The precipitation method was used for synthesis. Unit cell parameters showed that the apatite structure remained. There was an increase in c-axis parameter as the concentration of ions increased (Kannan et al., 2006). The crystal size was calculated as 50 nm which was similar to bone mineral size (Kannan et al., 2006). There was another study, which investigated the photoluminesent properties of Sb^{3+} and Mn^{2+} co doped HA. These two ions were substituted with Ca^{2+} ion. The samples were prepared by hydrothermal synthesis method. By adjusting the ratio of $Sb^{3+/}Mn^{2+}$, luminescent properties of HA could be improved (Wen et al., 2002).

Co-doping of Mg^{2+} and CO_3^{2-} ions alters the cell viability on HA. However, cell differentiation results showed that HA was superior to Mg^{2+} and CO_3^{2-} co-doped samples (Landi et al., 2006). Mg^{2+} and F^- co-doped samples were synthesized (Sun et al., 2010). Their effects on structural, mechanical and biological properties were studied. According to the results, Mg^{2+} addition did not have a significant effect on the density of HA. However, when Mg^{2+} was doped with F^- ion, the density of HA increased. As Mg^{2+} concentration increased, density started to decrease. Moreover, increase in Mg^{2+} addition triggered the β-TCP formation when the samples were sintered at 1100°C for 1h. Grain sizes of the samples decreased as expected. The microhardness values were also determined and it could be said that Mg^{2+} ion resulted in decrease in Vickers microhardness. However, with F^- addition, microhardness values improved. Osteoblast adhesion was also investigated for the samples.

It was found that up to a limit, Mg^{2+} addition increased osteoblast adhesion (Sun et al., 2010). However, when Mg^{2+} and F^- were co-doped, the osteoblast adhesion increased as the amounts of doping increased. In another study, Y^{3+} and F^- ion incorporation together was investigated in terms of structural and mechanical

properties (Evis et al., 2010). Three different sintering temperatures were used in experiments. Densities of the samples decreased with Y^{3+} addition when they were sintered at 900°C and 1100°C (Evis et al., 2010). In terms of mechanical test, diametral strength test was applied. The composition with 2.5 mol % Y^{3+} and 2.5 mol % F^- gave the highest value for the diametral strength when compared with 5 and 7.5 mol.% Y^{3+} and 2.5 mol.% F^- doped samples (Evis et al., 2010).

1.6. β - Tricalcium Phosphate

TCP ($Ca_3(PO_4)_2$), which has three polymorphic forms: β, α and α′, is bone-substitute material with high biocompatibility, favorable resorption properties and osteoconductivity (Koepp et al., 2004; Xin et al., 2005). Among these three forms, α′ changes into the α-form during cooling, so it is not of any interest in this study. One such TCP is pure-phase β-TCP, which is characterized by its precisely defined physical and chemo-crystalline properties, high level of uniformity of chemical composition and purity in comparison to other bone substitutes. Therefore, the prediction of its biological reactions can be reliable. It means that β-TCP is stable at room temperature, but reconstructively transforms at 1125°C and above up to 1430°C into α-TCP, at which α-TCP is a stable phase. However, the super α-TCP form becomes stable until the melting point of 1756°C at temperatures above 1430°C. This feature is meta-stably retained at room temperature during the cooling (Carrodeguas et al., 2010). Moreover, it is reported that β-TCP is the low-temperature phase in the $CaOP_2O_5$ phase diagram. Based on these observations, Mirhadi et al. consider 1.5 as the ideal Ca/P ratio of β-TCP and 3.07 g/cm^3 as the theoretical density (Mirhadi et al., 2011).

1.6.1. Crystal and Monoclinic Structure of β- Tricalcium Phosphate

Based on the reports by Dickens et al.(1974), the β-TCP has a hexagonal cell with a space group of *R*3*c* and 273 atoms per unit cell with unit-cell parameters a = 10.439 Å; c = 37.375Å. Six Ca sites are half occupied in β-TCP, which is represented through the dashed circles (I–VI) in Figure 1.5. In order to maintain the charge neutrality of the cell, it is necessary to have three Ca vacancies per unit cell even

though their distribution can be in different ways over the six sites, and this distribution is the model on which the structure of β-TCP is based.

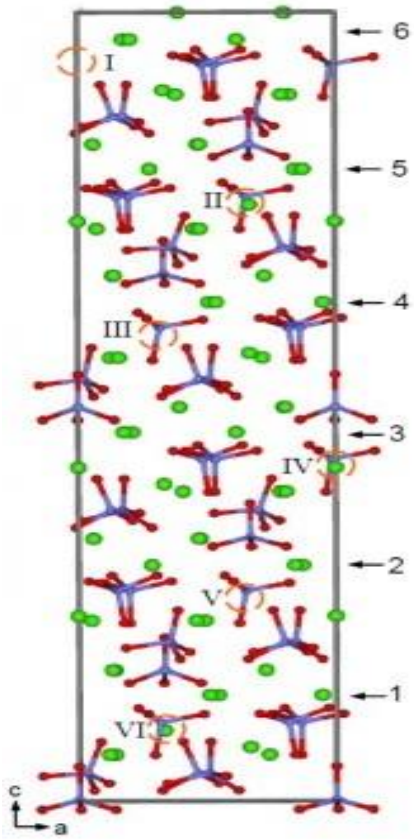

Figure 1.5. Crystal structure of β-TCP. β-TCP projected along the c-axis: roman numerals I–VI with the dashed circles denote six half occupied Ca sites; numerals 1–6 along the right side denote six possible cutting positions for making surface models (Liang et al., 2010).

Nucleation-aggregation-agglomeration-growth mechanism theory explains the crystal growth mechanism of β-TCP. Based on this theory, β-TCP nano-sized crystallites are formed by nucleation and growth after the reaction of calcium and phosphate precursors. Afterwards, aggregates are formed because of some molecular attractions between the nanocrystals with different forces. These aggregates minimize the surface free energy. Finally, agglomerate is formed by further crystal growth if aggregates are gathered as a last step. In this process, if we increase temperature, we

will have increase in particle size by addition of agglomerates. Because of this, secondary particles are formed (Sanosh et al., 2010). This process is summarized in Figure 1.6.

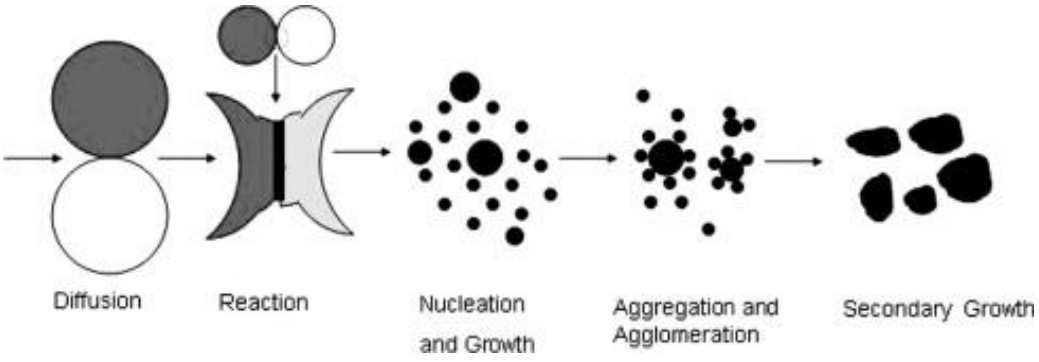

Figure 1.6. Nucleation-aggregation-agglomeration-growth mechanism of β-TCP (Sanosh et al., 2010).

The features, such as high chemical stability, bioresorption rate and mechanical strength, make β-TCP the most preferable polymorph among the three phases. Despite these advantageous features, its mechanical strength must be improved through densification to be used as an implant material. To achieve densification, effective sintering is needed as well as reaction routes, which also affect the phases formed during sintering. Here, it is possible to produce α-TCP through a wet chemical method instead of solid state reactions between 600 and 800°C (Ryu et al., 2002). Another way to affect the sintering of β-TCP is doping some compounds. For example, Bohner et al. investigated MgO and SiO_2 doping effects on β-TCP sintering (Bohner et al., 1996).

They observed that as MgO increased the β to α phase transformation temperature, whereas SiO_2 decreased. In other words, SiO_2 inhibits the sintering of β-TCP. Next parameter that affects the sintering is calcium to phosphorus (Ca/P) ratio (Bohner et al., 1996).

Ryu et al. in their investigation on sintering behavior of pure β-TCP found that the temperatures between 850°C and 1200°C created a rapid increase in sintering rate (Ryu et al., 2002). Another parameter can be grinding time which affects the crystal structure of β-TCP. To explain this, Gbureck et al. transformed β-TCP into calcium

deficient HA by hydrolysis, a reaction which can be accelerated by increasing the grinding time (Gbureck et al., 2003). By increasing grinding time, we can increase the amorphous phases in the structure, and this creates smaller particle size up to a critical level. By the time we reach this level, the given energy is used to form some defects in the crystal lattice, not to reduce the particle size. Consequently, formation of nanocrystals within a single particle results in the loss of crystallinity, and the reactive fraction in the material is the amorphous one. During setting process, the crystalline fraction remains unreacted, so it means that both the amorphous fraction and the solubility of the material increase. That is to say, because amorphous fraction depends on the grinding time, any increase in the grinding time causes increase in solubility (Gbureck et al., 2003). An increase in the grinding time also narrows down the range of pore sizes, increases the porosity, but decreases compressive strength (Gbureck et al., 2003).

1.6.2. Mechanical Properties of β- Tricalcium Phosphate

When used in biomedical applications, β-TCP has the most preferred chemical stability, mechanical strength and bioresorption rate in comparison to the other TCP phases. Elliott argued that it has increasingly been used as a biocompatible material for bone replacement or for the coating of bone prostheses and apatites (Elliott, 1994) because β-TCP solubility in water is about twice as high as that of HA (Yashima et al., 2003). In general, β-TCP comes in the form of powders and polycrystalline materials. Despite the investigations done on the features of β-TCP, it is important to consider that the crystal structural analysis using polycrystalline materials is the part that there has been little analysis in the literature (Rangavittal et al., 2000).

Liang, Rulis, and Ching compared α-TCP and β-TCP and reported that the mechanical properties of the two crystals are comparable and that α-TCP is somewhat softer than β-TCP. This softness most likely comes from the distribution of stronger P–O bonds in β-TCP (Liang et al., 2010). When analyzing β-TCP structures, Yin et al. observed that they have complex crystal structures containing several hundred atoms in the unit cell. Moreover, α, and β types of tricalcium phosphate play important roles in present day bone grafting procedures. They also observed that there are different

temperatures needed for stability. For example, the β -TCP phase becomes stable at the temperature up to 1125°C; the α -TCP becomes stable at the temperature ranging from 1125 to 1430°C but becomes metastable at room temperature (Yin et al., 2003).

An increase in the mechanical strength of β-TCP happens through the densification process, and there is a correlation between sintering temperature and the densification process. When temperature is up to 800ºC, the shrinkage rate of β-TCP is close to zero (Boanini et al., 2010b); when it is between 850 and 1200ºC, the shrinkage rate increases dramatically; when it is above 1200ºC, the shrinkage rate becomes close to zero again. It is at this point that β-TCP transforms into α-TCP, and this transformation prevents further densification. However, transformation in α-TCP creates expansion in the sample volume, and as a result a decrease in the density of the compound. Boanini et al. also observed microcrack formation, which decreases the strength of the material, due to expansion of the sample volume in α-TCP. These features mean α-TCP is not a good candidate for surgical implants. Kurashina et al. also studied the effect of pyrophosphate ($Ca_2P_2O_7$) on β-TCP sintering temperature. They found that as they added small portions of pyrophosphate (3% wt.), the phase transformation temperature of β-TCP to α-TCP increased by 50ºC. Moreover, they reported that the doped β-TCP had higher density than pure β-TCP at 1200ºC (Kurashina et al., 1997). However, Boanini et al. observed that only β-TCP phase was present in pyrophosphate doped TCP when temperature was up to 1300ºC, and they observed the microcrack formation when temperature was above 1300ºC, consequently, the density of doped β-TCP decreased (Boanini et al., 2010b).

Another advantage of β-TCP is its resorbability, which is required in implants in repairing periodontal bone defects or lifting sinus because it is important that this resorbable material to be easily replaced with the bone minerals. Yeong et al. also observed that β-TCP can be used as bone fillers in socket preservation and sinus augmentation applications (Yeong et al., 1999), and it should have adequate mechanical strength. Therefore, densification of β-TCP is very important in achieving the desirable mechanical strength. Additionally, densification, crystallinity, purity and appropriate stoichiometry affect osteointegration and bioactivity (Yeong et al., 1999).

1.6.3. Biological Properties of β- Tricalcium Phosphate

Due to β-TCP's quality of fusion in terms of resorption capacity, limited loss of correction and bioactivity, there is a wide use of it in bone substitution. However, it is not possible to find β-TCP in biological calcifications (Ma et al., 2006). Instead, whitlockite (magnesium substituted) can be found in dental calculi and urinary stones, dentinal caries, salivary stones, arthritic cartilage and some soft tissue deposits (Ma et al., 2006). One important property of β-TCP in comparison to allograft substitutes for idiopathic scoliosis is its higher resorption rate. Le Huec et al. observed that it took 2 years for TCPs to be resorbed totally and the same period of time for allograft particles to be seen the X-ray detection. Also, when observed that the loss of correction was not present in β-TCP after 6 months while it lasted 2 years for allografts. The resorption process of β-TCP in vivo results in the replacement of the pores by connective tissue and then bone tissue. Le Huec et al. observed that the resorption percentage was 40, while the percentage for the replacement of the biological tissue was 80 (Le Huec et al., 2009). They also observed that the replacement and resorption occurred inside the pores and at the outer surface of the material, and the results were consistent with the theoretical mineral content of woven bone in early stages of endochondral ossification. They were also able to detect the dissolved ions from the β-TCP with radioactive labelling, and discovered that osteoblast cells reused these ions to form the extracellular bone matrix. Depending on the situation and features, it is possible for β-TCP to be used in both load and non-load bearing applications. The latter application is more common and general, while the former application occurs in case of adjusted porosity and mechanical strength (Le Huec et al., 2009). The improvement in β-TCP properties, such as improved modulus of elasticity and tensile strength, could be done through producing the composite of β-TCP and poly-L-lactic acid (Le Huec et al., 2009). They also observed that there was the biological activity of this material in vivo and in vitro. While, the increase in the osteogenesis cell proliferation and extracellular bone matrix formation happened because of the increase in the β-TCP weight percentage in vitro experiments, the increase in degradation kinetics in β-TCP containing materials resulted in less inflammatory reactions when compared with pure poly-L-lactic acid in vivo experiments. In terms of osteogenesis, pure β-TCP with β-

TCP/poly-L-lactic acid composite including 60 % β-TCP by weight, gave the same results (Le Huec et al., 2009). In addition, Ogose et al. used β-TCP as a bone morphologic protein carrier to induce bone formation in the body. It was more common in the studies to combine β-TCP with some degredable polymer, such as p-dioxanone and polyethylene glycol and recombinant bone morphogenic proteins. These proteins leads to the alteration in the bone inducing capacity of the β-TCP, known to be a biodegradable and osteoconductive material (Ogose et al., 2002). In terms of carrying capacity, the porosity of β-TCP is also important (Matsushita et al., 2004). Matsushita et al. argued that β-TCP is used as a constituent of calcium phosphate bone cements, and HA and β-TCP biphasic components are widely used as a bone substitution bioceramics (Matsushita et al., 2004). Kasten et al. observed that β-TCP created lower seeding efficacy values of bone marrow stromal cells in comparison to demineralized bone matrix and calcium deficient HA (Kasten et al., 2003). But regarding protein content and alkaline phosphatase activity, they showed that there were similar results with demineralized bone matrix and calcium deficient HA (Kasten et al., 2003).

1.6.4. Doping of Ions into β- Tricalcium Phosphate

It is shown in a number of studies that doping β-TCP with trace metal ions creates changes in its biological activity and chemical nature. When this doping occurs with magnesium ions (Mg^{2+} ions), it also decreases the formation temperature of β-TCP from Ca-deficient apatite. Moreover, these Mg^{2+} ions may lead to the acceleration of bone growth and mineralization and the increase in bone quality, strength, and density in vivo since magnesium-deficiency impairs these factors (Ito et al., 2006; Kannan et al., 2007; Li et al., 2009). To improve the thermal stability of β-TCP, it is possible to add metal ions to β-TCP. For example, Enderle et al. and Marchi et al. are among many researchers who reported that when β-TCP was doped with Mg^{2+}ions (Mg-TCP), it got a stabile β-phase at high temperatures (Enderle et al., 2005; Marchi et al., 2007). Therefore, when used as a sintering additive for β-TCP, MgO results in an increase in the β–α-transformation temperature to 1500 °C. Additionally, β–α transformation of TCP in Mg^{2+} ion-substituted HA/TCP biphasic ceramics is inhibited

at high temperatures (Kannan et al., 2005). When the thermal stability of β-TCP increases, it creates the possibility of sintering at temperatures above 1150 °C. Moreover, Li et al. reported that the standard free energy of the β-TCP solution can increase through the structural stabilization of Mg-TCP, demonstrated by the thermal stability of the β-phase. This, in turn, decreases the solubility constant (Li et al., 2009). As a result, it is important to evaluate the thermal stability of β-TCP in order to determine the various characterizations, like mechanical properties, solubility and biomineralization. Yoshida et al. (2006) also observed that it was possible to dope β-TCP with monovalent metal ions (lithium (Li^+), sodium (Na^+), and potassium (K^+) ions), and proposed a substitution model for these metal ions in the β-TCP structure regarding the resulting lattice constant changes and maximum substitution (Yoshida et al., 2006). Matsumoto et al. (2009) also evaluated the thermal stability of β-TCP which was doped with monovalent metal ions (Li^+, Na^+ and K^+) by using the formation ratio of α-TCP and the rate constant which was calculated by the Johnson–Mehl–Avrami formula. Then, they compared it with that of pure β-TCP and β-TCP which was doped with magnesium ions. In addition, they analyzed the factors inducing thermal stability of β-TCP which was doped with monovalent metal ions. Doping β-TCP with monovalent metal ions decreased the formation ratio of α-TCP and the rate constant and increased the amount of metal ions. Regardless of the metal species and the additive amount, the β–α transformation of β-TCP and β-TCP doped with monovalent metal ions went through the nucleation and growth processes. Moreover, the species at the same amounts of metal ions and heating temperature hardly changed their rate constants. Its thermal stability was also attributed to the structure stabilization of β-TCP structure. This structure was caused by the occupancy of calcium ions and monovalent metal ions in all calcium sites including vacancy in β-TCP structure, which induced by substitution of monovalent metal ions into Ca(4) sites and vacancy in β-TCP with maintaining the charge balance. However, its thermal stability was lower than that of β-TCP doped with magnesium ions. With ionic radii smaller than those of calcium ions, magnesium ions were substitutes for Ca(5) and Ca(4) sites in β-TCP. Also, the stability of the crystal structure occurred because of the structural optimization by the shrinkage of bond length between magnesium or calcium and

oxygen. As a result, it was concluded that the structural stabilization caused by substituting metal ions for calcium sites and vacancy in β-TCP led to the thermal stability of β-TCP , and that also varied by the calcium sites doped with metal ions, i.e., valence and ionic radii of the doping metal ions. In addition, diffusion-controlled growth dominated the β–α transformation for β-TCP doped with monovalent metal ions, but interface-controlled growth mainly dominated by that of β-TCP. Therefore, sintering β-TCP doped with monovalent metal ions at high temperatures and control bioresorbability would become possible as they were thermally and structurally stabilized (Matsumoto et al., 2009).

1.7. HA- β- Tricalcium Phosphate Composites

The β-TCP, represented by the chemical formula of $Ca_3(PO_4)_2$ with Ca/P ratio of 1.5, has also an hexagonal crystal structure (Thamaraiselvi & Rajeswari, 2004). The biocompatibility and similarity of calcium phosphates like HA and TCP to the mineral composition of human bone and teeth have made them suitable for substitution of damaged segments of human skeleton system (Li et al., 2007a). Within several compositions among calcium and phosphorous, hydroxyapatite-β-tricalcium phosphate HA-β-TCP, and their composites (biphasic calcium phosphates, BCP) have received particular attention. HA is considered to be a bioactive and non-biodegradable bone replacement material, and is stable in the body fluid while TCP is resorbable and significantly more soluble than HA (Radin & Ducheyne, 1993). The dissolution rate of HA in body fluid is too low but that of β-TCP is too fast for bone bonding. Therefore, BCP consisting of HA and TCP can be used to control the bioresorbability and achieve optimal results. BCP ceramics were developed in order to combine the high bioactivity of HA and the solubility characteristics of TCP in a composite material. BCP, consisting of HA and β-TCP have many applications in human body (Farzadi et al., 2011; Rabiee et al., 2008).

The concurrent existence of both HA and β-TCP forms BCP that combine the excellent bioactivity of HA with the good resorbability of β-TCP, and thus HA and β-TCP have been used as materials for bone replacement. BCP is composed of a controlled mixture of HA and β-TCP (Jensen et al., 2007). According to the

manufacturer's description, it is a fully synthetic bioactive, osteoconductive bone substitute, available in powder form and is already used clinically. This BCP ceramic, composed of 60% HA and 40% TCP, has a chemical composition close to that of bone. It is able to gradually degrade, leaving room for natural bone (Frenken et al., 2010). The results of its implantation indicate good biocompatibility and bioresorbability, when firmly packed into the bone (Fanghänel et al., 2006). Solubility appears to be the characteristic of primary importance in the remineralization process; results showed that β-TCP has the highest solubility, followed by BCP, than HA (Rumpel et al., 2006). In addition, the biodegradation rate increases with increasing specific surface area (powders > porous solid > dense solid), and with decreasing crystallinity and grain size (Ducheyne & Qiu, 1999). In BCP, the limiting factor is the HA: β- TCP ratio (Yamada et al., 1997).

F^- is well-recognized for its potential behavior relating to the stability of the apatite and for its prevention role in dental caries (Caverzasio et al., 1997; Ten Cate & Featherstone, 1991). However, combined substitution of these elements with the simultaneous formation of biphasic mixtures of HA and β-TCP is a new contribution to improving and refining calcium phosphates in the market. Hence the goal of the present work is an effort toward the synthesis of biphasic mixtures of HA and β-TCP with combined substitution of Sr^{2+}, and F^- through precipitation method. Generally, biphasic mixtures are formed by the calcination of calcium-deficient apatites beyond 700 °C, and the proportions of the resulting mixtures are dependent on the Ca:P ratios of the precursors (Kannan & Ferreira, 2006; Legeros, 1991).

According to a study, one of the essential criteria in the apatite-based materials for medical applications is their aptitude for maintaining thermal stability. Some of their critical applications as (i) porous or granulated materials useful in bone surgery, (ii) additives to organic polymers that improve their bio-functionality, and (iii) coatings, plasma sprayed or prepared by laser ablation, necessarily need treatments of the materials at elevated temperatures. The pure HA has not shown thermal stability above 1200°C by the precipitation method of synthesis, whereas the biphasic mixtures with substituted elements have indicated thermal stability to 1400°C without decomposition to undesirable phases such as α-TCP. It is a well-established fact that

pure β-TCP undergoes allotropic transformation to α-TCP beyond 1120°C (Marchi et al., 2009) and therefore, the high thermal stability of phase mixtures obtained from the present method of synthesis confirms the positive influence of additives (Kannan & Ferreira, 2006).

Numerous studies have been reported on the mechanical properties of the HA ceramics at room temperature. It has been revealed that the mechanical properties strongly depend on the conditions for synthesis and sintering of HA powder (Zyman et al., 1999). Some of the reports pointed out that dispersion of β–TCP improved the mechanical properties. Raynaud et al. showed that HA/10% β-TCP had the highest strength (Raynaud et al., 2002), whereas Akao et al. reported that HA/70% β-TCP exhibited the highest (Akao et al., 1981). The results of this study showed that the mechanical properties were convexly increased with the β-TCP content. This is considered to be due to the two opposite reasons, the reinforcing effect and the microcrack. The compression test at 1100°C showed that the yield stress and work hardening were reduced by the β–TCP dispersion. Since the composites were largely deformed without growth and deformation of each grain, superior superplasticity will be exhibited in the composites (Shiota et al., 2008).

Furthermore, HA and β-TCP ceramics are biocompatible and osteoconductive materials that offer a chemical environment and a surface conducive to new bone formation (Hak, 2007). These are brittle materials and have low fracture resistance (Ogose et al., 2005). Different preparative methods lead to either a compact or porous material with interconnective macropores that are spatially and structurally equivalent to cancellous bone (Samavedi et al., 2013). Commercially available HA is resorbed very slowly, under normal physiological conditions, whereas β-TCP is generally resorbed within 6 weeks after implantation (Spivak & Hasharoni, 2001). When used as a mixture, biodegradable biphasic HA-β-TCP (HT) ceramics have the ability to dissolve, break down, and allow new bone formation and remodeling required to attain optimal mechanical strength without interference.

There is also another research by França et al., regarding the aspects of biphasic material (França et al., 2014), which indicated that both HA and β-TCP are

biocompatible, nontoxic, resorbable, non-inflammatory, cause neither immune nor irritating responses, and have excellent osteoconductive abilities (McLeod et al., 2010)

1.8. Aim of the Study

The purpose of this study was to investigate the microstructural, mechanical and biocompatibility properties of pure and Sr^{2+} & F^{-} doped HTs in order to achieve an improved mechanical and biological properties. Pure and doped HTs were synthesized by precipitation method and sintered at 1100°C for 1 h. The density of the samples was determined by Archimedes method. X-ray diffraction (XRD) and Fourier transform infrared spectroscopy (FTIR) analysis were used in order to investigate the presence of phases and bonds. Scanning electron microscopy (SEM) was used for investigating the microstructure of the samples. The mechanical properties of samples were tested by micro hardness test. For biocompatibility analysis, in vitro cell culture tests were performed using Saos-2 cells. PrestoBlue™ viability test was used to study cell proliferation on HT and doped HT discs. Morphology of the cells on HT discs was investigated by SEM examinations.

CHAPTER 2

MATERIALS AND METHODS

2.1. Materials

2.1.1. Materials used in pure and Sr^{2+} & F^{-}- Doped Composite Synthesis

In this thesis, the main precursors used for the synthesis of HT were calcium nitrate tetra hydrate ($Ca(NO_3)_2 \cdot 4H_2O$) and di-ammonium hydrogen phosphate ($(NH_4)_2HPO_4$) (Merck, Germany). Besides these precursors, additional compounds were required for doped samples. Strontium nitrate ($Sr(NO_3)_2$) was used for preparation of Sr-doped samples (Merck, Germany), and ammonium fluoride (NH_4F) was used for the preparation of F^{-}-doped (Aldrich, Germany).

2.1.2. Materials Used in Cell Culture Studies

For cell culture studies, the following materials were used in the thesis: Dulbecco's modified Eagle's medium (DMEM) (high and low glucose) and fetal bovine serum (FBS) were obtained from Biochrom, Germany; penicilin-streptomycin, sodium pyruvate solution, bovine serum albumin and trypsin-EDTA used for cell detachment were the products of PAA Laboratories GmbH, Austria; dimethly sulfoxide (DMSO) (molecular biology grade) was purchased from AppliChem, Germany; PrestoBlue™ was obtained from Invitrogen, USA; gluteraldehyde, hexamethyldisilizane and 100% ethanol (Sigma-Aldrich, Germany) were used for preparing SEM specimens.

2.2. Methods

2.2.1. Synthesis of HT and Doped Samples

2.2.1.1. Synthesis of HT Samples

To produce HT and doped samples, precipitation method was used, and the precursors were $Ca(NO_3)_2 \cdot 4H_2O$ and $(NH_4)_2HPO_4$. In this method, the first step was to dissolve these two powders separately in distilled water with different amounts to obtain a theoretical Ca/P ratio of 1.58 and stir for 1h.

At the end of 1h stirring, some ammonia solution (NH_4OH) was added to the solution with $(NH_4)_2HPO_4$ and the solution was stirred for 10 minutes. Then, $Ca(NO_3)_2 \cdot 4H_2O$ and ammonia solutions were added drop wise. The purpose of adding ammonia was to adjust the pH level between 11 and 12. After that, the final mixture was left for stirring and the heater was turned on to speed up the reaction. It was heated until boiling. After boiling for 10 minutes, the heater was turned off and the boiled mixture was left for stirring overnight, and the prepared mixture was left for aging for 1 day, after which the mixture was filtered using a vacuum filter. By filtration with a fine filter paper, a wet cake was obtained, which later was dried overnight at 200ºC to remove excess water and ammonia. Finally, the dried samples were sintered at 1100ºC for 1h.

2.2.1.2. Synthesis of Doped HT Samples

To obtain strontium and fluoride doped HT, in addition to the main precursors used in the synthesis of HT, $Sr(NO_3)_2$ and NH_4F were used. Four different compositions of doped HT were prepared. Fluoride amount was kept constant at 1 mole %, while strontium amount was increased from 0.5 % mole percent to 1, 2, and 5 mole %. Descriptions of HT and doped samples according to their strontium and fluoride compositions are summarized in Table 2.1.

Table 2.1. Compositions and Ca/P ratios of HT and doped samples.

Sample ID	Mole % Sr^{2+}	Mole % F^{-}	Ca/P ratio
HT	0	0	1.596
HT0.5Sr1F	0.5	1	1.588
HT1Sr1F	1	1	1.58
HT2Sr1F	2	1	1.564
HT5Sr1F	5	1	1.516

In order to adjust percentage of the substitutions, the amounts of the main precursors were decreased. The changes in the moles of the main precursors are given in Table 2.2.

The procedure of synthesizing was the same as the procedure for HT synthesis. Strontium nitrate was added into the calcium nitrate solution and ammonium fluoride was added into the di-ammonium hydrogen phosphate solution. After the two solutions were mixed with the same procedure, the final mixture was stirred, aged for one day, filtered, dried at 200°C and sintered at 1100°C for 1h.

Table 2.2. Moles of the precursors used for the synthesis of HT and doped samples.

Sample ID	$Ca(NO_3)_2 \cdot 4H_2O$ (mole)	$(NH_4)_2HPO_4$ (mole)	$Sr(NO_3)_2$ (mole)	NH_4F (mole)
HT	0.07500	0.047	0	0
HT0.5Sr1F	0.07463	0.047	0.00037	0.00075
HT1Sr1F	0.07425	0.047	0.00075	0.00075
HT2Sr1F	0.07350	0.047	0.00150	0.00075
HT5Sr1F	0.07125	0.047	0.00375	0.00075

2.2.2. Characterization Methods

2.2.2.1. Structural Characterization

2.2.2.1.1. Density Measurements

Densities of the sintered materials were determined by Archimedes method, this method is based on the formula;

$$d=m/V \tag{2.1}$$

Where d is density, m is mass and V is the volume of the sample.

By using the Precisa Gravimetrics density determination kit (Switzerland), first the dry weight of the sintered samples was measured by putting the sample in the upper part of the kit. Then, the weight of the samples in distilled water was measured by putting the sample in the lower part of the kit. The volume (V) of the samples was calculated by using this formula:

$$V= mass\ of\ the\ object\ in\ the\ air - mass\ of\ the\ object\ in\ the\ water \tag{2.2}$$

Then the density formula becomes with d density (Kuwahara et al., 2001);

$$Density(g/cm^3) = \frac{W_{air}}{W_{air} - W_{water}} \tag{2.3}$$

where W_{air} is mass of the object in the air and W_{water} is mass of the object in the water.

The theoretical densities of HA and β-TCP are 3.156 and 3.07 g/cm3, respectively. The theoretical densities (ρ_t) of the sintered samples were calculated according to their weight percentages (wt % of HA (W_{HA}) and wt % of β-TCP ($W_{\beta-TCP}$), which were calculated from the ratios of the most prominent XRD peaks of the respective phases) in the samples by the following formula (Evis et al., 2005).

$$\rho_t = \frac{1}{\frac{W_{\beta-TCP}}{3.07} + \frac{W_{HA}}{3.156}} \quad (2.4)$$

By using this value, relative densities of the HT and doped samples were calculated.

$$relative\ density = \frac{density}{\rho_t} \quad (2.5)$$

2.2.2.1.2. X-Ray Diffraction Analysis

For XRD analyses, Rigaku DMAX 2200 device was used. The specimens were exposed to Cu-Kα radiation at 40 kV/ 40 mA and scanned from different angles between 20º and 70º in 2θ with the scan rate of 2.0º/min. The results were compared with Joint Committee on Powder Diffraction Standards (JCPDS) files.

2.2.2.1.2.1. Lattice Parameters of HT and Doped HT samples

Unit lattice structure of HA is hexagonal. The hexagonal lattice parameters "a" and "c" of all the samples were calculated by using successive approximations. For the calculation "a" of HT, the following formula which is based on Bragg's equation was used (Cullity & Stock, 2001):

$$a_0 = \left(\frac{\lambda}{2\sin\theta}\right)\sqrt{\left(\frac{4}{3}(h^2 + hk + k^2) + \left(\frac{a}{c}\right)^2 l^2\right)} \quad (2.6)$$

where: a_0: the calculated lattice constant; λ: x-ray wavelength; θ: the Bragg angle for corresponding (hkl); a/c: the last calculated ratio in successive approximation.

This formula was used to calculate a_0 when the value of the term "$\frac{4}{3}(h^2 + hk + k^2)$" was larger than the value of the term "$(\frac{a}{c})^2 l^2$" for a reflection of (hkl). It was used to calculate c_0 if the value of the term "$h^2 + hk + k^2$" was less than the value of "l^2". In order to minimize the error caused by incorrect axial ratio, another formula was used for the calculation of c_0 (Cullity & Stock, 2001):

$$c_0 = \left(\frac{\lambda}{2\sin\theta}\right)\sqrt{(\frac{4}{3}\ (\frac{c}{a})^2(h^2 + hk + k^2) + l^2)} \tag{2.7}$$

The following formula was used to calculate the hexagonal unit cell volume of the materials:

$$V = 2.589(a^2)c \tag{2.8}$$

The degree of crystallinity was calculated according to the fraction of crystalline phase available in the analyzed volume, from the X-ray diffraction data using the expression (Landi et al., 2000):

$$X_c = 1 - (V_{112/300}/I_{300}\ ) \tag{2.9}$$

where X_C is the degree of crystallinity, I_{300} is the intensity of (300) reflection and $V_{112/300}$ is the intensity of the hollow between (112) and (300) reflection.

Phase percentages of HT and doped HT were determined by evaluating relative intensity ratio of the corresponding major phases by using the equations (2.10) and (2.11) (Sun et al., 2010).

$$\frac{W_{HA}}{W_{\beta-TCP}} = \frac{R}{R_0} = \frac{\frac{I_H}{I_{\beta-TCP}}}{1.755} \tag{2.10}$$

$$W_{HA} + W_{\beta-TCP} = 1 \quad (2.11)$$

where W_{HA} and $W_{\beta\text{-}TCP}$ are the wt % of the HA and β-TCP phases, respectively. The ratio R_0 of the peak heights of HA to that of β-TCP was taken as 1.755 (Evis, 2007). R is the ratio of the intensities of the HA (I_H) to that of β-TCP ($I_{\beta\text{-}TCP}$) measured from the XRD peaks.

2.2.2.1.3. Fourier Transform Infrared Spectroscopy (FTIR)

In order to determine the types of bonds formed in the doped and undoped HT structure, FTIR spectra were used. With this aim, the samples were first crushed into the powder form with the use of mortar and pestle. Ceramic powders were mixed with potassium bromide (KBr) with a weight ratio of 1 to 300. In order to obtain transparent pellets the prepared powder mixtures were dried in vacuum by freeze drying for 1 day. The spectra records were performed from 1400 cm^{-1} to 400 cm^{-1} with a 512 scan on FTIR spectrometer (Brukers IFS 66/S; Bruker Optics, Germany).

2.2.2.1.4. Scanning Electron Microscopy Analysis

During experimentation period, the sintered HT and doped HT were investigated by scanning electron microscopy (SEM). The analysis was performed by a QUANTA 400F Field Emission (FEI Inc., USA) at a voltage of 20 kV. These images were then used for microstructural evaluation and calculating the grain size. The intercept method was performed in order to determine the grain size of the sintered samples.

$$G_{av} = \frac{L}{N * M} \quad (2.12)$$

Where; G_{av}: Average grain size; L: circumference of the circle; N: number of the intersections along the intersection line; M: magnification.

2.2.2.2. Mechanical Characterization

2.2.2.2.1. Vickers Micro-hardness

Vickers micro-hardness measurements (Type II) were performed by a HMV-2 Vickers micro hardness tester (Shimadzu Co., Kyoto, Japan). Samples were first embedded in epoxy molds (Struers, Denmark) for easy handling, then polished with SiC papers (Buehler Ltd., Lake Bluff, IL, USA) from 200 to 1200 grades before examination. Final polishing was applied with a 1 μm monocrystalline diamond suspension (Buehler Ltd., Lake Bluff, IL, USA). At least 10 measurements were done on each sample with a diamond indenter at 9.807 N load for 20 seconds. The average Vickers hardness was calculated using the formula below:

$$HV = \frac{F}{A} = \frac{0.001854\,P}{d^2} \qquad (2.13)$$

HV: Vickers hardness; P: Applied force (N); d: Average length of two diagonals (mm).

2.2.2.3. Cell Culture Studies

2.2.2.3.1. Cell Proliferation

For cell attachment and proliferation tests, Saos-2 cells were seeded on HT and doped HT discs sintered at 1100°C for 1 hr. The discs were sterilized at 200°C for 2 h prior to seeding. Saos-2 cells were grown in DMEM high glucose supplemented with 10 % fetal bovine serum (FBS) and 0.3 % penicillin-streptomycin. The initial cell seeding density was 2×10^4 cells/disc. The cells were incubated on HT discs for three different time periods: 1, 4 and 7 days in a carbon dioxide incubator (5215, Shel Lab., USA) at 37°C under 5% CO_2 humidified environment. The medium was refreshed every 3 days. Proliferation of the cells on the discs was analyzed by PrestoBlue™ viability assay at different incubation periods. On each of the designated time points, PrestoBlue™ viability reagent was added to wells containing cell seeded discs and then the well plates were incubated at 37ºC under 5% CO_2 environment for 6h. During incubation PrestoBlue™ reagent was reduced into intensely colored resazurin, as a

result of enzymatic activity of the viable cells. After 6h of incubation, the medium in each well was collected and their absorbance was read by μQuant™ spectrophotometer (Biotek Instruments Inc., USA) with an excitation wavelength of 570 nm and emission wavelength of 600 nm. The amount of metabolic reduction caused by cells was calculated as % reduction using the following formula provided by the manufacturer:

$$\text{Percent Reduction} = \frac{(02 \times A1) - (01 \times A2)}{(R1 \times N2) - (R2 \times N1)} \quad (2.14)$$

where O1 stands for molar extinction coefficient of oxidized PrestoBlue™ reagent at 570 nm, O2 stands for molar extinction coefficient of oxidized PrestoBlue™ reagent at 600 nm, R1 stands for molar extinction coefficient of reduced PrestoBlue™ reagent at 570 nm, R2 stands for molar extinction coefficient of reduced PrestoBlue™ reagent at 600 nm, A1 is the absorbance of test wells at 570 nm, A2 is the absorbance of test wells at 600 nm, N1 is the absorbance of media only wells at 570 nm and N_2 is the absorbance of test wells at 600 nm. After collection the medium, cells were washed with PBS once more and growth medium was added for further culturing of cells. All experiments were run in quadruplicate and cell adhesion was evaluated based on the mean number of adherent cells. Numerical data were analyzed using standard analysis of variance (one-way ANOVA) techniques and statistical significance was considered at $p<0.05$.

2.2.2.3.2. Morphology of Cells

In order to investigate the morphology of Saos-2 cells on composite discs SEM analysis was performed. Two samples of each composition were seeded with cell at a seeding density of 2×10^4 cells/disc. After 1 and 7 days of incubation, the medium was removed and cells were washed with PBS and then fixed with 3% gluteraldehyde in PBS for 15 minutes. Following fixation, cells were washed with PBS again and then dehydrated with graded ethanol-water solution series (30, 50, 80, 90 and 100%). Following dehydration in ethanol series the discs were immersed in

hexamethyldisilazane (HMDS) in order to achieve further dehydration and higher conductivity in SEM analysis and then dried in laminar flow. Prior to SEM analysis, discs were coated with gold-palladium via a precision etching coating system (PECS, Gatan 682, USA) at a thickness of 5 nm.

Chapter 3

RESULTS AND DISCUSSION

3.1. Structural Analysis

3.1.1. Density of the Samples

Average densities of the materials and their relative densities compared to theoretical density, sintered at 1100°C for 1h are presented in Table 3.1.

Table 3.1. Density of HT and doped HT samples.

Sample	Theoretical Density (g/cm^3)	Sintered Density (g/cm^3)	Relative Density (%)
HT	3.117	2.95	94.9
HT0.5Sr1F	3.121	2.93	94.7
HT1Sr1F	3.119	2.92	93.8
HT2Sr1F	3.128	3.02	96.6
HT5Sr1F	3.106	3.00	96.2

Although all the densities of doped samples were close to that of undoped HT, increasing the amount of Sr^{2+} ions, first led to decrease in density of the samples doped with Sr^{2+} and F^{-} ions after the sintering a small decrease was observed step by step in two of the doped ones, however by adding more Sr^{2+} ions, the density increased for samples of HT5Sr1F, and HT2Sr1F, which had the highest density of doped ones, after sintering.

In an investigation, a series of Sr-substituted HAs was studied. Lattice parameters (a, and c) increased linearly with Sr^{2+} addition. As a result of this, the unit cell volume also increased linearly. Density also increases linearly with Sr-addition due to the replacement of a heavier ion for Ca in the crystal structure (O'Donnell et al., 2008). It has been indicated that strontium addition to HA broadens the crystal size distribution, which contributes to the improved mechanical strength of bone (Li et al., 2007b).

In addition, based on the previous studies, addition of F^- ion led to a decrease in the density of samples, and it stays the same due to its fixed amount (Curran et al., 2011). It was reported that doping of HA with F^- ion causes a decrease in density of products due to reduction of decomposition rate of the synthesized materials by formation of FHA (fluorapatite) which shows high thermal and chemical stability at sintering temperatures (Gross & Rodríguez-Lorenzo, 2004a).

Furthermore, Grynpas et al. had an investigation on bone volume of rats by supplying low doses of strontium and fluoride. Thus, as a result, strontium and fluoride have been shown to have beneficial effects on bone formation and trabecular bone density. However, the effects of these elements on bone mass appear to depend on the doses used (Grynpas et al., 1996).

3.1.2. X-Ray Diffraction Analysis

XRD patterns of each sintered samples are shown in Figure 3.1.

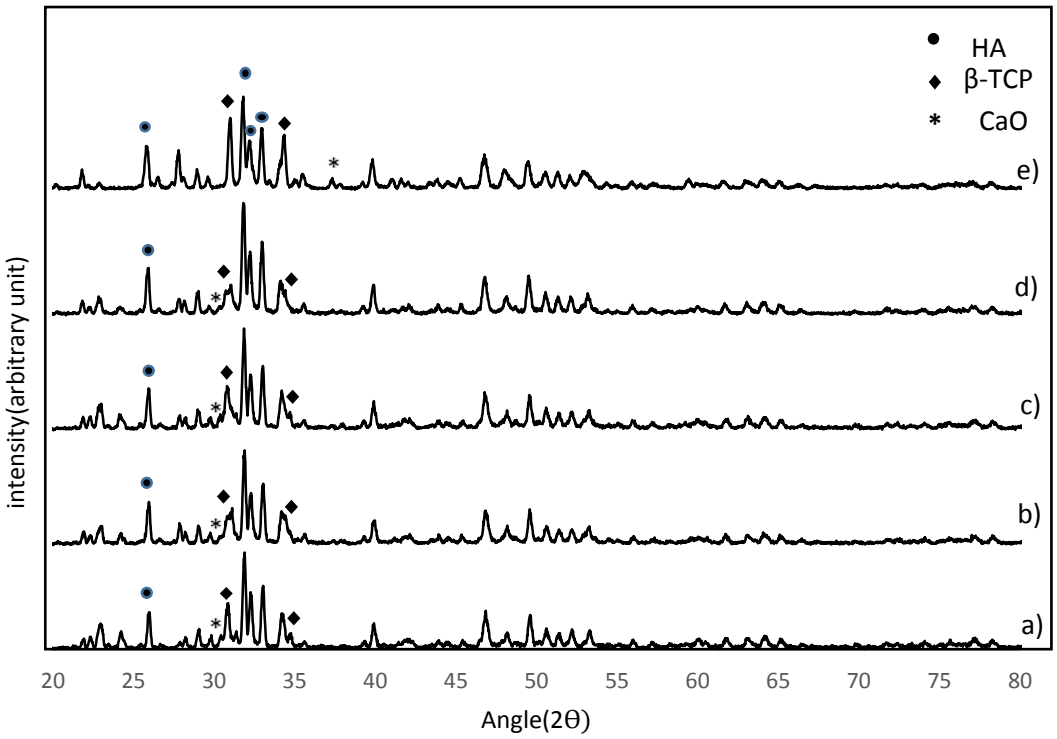

Figure 3.1. XRD analysis for the samples synthesized at a pH of 12; a) HT; b) HT0.5Sr1F; c) HT1Sr1F; d) HT2Sr1F; e) HT5Sr1F.

XRD patterns of all the samples were found to match with (JCPDS file # 9-432) for HA, (JCPDS #9-0169) for β-TCP, and (JCPDS#28-0775) for CaO. Most of the peaks of HT, are the same and comparable with the standard one. There is also β-TCP and CaO phases in HT, and according to previous studies, it was reported that β-TCP phase was observed in HT sintered at 1100°C (Metsger et al., 1999). Moreover, according to the matching of β-TCP peaks with the JCPDS file, it is observed that (0 2 10) peak, is belong to β-TCP.

In another study investigated by Curran et al. (2011), XRD results for the samples showed a higher level of decomposition of HA in the 5% Sr–HA samples by the emergence of the TCP peak at 2θ = 27°. Peak broadening also occurs in the

samples. The results illustrated TCP peaks with higher intensities relative to the main HA peaks (Curran et al., 2011).

However, the level of stabilization would be highly dependent on the crystal structure of the HA phase and the available sites for Sr^{2+} incorporation. In the undoped HA the dominant second phase is α-TCP (~30%), which decreases to virtually 0% with Sr^{2+} substitution and is replaced by β-TCP which becomes the major phase at 10% Sr^{2+} substitution for Ca. Hence β-TCP stabilization, which is known to occur with Sr^{2+} incorporation (Leroux & Lacout, 2001; Renaudin et al., 2009), may be occurring in the samples, thereby reducing α-TCP formation with increasing amounts of Sr^{2+} (Curran et al., 2011). Thus, in this investigation, the dominant second phase of the undoped HT, is β-TCP (~45%), which tends to be the major phase at 5% Sr^{2+} substation.

Figure 3.1 shows peaks attributed to HA as the main phase and β-TCP and CaO as the secondary phase. This confirmed that at this temperature, the synthesized powder tends to form BCP as it contains both phases.

The intensity of β-TCP peak first decreased gradually as concentration of Sr^{2+} increased. But at HT5Sr1F, it suddenly increased. This originates from lattice concentration due to the large radii atom (Sr) substitution for the small radii atom (Ca) (ionic radii: Sr^{2+} = 1.13 Å, Ca^{2+} = 0.99 Å) (Saint-Jean et al., 2005). Mardziah et al. reported that HA contains larger cation site compared to β-TCP (Mardziah et al., 2009). Thus, it is more suitable for larger Sr^{2+} to substitute Ca^{2+} in the HA rather than in β-TCP. Due to the incorporation of Sr^{2+} into the HA, the diffraction peaks of the strongest HA planes shifted to smaller angles of 2 theta, compared to undoped powder (Mardziah et al., 2009).

Incorporation of Sr^{2+} and F^{-} ions also caused some fluctuations in XRD patterns of the samples like little shifts from the pattern of HT towards lower diffraction angels. For example, when the HT and doped samples are compared, it was more evident in the most intense peak which shifted from the 2θ value of 31.90° in HT, to 2θ= 31.86° in HT1Sr1F and 2θ= 31.82° in HT2Sr1F, and HT5Sr1F (Figure 3.2). These small shifts might be due to the incorporation of doping ions into the unit cell structure of HT, which was attributed to the replacement of Ca^{2+} ions (0.99 Å) with larger sized Sr^{2+}

ions (1.13 Å). Furthermore, this shift became clearer as the amount of Sr^{2+} ions increased. This growth inside the doped HT structure led to a broadening in peaks, which states reduction in crystallite size (Alshemary et al., 2015).

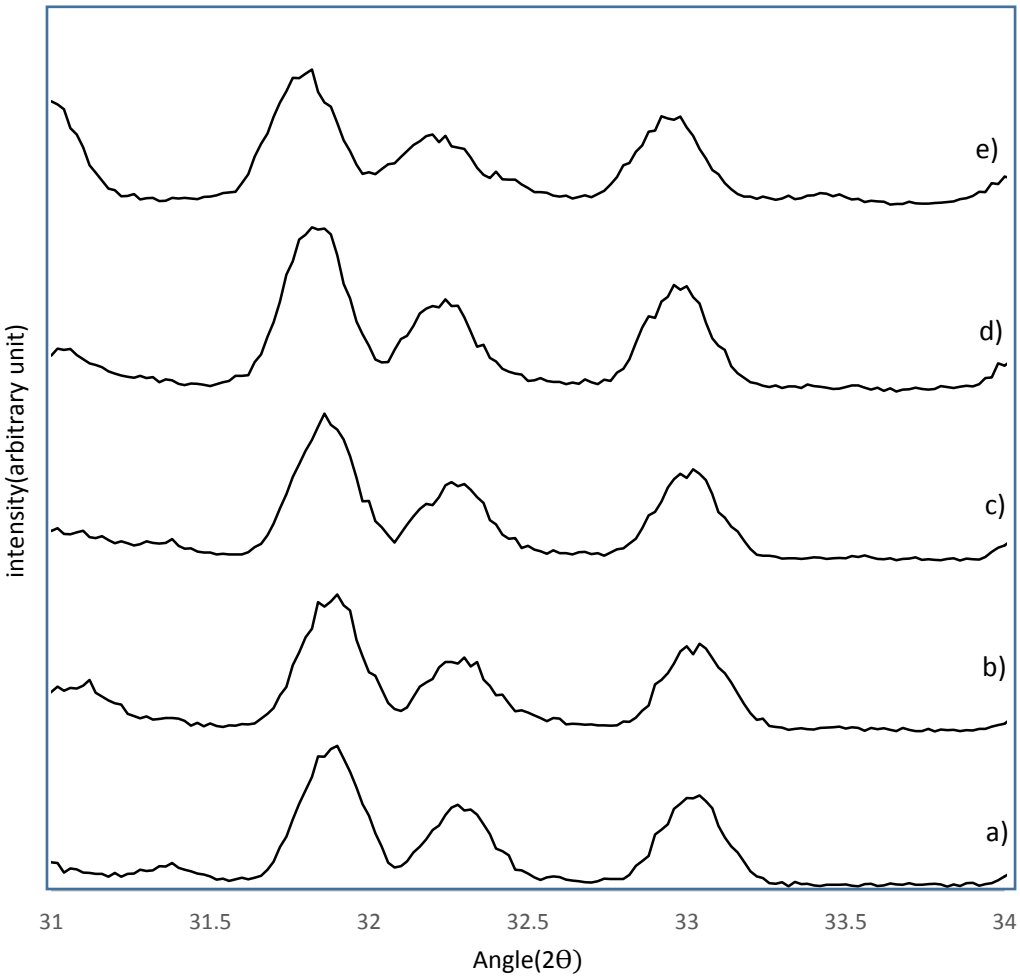

Figure 3.2. XRD patterns of; a) HT; b) HT0.5Sr1F; c) HT1Sr1F; d) HT2Sr1F; e) HT5Sr1F, sintered at 1100°C between the 2Θ ranges 31-34.

It has also been observed that the intensity of the peaks change with Sr^{2+} and F^{-} ion doping. For instance, the intensity of the most intense peak reached to 934 for HT while this value reached to 1081 for HT2Sr1F. This might indicate an improvement in the crystallinity of the samples, which was expected since F^{-} ion incorporation results in an increase in crystallinity (Legeros et al., 2003). Among the doped samples,

HT2Sr1F exhibited relatively higher intensity compared to the others, indicating that HT2Sr 1F had the highest crystallinity. It was also observed that the instability of HA as well as intensity of β-TCP increased steadily as the amount of Sr^{2+} doped increased.

3.1.2.1. Lattice Parameters of HT and doped HT samples

In Table 3.2, lattice parameters of HT and doped HT samples, volumes of the samples, degree of crystallinity, and the percentage of phases are presented.

Table 3.2. Hexagonal lattice parameters, unit cell volumes, degree of crystallinity, and the percentage of phases for HT and doped HT samples.

Sample ID	a (Å)	c (Å)	V (Å^3)	χ_c (%)	Phase %	
					β-TCP	HA
HT	9.3564	6.8594	1554.7	92	44.98	55.02
HT0.5Sr1F	9.3567	6.8597	1554.8	90	40.91	59.08
HT1Sr1F	9.3826	6.8413	1559.3	91	42.18	57.81
HT2Sr1F	9.3985	6.8641	1569.8	92	32.19	67.80
HT5Sr1F	9.4072	6.9054	1582.1	89	57.60	42.39

It was observed that Sr^{2+} ion substitution resulted in an increase in lattice parameters in both a, and c directions and the unit cell volume. It was also observed that by adding more Sr^{2+}, the intensity of peaks and consequently degree of crystallinity changed. For example, for HT2Sr1F which had the highest intensity, an increase in degree of crystallinity was observed. This result can be explained by the differences in the ionic radii of Ca^{2+} ion (0.99 Å) and Sr^{2+} ion (1.13 Å), which substitutes for Ca^{2+} (Webster et al., 2004). Since Sr^{2+} ion is larger than Ca^{2+} ion, an increase in lattice

parameters and unit cell volume due to Sr^{2+} doping is reasonable. This result is in agreement with previous studies (Mardziah et al., 2009; Webster et al., 2004).

It was reported that substitution of other cations with smaller radii than Ca^{2+} ion such as Cd^{2+}, Mg^{2+}, $Zn^{2+,}$ In^{3+} resulted in a reduction in lattice parameters while addition of cations with larger ionic radii such as Bi^{3+}, La^{3+} led to an increase in lattice parameters due to the differences in their ionic radii (Legeros et al., 2003; Mardziah et al., 2009; Webster et al., 2004).

When ions with higher ionic radii differences are substituted into HA, changes can be observed in the crystallinity or structure of HA in addition to lattice parameters (Li et al., 2007b). In this study, the structural incorporation of Sr^{2+} ion for Ca^{2+} was found to cause increase in the lattice parameters and also expansion in the structural size of HA due to the larger ionic radius of Sr^{2+} (1.13 Å) compared to that of Ca^{2+} ion (Li et al., 2007b). Therefore, due to their larger radius, Sr^{2+} ions substitute for Ca (II) site, causing a distortion in the crystal structure of the material (Li et al., 2007b). These results show that there is a high correlation between ionic radii and lattice parameters for ion substitutions.

While, studies showed that incorporation of F^{-} into HA resulted in a slight shift of XRD peaks to the higher 2θ value, indicating the decrease in lattice parameters due to the successful substitution of smaller sized F^{-} ion, compared to OH^{-} (Cheng et al., 2005; Wei et al., 2003). Furthermore, a very slight increase in the degree of crystallinity was also observed upon F^{-} substitution (Rameshbabu et al., 2006). The percentage of phases values for the HA and β-TCP are also presented in Table 3.2. HA phase exhibited as the main phase of HT beside β-TCP as the second phase. With an incorporation of Sr^{2+} and F^{-} ions led to decomposed HA phase into β-TCP and little amount of CaO phases. Furthermore, percentage of β-TCP phase increased gradually with increasing of Sr^{2+} amount into HT lattice.

3.1.3. FTIR Analysis

Functional groups of entire materials were investigated using FTIR technique and the obtained spectra are illustrated in Figure 3.3. The characteristic peaks of HA and β-TCP were observed for all samples.

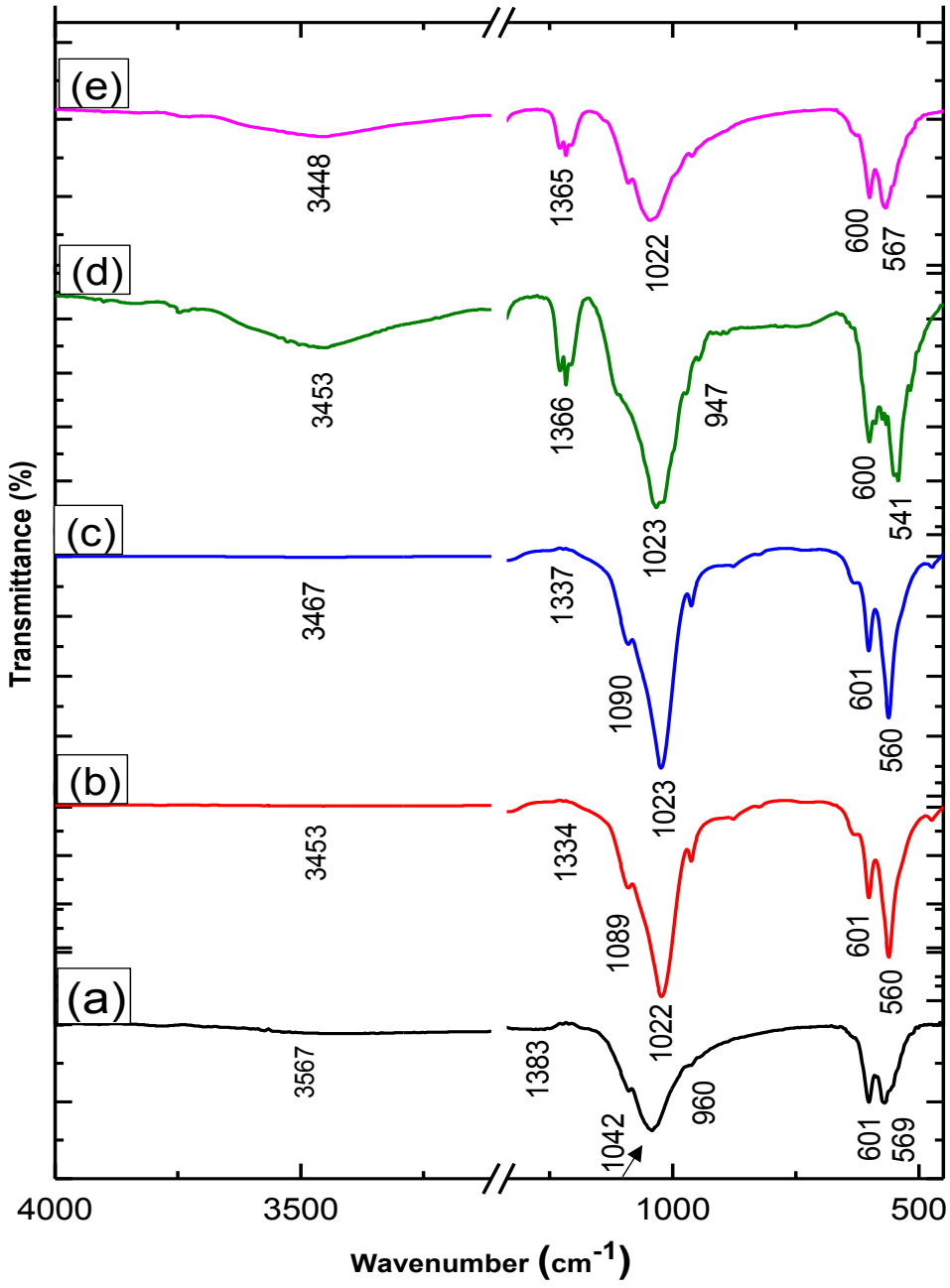

Figure 3.3. FTIR spectra of the samples synthesized at a pH of 12; a) HT; b) HT0.5Sr1F; c) HT1Sr1F; d) HT2Sr1F; e) HT5Sr1F

In all samples, the characteristic peaks of the vibrations of PO_4^{3-} groups were observed (Figure 3.3). The alterations observed in the spectra due to the incorporation of doping elements are discussed below.

The band at 462 cm^{-1} was assigned to the bending mode (υ_2) of PO_4^{3-} group, the vibration at 569 cm^{-1} and 601 cm^{-1} were attributed to the bending mode (υ_4) of PO_4^{3-} group. The band at 960 cm^{-1} was assigned to the stretching mode (υ_1) of PO_4^{3-} group. Moreover, stretching mode (υ_3) of PO_4^{3-} group was observed at 1042 cm^{-1}. OH^- bending and stretching modes were also observed at 632 cm^{-1} and 3571 cm^{-1}, respectively. Incorporation of F^- and Sr^{2+} into HT structure, caused a shifting of OH^- vibration peak from 632 cm^{-1} to 626 cm^{-1} (Table 3.3), due to the OH-F interaction (Alshemary et al., 2015). The spectra of OH^- group (stretching mode) showed shift towards high value of wavenumber from 3567 cm^{-1} for HT to 3571 cm^{-1} for HT5Sr1F, suggesting that high temperature accelerates decomposition rate of OH group for HT, same observations were highlighted by Bahrololoom et al. (2009).

Table 3.3. Frequencies (in cm^{-1}) and assignments of bands in FTIR spectra of HT and doped samples.

Functional Groups	**Vibration Mode**	**Wavenumber (cm^{-1}) HT**	**Wavenumber (cm^{-1}) Doped HT**	**Characteristic peaks of HA/β-TCP**
OH^-	(stretching)	3567	3569-3571	HA
OH^-	(bending)	632	626	HA
H_2O	(stretching)	3450	3448-3467	HA
PO_4^{3-}	υ_4	569,601	515-600	HA/β-TCP
PO_4^{3-}	υ_3	1042,1091	1033-1228	HA/β-TCP
PO_4^{3-}	υ_2	462-474	423-437	HA/β-TCP
PO_4^{3-}	υ_1	960	901-961	HA
PO_4^{3-}	υ_1	960	945-972	β-TCP
CO_3^{2-}	-	1383	1365-1435	HA

Furthermore, other peaks observed at 870 and 1383 cm^{-1} were due to the B-type substitution of the carbonate group CO_3^{2-} (Xu et al., 2001). While, the peak located at 1435 cm^{-1} was assigned to A-type CO_3^{2-} substitution of the carbonate group (Xu et al., 2001). In addition, incorporation of Sr^{2+} ions resulted in decreasing the intensity and sharpness of the bands, hence confirming that the crystallinity of HA decreased upon Sr^{2+} doping (Table 3.2). The intensity of OH^- band gradually decreased as the doping of Sr^{2+} ions increased inside the HT lattice due to the partial replacement of OH^- by CO_3^{2-} (A type) of HT lattice (Gibson & Bonfield, 2002).

It is evidently seen, as the amount of Sr^{2+} ion substitution was increased, the curve in the OH^- stretching band (~3450 cm^{-1}) became clearer. In the spectra of Sr^{2+} and F^- ions doped samples, a curvature was observed around 3448-3467 cm^{-1} bands which indicated the presence of doped ions in the structure of HT. These findings prove the substitution of F^- for OH^- ions (Wei et al., 2003).

Based on previous studies it was observed that the most prominent bands in the FTIR spectrum of β-TCP are present at 945 and 972 cm^{-1}. These bands arise due to the factor group splitting of the υ_1 fundamental vibrational mode corresponding to the symmetric P-O stretching vibration of the phosphate ion (938 cm^{-1}) (Jillavenkatesa & Condrate, 1998).

3.1.4. SEM Analysis

Figures 3.4 represents the SEM pictures of HT and doped HTs. As seen in Figure 3.4, ion incorporation in HT structure resulted in changes in grain size and shape. Compared to the microstructure of HT, different grain sizes were observed in the microstructure of the doped samples. For more precise results, these observations were verified by the grain size measurements. It was proved that there was a relationship between the amount of dopant and grain sizes of apatites (Basar et al., 2010). HA sintered at low temperatures had more uniform microstructures, however, its grain sizes exhibited severe increase with increase in the sintering time (Basar et al., 2010). They proved that HA had a nano size grain structure after sintering at 900°C and 1100°C, while there was severe grain growth after sintering at 1300°C (Basar et al., 2010).

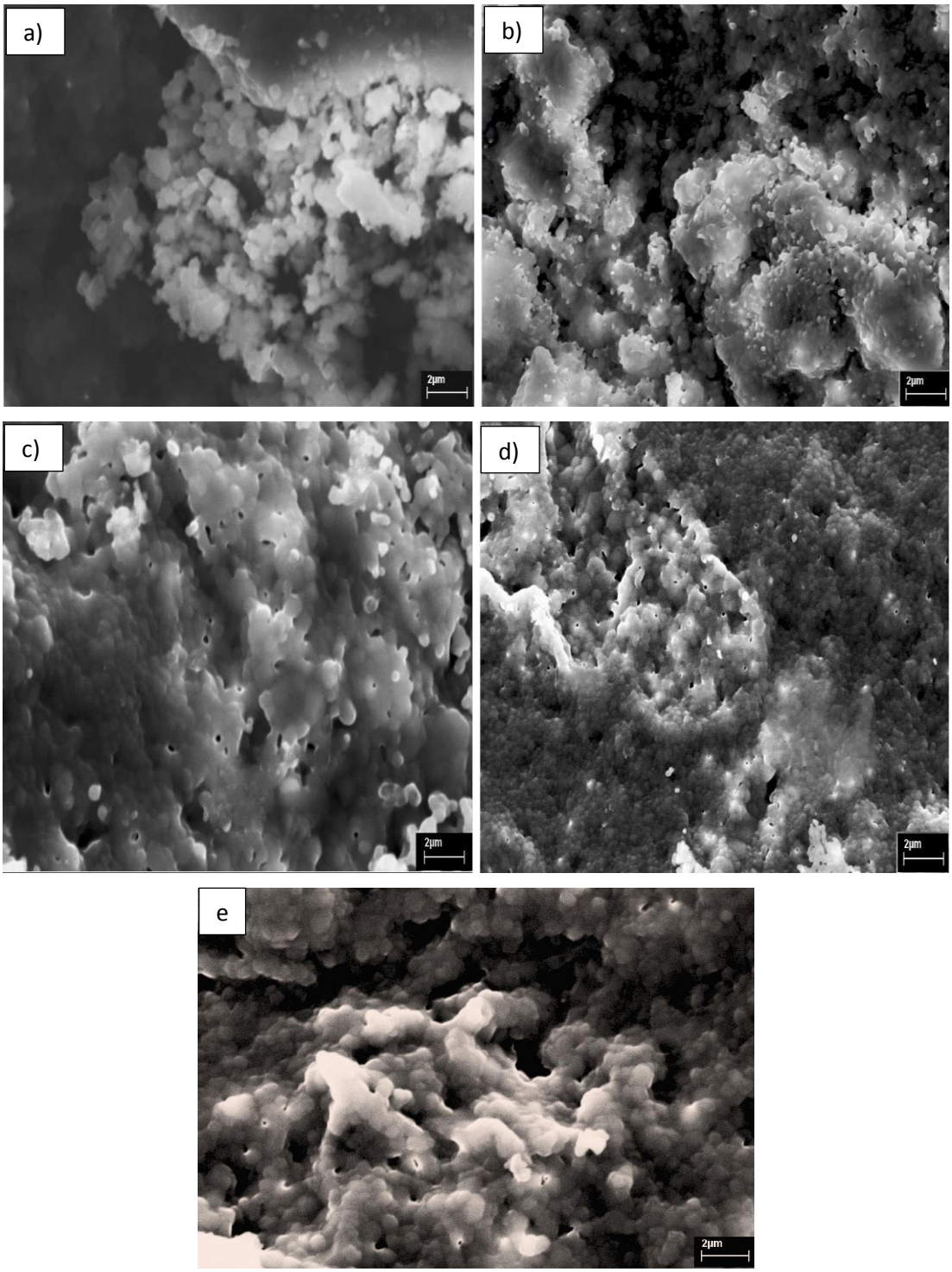

Figure 3.4. SEM images for the samples synthesized at a pH of 12 (Mag: 5000×; scale bar: 2 µm): a) HT; b) HT0.5Sr1F; c) HT1Sr1F; d) HT2Sr1F; e) HT5Sr1F.

Grain sizes of HT and doped samples are given in Table 3.4. As seen in Table 3.4, all of the doped samples exhibited smaller grain sizes compared to HT. The bond that forms between F^- and OH^- ions, which lowers densification rate, also decelerates the grain growth thus resulting in smaller grains (Gross & Rodríguez-Lorenzo, 2004a) . In addition, the results of a study showed that with incorporation of fluoride into HA structure, crystallites size markedly decreased. It is meaningful to the fluoride which significantly prevented growth of grains in HA structure (Eslami et al., 2009). The addition of Sr^{2+} ion resulted in a decrease in grain size, which was in agreement with a previous study (Terra et al., 2009). Moreover, in another study by Curran et al., grain growth occurred in the undoped HA to a size of 3.2 μm, while no further grain growth was seen with the substitution of Sr^{2+} (Curran et al., 2011).

In the first doped sample (HT0.5Sr1F) there is a drop in grain size, The average grain size of all the doped samples are smaller than the undoped one and the smallest is for the last one HT5Sr1F, with a dramatic reduction in the amount of grain size.

Table 3.4. Average grain size values of HT and doped HT.

Sample ID	**Average Grain Size (nm)**
HT	1052
HT0.5Sr1F	689
HT1Sr1F	975
HT2Sr1F	1000
HT5Sr1F	597

3.2. Mechanical Analysis

In terms of mechanical analysis, Vickers micro-hardness test was applied to the samples.

3.2.1. Vickers Micro-hardness

In order to compare the mechanical properties of HT and doped HT, micro-hardness values of the samples were determined. In Table 3.5, average micro-hardness of each sample is given.

Table 3.5. Average micro-hardness and standard deviation of HT and doped HT, (n= 10)

Sample	Micro-Hardness (GPa)
HT	1.36±0.39
HT0.5Sr1F	1.62±0.44
HT1Sr1F	1.83±0.46
HT2Sr1F	2.83±0.51
HT5Sr1F	3.79±0.35

As seen in Table 3.5, micro-hardness values of most of the doped samples were close to micro-hardness of HT. The highest increase in micro-hardness among the doped materials was seen in HT5Sr1F. So, results showed an increase in values of micro-hardness in comparison with HT. Thus, an improvement in the mechanical properties happened, as the amount of strontium was increased.

This result was similar to the findings of the study investigated by Curran et al., which showed that Sr^{2+} incorporation improved mechanical properties only in certain values. After increasing the Sr^{2+} amount, a decrease in mechanical properties was

observed, and after that by increasing the strontium amount, the mechanical properties improved as well (Curran et al., 2011).

The variations in the microhardness values of the samples depending on the changes in Sr^{2+} ion content, exhibited a similar pattern with the variations in the densities of the samples. Among the strontium doped samples, highest density and highest microhardness values were seen in HT5Sr1F.

There are some other studies, in which HA was doped with other ions such as yttrium, magnesium, zinc, and fluoride. According to the results of a study about HA doped with Zn^{2+} and F^{-}, Zn^{2+} addition decreased the microhardness of HA, slightly. Based on a study investigated by Kim et al., F^{-} addition into HA also increased the microhardness of HA. However, its standard deviation was the highest. Therefore, it can be said that by F^{-} addition, microhardness values increase. This is due to the fact that F^{-} decreased the porosity of the samples which resulted in more compact and hard structure (Kim et al., 2003). Moreover, the high affinity between F^{-} and H^{+} ions played an important role in formation of this compact structure (Edwards & Ramulu, 2009).

Results of another study of HA doped with Mg^{2+} and F^{-} demonstrated that the highest microhardness value was obtained for HA1Mg2.5F. Increasing the Mg^{2+} content from 1 to 7.5%, resulted in lower microhardness values. Moreover, increasing the F^{-} amount improved the microhardness values for the 2.5% Mg^{2+} -doped HA (Sun et al., 2010).

Moreover, in another study of HA doped with a fixed amount of yttrium and variable amounts of F^{-}, the microhardness values of the samples were found to increase upon addition of F^{-} ions up to a certain extent, however further increase in F^{-} ion incorporation led to a decrease in microhardness of the samples. Eslami et al. also agree that the partial replacement of OH^{-} ions by F^{-} ions leads to improvements in mechanical properties and states that during the partial replacement of OH^{-} ions by F^{-} ions, hydrogen ions from the former OH^{-} ions bound to high affinity F^{-} ions instead of O^{2-} ions, producing a good ordered apatite structure with better mechanical properties (Eslami et al., 2010).

3.4 Biological Characterizations

3.4.1 PrestoBlue™ Assay

Viability of Saos-2 cells on HT and different composites pellets sintered at 1100ºC for 1h was investigated via PrestoBlue™ viability assay. HA is well known cytocompatible material. It has been shown that it did not have toxic effect on hFOB cell line (Zhang et al., 2015), furthermore, it was reported that it promotes cell proliferation as well as it does not induce any genetic problems (Bose et al., 2010; Lee et al., 2013). For this reason, cell viability on HT discs was taken as 100% and used as control to analyze the effect of dopants on biological properties of HT.

It was observed that cells seeded on the discs showed perfect attachment on the first day. This finding was also supported both by SEM images (Figures 3.6-3.9) and literature (Romieu et al., 2010). Highest cell attachment was observed on HT0.5Sr1F, while the lowest cell attachment was observed on HT sample. No statistical difference was observed between HT and doped discs on day 1, except for HT5Sr1F. The reason for the high rate of cell attachment on most of the samples lies within the microstructure of the discs. The disc samples were porous and had lower grain size. As seen in Figure 3.5, HT5Sr1F was statistically different from HT in day 1, as well as HT0.5Sr1F of day 7 with the HT sample of that day.

After 4 days of incubation, a considerable decrease in cell number was observed for all samples, which could be due to the confluency on day 4. It was observed that incorporation of Sr^{2+} and F^{-} ions have positive effects on the biocompatibility of HT (Figure 3.6). Moreover, F^{-} ion incorporation was found to improve cell proliferation on HT with longer incubation periods. On day 4, F^{-} ion doped samples exhibited slightly lower percent reduction values compared to those of HT. This finding is in agreement with the former studies which reported that OH groups provided binding sites for cell attachment and when F^{-} ions replace OH groups, a decrement was observed in the cell attachment and proliferation rates of HA in the first place (Eslami et al., 2009; Qu & Wei, 2006b). However, it was reported that cell attachment and proliferation on HA increased with incubation due to release of more F^{-} ions into the cell culture medium, (Kim et al., 2005; Qu & Wei, 2006b). This

explains the significantly higher cell proliferation observed on F^- ion doped samples on day 7 compared to HT.

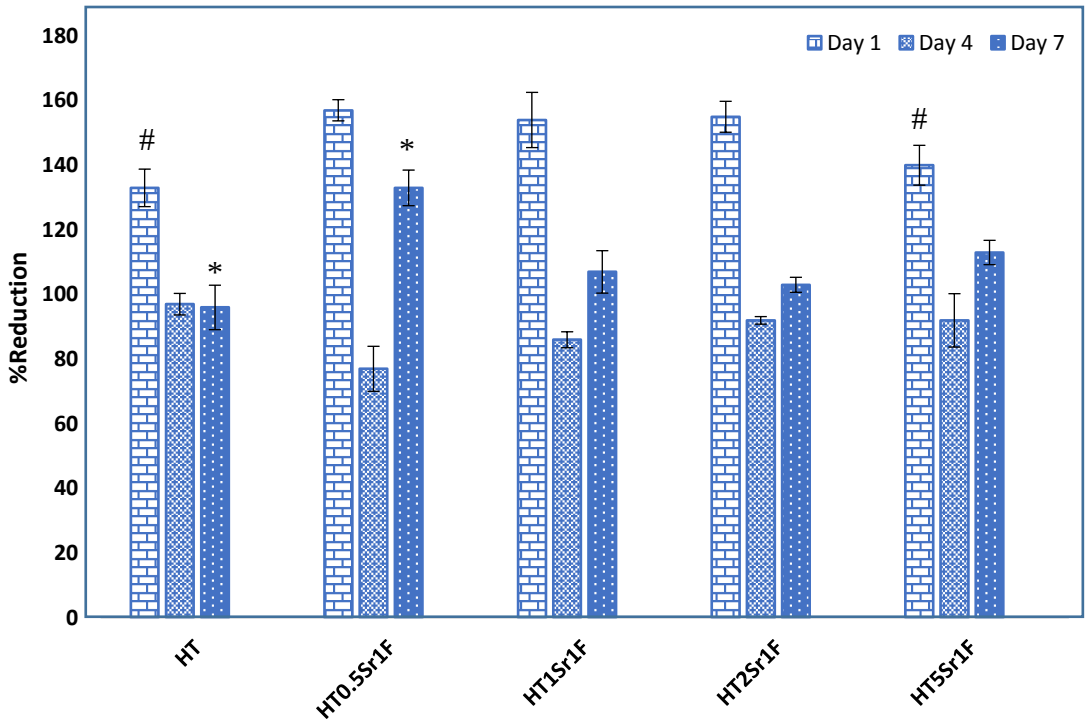

Figure 3.5. Cell proliferation on HT and doped HT discs sintered at 1100°C. (Statistically significant differences between the groups: #, *, $p \leq 0.05$)

Sr^{2+} incorporation was also found to have a positive effect on cell proliferation especially at 7 days of incubation (Figure 3.5) in accordance with the previous results (O'Donnell et al., 2008; Pors Nielsen, 2004). As reported previously, the highest degree of proliferation was observed on HT0.5Sr1F after 7 days of incubation. It was seen that co-substitution of Sr^{2+} and F^- ions resulted in higher cell proliferation. The smaller grain sizes obtained with doping (Table 3.4) might be another contributing factor to enhance cell proliferation since HA with smaller grains sizes was reported to result in improved cell attachment and proliferation (Shi et al., 2009; Webster et al., 1999). Apart from these, other works also suggested that addition of Sr^{2+} significantly improved the biocompatibility of the material (Terra et al., 2009).

In this study, in agreement with previous works, it was observed that HA containing from 0.5 to 5 mol. (%) of Sr^{2+} was successfully produced and presented no cytotoxicity. For example, in an investigation by Wen et al., (2002) In vitro studies of Sr-HA containing 0, 1, 5, 10 and 100 mol. (%) Sr^{2+} presented good biocompatibility in low percentages of Sr^{2+}, while the cytotoxicity increased with increasing concentration of the strontium. Similarly, another study also confirmed that Sr^{2+} was not cytotoxic, however, some adverse responses were observed which was due to presence of Sr^{2+} more than 5 mol.(%) (Tavares et al., 2011).

3.4.2 Scanning Electron Microscopy

SEM images of the cells cultured on HT and doped HT discs for 1 and 7 days are presented in Figures 3.6-3.9. It was observed that after 1 day of seeding, cells attached and they even started to spread on the surfaces of all discs. Complete coverage indicated that surface properties were ideal for cell attachment and spreading. At lower magnifications, the cells were observed more in the center of HT discs after 1 day of incubation. The cells were near confluency at the center. This was due to seeding of the cells in a sample volume at the center of the discs (35µl). The number of attached cells was relatively lower on HT compared to the doped samples. However, better cell attachment was observed on doped HT discs with Sr^{2+} ion. Higher cell attachment was observed as the Sr^{2+} ion content in HT was increased.

After 7 days of incubation, the cells were observed to be spread on all disc surfaces. Cells were also observed at the edge of the discs (data not shown), which showed that HT and doped HT discs provided a favorable environment for cell proliferation. This finding was in agreement with cell proliferation results (Figure 3.5). Cell layer formed on the samples exhibited a more compact structure on day 7 compared to day 1. The cells proliferated forming a thick layer, such that material surface could not be observed in most areas (Figure 3.9). HT2Sr1F and HT5Sr1F especially exhibited very intense layers of cells on day 7, which showed that these doping compositions were relatively more favorable for cell morphology, as well as cell proliferation results.

It was reported that pores and tiny cracks make specific surface area larger and easier to bond with surrounding tissue in vivo, thus providing brackets and passages for the growth of the new bone tissue, hence the better biocompatibility (Brook et al., 2012).

In another study, it was reported that cell division and proliferation are known to be a coordinated process ruled by cell-cell signaling. Once the cell-layer on a substrate becomes confluent, the cell signaling for the proliferation gets restricted, causing cellular division and proliferation to stop. Also in some SEM images, filopodia of cells were broken which was reported to be a result of drying out during the fixation process, or is a sign of a necrotic cell (Capuccini et al., 2008).

In this study, it was observed that HT5Sr1F disc samples (Figures 3.7 and 3.9), had the highest surface coverage with cells, both at days 1 and 7. The fact that cells covered the entire surface of discs from day 1 could be due to high initial cell seeding density. Due to confluency on most of the samples the structure of the surface was not visible. In Figure 3.8 it was observed that samples had a thin layer of cell sheet spread all over, which was distinguishable as an opaque layer covering small grains. After 7 days of incubation, both cuboidal and dendritic shaped cell clusters were observed in scattered patterns over the disc surface. This was due to lack of attachable surface for proliferated cells (Figure 3.7-c, 3.7-d, and 3.7-e), which in turn caused viability of cells to reduce with culture time (Figure 3.5).

Cell sheet coverage was observed at the end of day 7 at the periphery of discs and also inside the cracks and grooves of the surface. Also, it was observed that at the end of day 7 thick layers of cell sheets have covered the surface of the discs which resulted in reduced viability readings since the cell layers underneath others did not have access to culture medium (Figures 3.8, and 3.9), which was in agreement with cell viability results. It was observed that samples HT5Sr1F (Figures 3.7-c, 3.7-d, and 3.7- e) had the highest value of cell viability at the end of day 1 among the other samples. As for samples of day 7, again it was observed that HT5Sr1F (Figures 3.9-c, and 3.9-d) had the best result of morphology among all groups.

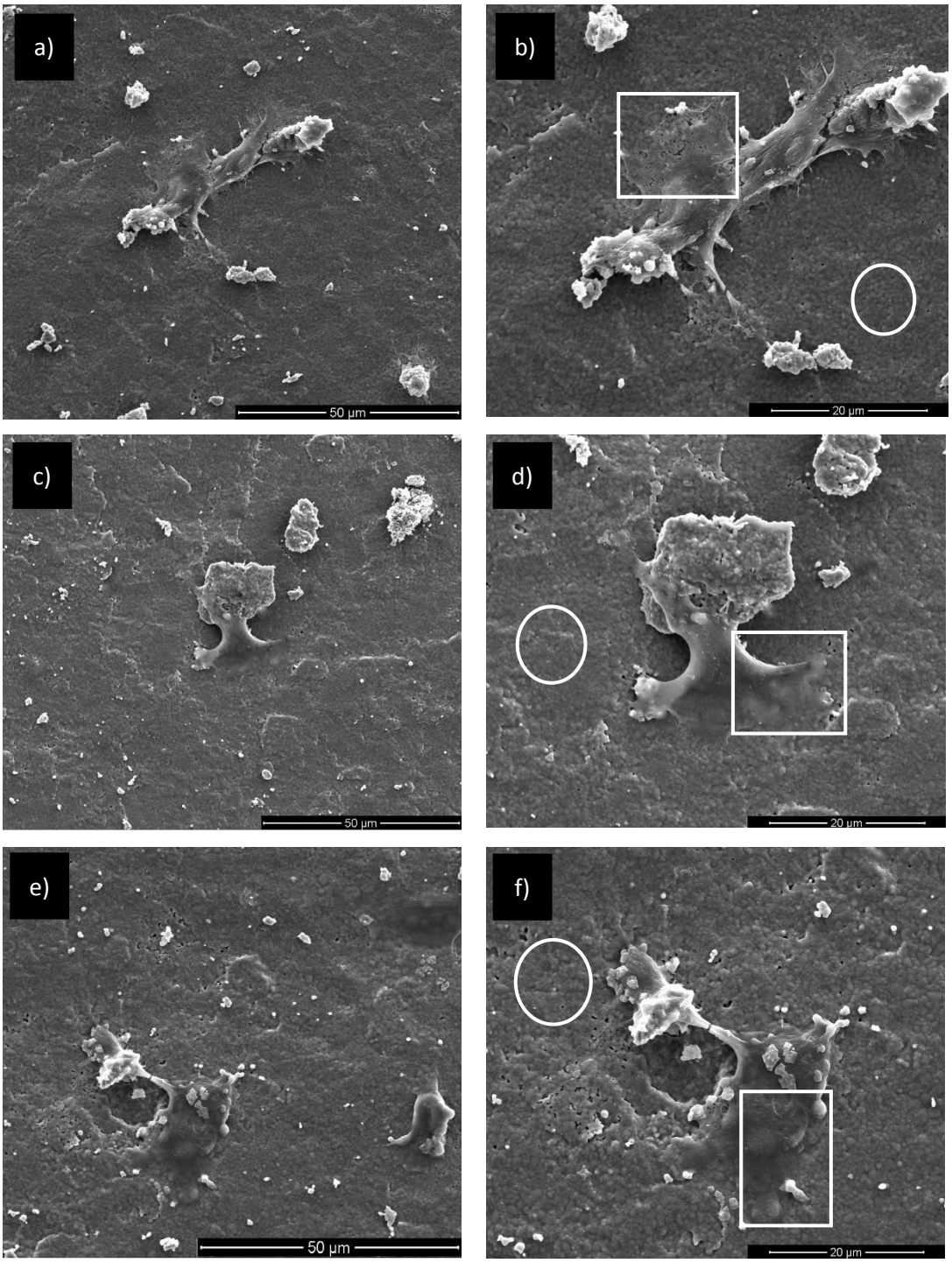

Figure 3.6. SEM images of cells on a and b) HT; c and d) HT0.5Sr1F; e and f) HT1Sr1F discs (day 1).

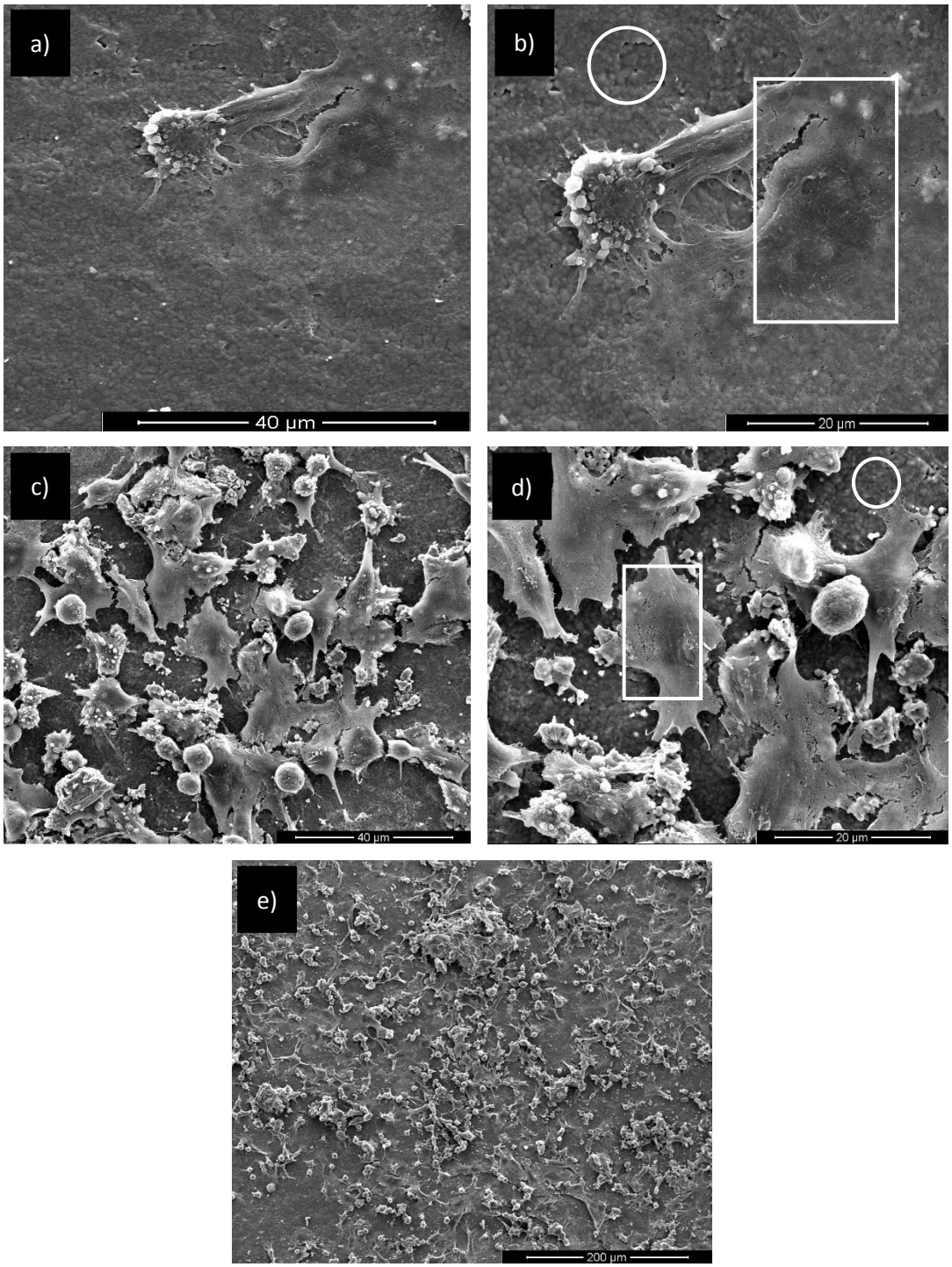

Figure 3.7. SEM images of cells on: a and b) HT2Sr1F; c, d and e) HT5Sr1F discs (day 1). (Rectangles represent cell sheet and circles represent material surface.)

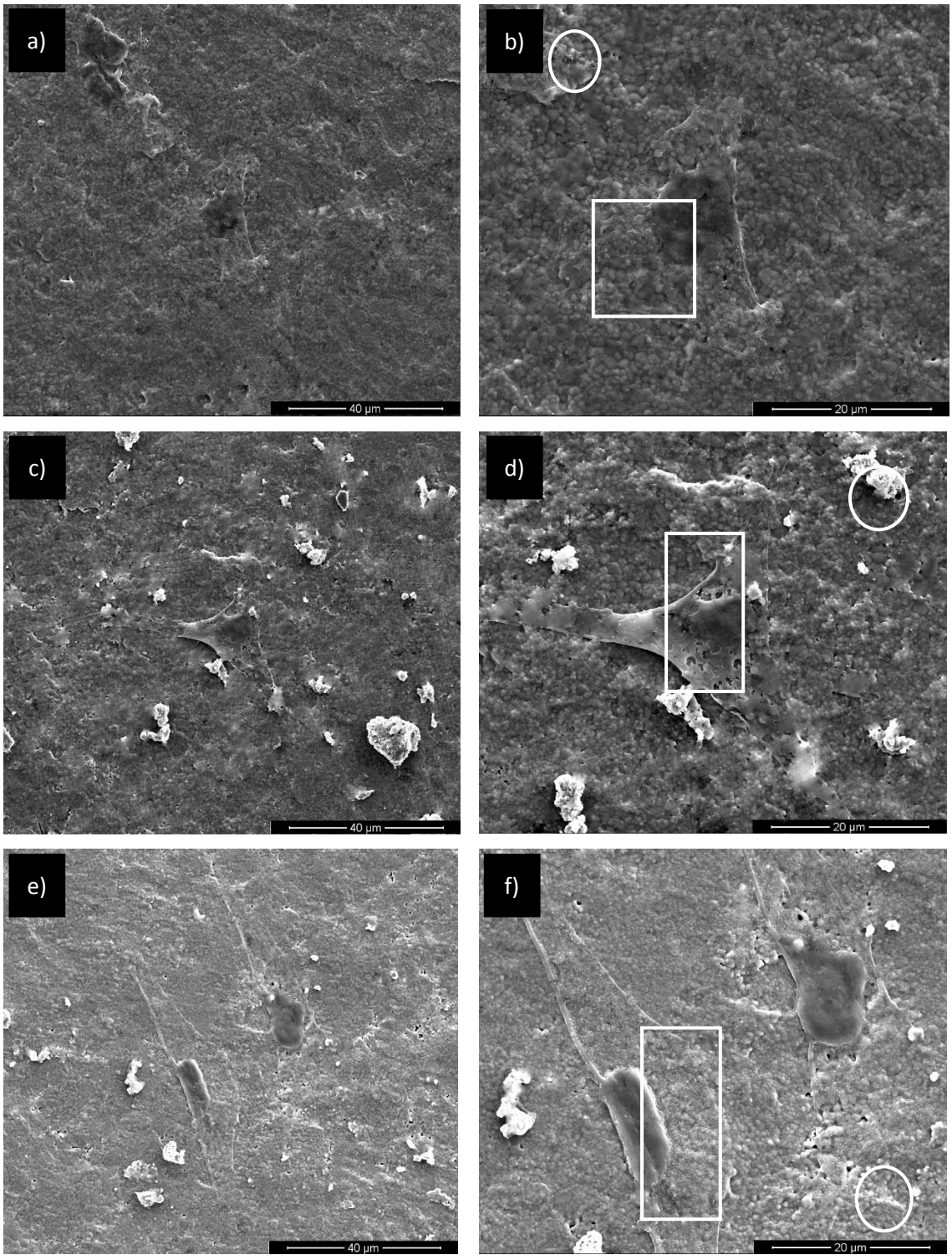

Figure 3.8. SEM images of cells on a and b) HT; c and d) HT0.5Sr1F; e and f) HT1Sr1F discs (day 7). (Rectangles represent cell sheet and circles represent material surface.)

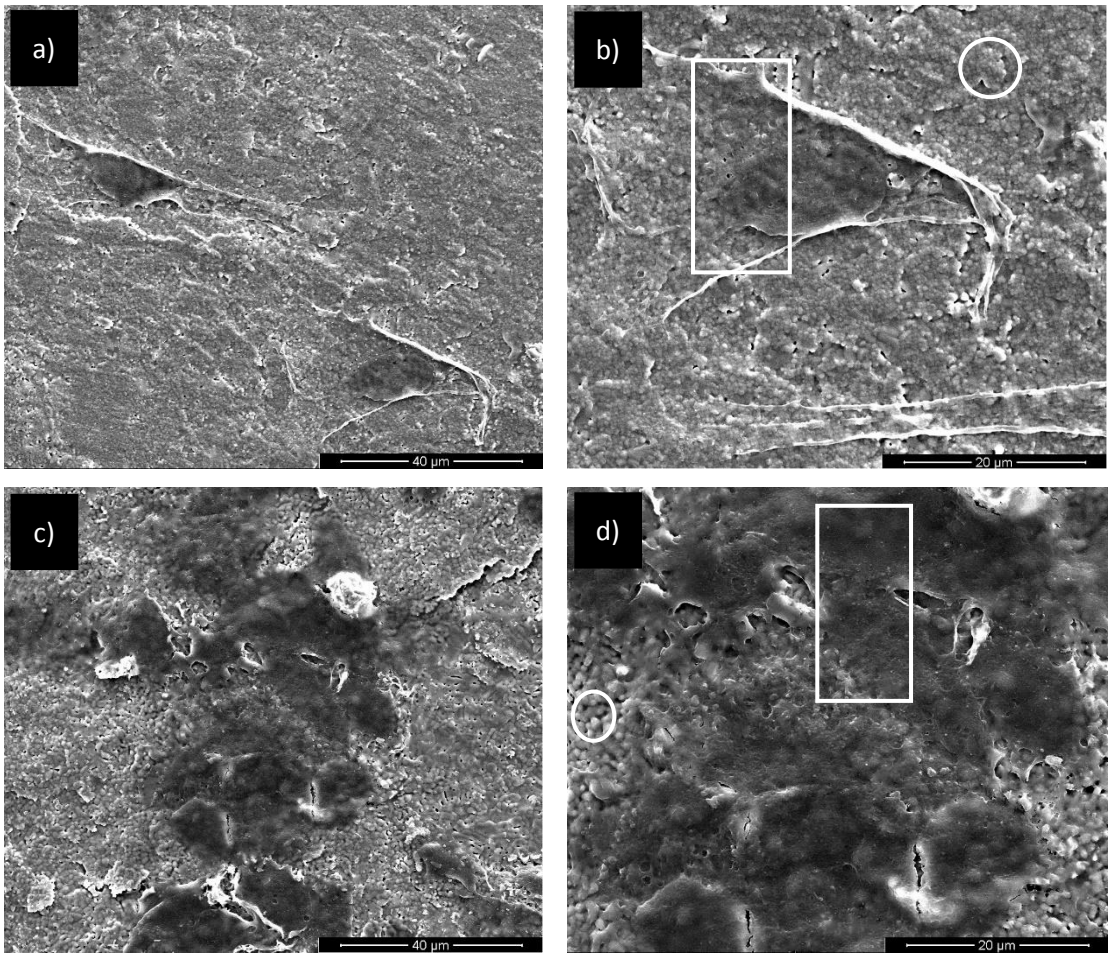

Figure 3.9. SEM images of cells on a, and b) HT2Sr1F; c and d) HT5Sr1F discs (day 7). (Rectangles represent cell sheet and circles represent material surface.)

CHAPTER 4

CONCLUSION

In this study, HT was synthesized by a precipitation method and doped with constant amount of F^- and varying amounts of Sr^{2+} ions in order to investigate its structural, mechanical and biocompatibility properties. All the samples were sintered at 1100°C for 1 h.

Sr^{2+} and F^- doped samples had slightly lower density than HT which could be due to the addition of F^- ions that resulted in a decrease in density in small amounts of Sr^{2+}, while by increasing the Sr^{2+} amount, density of the samples increased. From XRD analysis of Sr-F doped HT samples, shift towards lower angle in the powder pattern was observed due to the expansion of lattice parameters. Moreover, the intensity of peaks were decreased by increasing the amount of Sr. Grain size of powders analyzed by SEM showed that incorporation of Sr^{2+} and F^- ions resulted in smaller grain size. In FTIR spectroscopy analysis, doped samples exhibited the characteristic bands of HA and -βTCP. The micro hardness values of the samples were found to increase upon addition of Sr^{2+} and F^- ions.

In cell culture studies, proliferation, morphology of Saos-2 cells on the sample discs were analyzed. Cell proliferation results revealed that incorporation of Sr^{2+}, and F^- ions had a positive effect on cell proliferation.

Higher proliferation was observed on the discs with increasing the amount of strontium. SEM investigations showed that the cells attached and proliferated with time on HT and doped HT discs. According to the results of structural, microhardness and biocompatibility analysis, HT5Sr1F was found promising for biomedical applications. This material gave the highest microhardness value, as well as relatively high density, and small grain size. It also yielded good cell proliferation and viability.

REFERENCES

Aaseth, J., Shimshi, M., Gabrilove, J. L., & Birketvedt, G. S. (2004). Fluoride: A Toxic or Therapeutic Agent in the Treatment of Osteoporosis? *Journal of Trace Elements in Experimental Medicine*, *17*(2), 83–92. http://doi.org/10.1002/jtra.10051

Akao, M., Aoki, H., Kato, K. (1981). Flexural strength of mixed hydroxyapatite-tricalcium phosphate ceramics. *Tokyo Ika*, (15), 17–22. PubMed PMID: 6955906.

Alshemary, A. Z., Goh, Y.-F., Akram, M., Kadir, M. R. A., & Hussain, R. (2015). Barium and Fluorine Doped Synthetic Hydroxyapatite: Characterization and In-Vitro Bioactivity Analysis. *Science of Advanced Materials*, *7*(2), 249–257. http://doi.org/10.1166/sam.2015.2103

Bahrololoom, M. E., Javidi, M., Javadpour, S., & Ma, J. (2009). Characterisation of natural hydroxyapatite extracted from bovine cortical bone ash. *Journal of Ceramic Processing Research*, *10*(2), 129–138.

Basar, B., Tezcaner, A., Keskin, D., & Evis, Z. (2010). Improvements in microstructural, mechanical, and biocompatibility properties of nano-sized hydroxyapatites doped with yttrium and fluoride. *Ceramics International*, *36*(5), 1633–1643. http://doi.org/10.1016/j.ceramint.2010.02.033

Best, S. M., Porter, A. E., Thian, E. S., & Huang, J. (2008). Bioceramics: Past, present and for the future. *Journal of the European Ceramic Society*, *28*(7), 1319–1327. http://doi.org/10.1016/j.jeurceramsoc.2007.12.001

Bhattacharyya, M. H. (2009). Cadmium osteotoxicity in experimental animals: Mechanisms and relationship to human exposures. *Toxicology and Applied Pharmacology*, *238*(3), 258–265. http://doi.org/10.1016/j.taap.2009.05.015

Bigi, A., Boanini, E., Capuccini, C., & Gazzano, M. (2007). Strontium-substituted hydroxyapatite nanocrystals. *Inorganica Chimica Acta*, *360*(3), 1009–1016. http://doi.org/10.1016/j.ica.2006.07.074

Boanini, E., Gazzano, M., & Bigi, A. (2010a). Ionic substitutions in calcium phosphates synthesized at low temperature. *Acta Biomaterialia*, 6(6), 1882-1894. 6http://doi.org/10.1016/j.actbio.2009.12.041

Boanini, E., Panzavolta, S., Rubini, K., Gandolfi, M., & Bigi, A. (2010b). Effect of strontium and gelatin on the reactivity of β-tricalcium phosphate. *Acta Biomaterialia*, *6*(3), 936–942. http://doi.org/10.1016/j.actbio.2009.10.014

Bohner, M., Lemaitre, J., Legrand, A. P., d'Espinose de la Caillerie, J. B., & Belgrand, P. (1996). Synthesis, X-ray diffraction and solid-state 31P magic angle spinning NMR study of a-tricalcium orthophosphate. *Journal of Materials Science: Materials in Medicine*, *7*, 457–463. http://doi.org/10.1007/BF00122016

Bonnelye, E., Chabadel, A., Saltel, F., & Jurdic, P. (2008). Dual effect of strontium ranelate: Stimulation of osteoblast differentiation and inhibition of osteoclast formation and resorption in vitro. *Bone*, *42*(1), 129–138. http://doi.org/10.1016/j.bone.2007.08.043

Bose, S., Banerjee, A., Dasgupta, S., & Bandyopadhyay, A. (2009). Synthesis, processing, mechanical, and biological property characterization of hydroxyapatite whisker-reinforced hydroxyapatite composites. *Journal of the American Ceramic Society*, *92*(2), 323–330. http://doi.org/10.1111/j.1551-2916.2008.02881.x

Bose, S., Dasgupta, S., Tarafder, S., & Bandyopadhyay, A. (2010). Microwave processed nanocrystalline hydroxyapatite: Simultaneous enhancement of mechanical and biological properties. *Acta Biomater.*, *48*(Suppl 2), 1–6. http://doi.org/10.1097/MPG.0b013e3181a15ae8.Screening

Brook, I., Freeman, C., Grubb, S., Cummins, N., Curran, D., Reidy, C., Towler, M. (2012). Biological evaluation of nano-hydroxyapatite-zirconia (HA-ZrO2) composites and strontium-hydroxyapatite (Sr-HA) for load-bearing applications. *Journal of Biomaterials Applications*, *27*(3), 291–298. http://doi.org/10.1177/0885328211403020

Capuccini, C., Torricelli, P., Sima, F., Boanini, E., Ristoscu, C., Bracci, B., Bigi, A. (2008). Strontium-substituted hydroxyapatite coatings synthesized by pulsed-laser deposition: In vitro osteoblast and osteoclast response. *Acta Biomaterialia*, *4*(6), 1885–1893. http://doi.org/10.1016/j.actbio.2008.05.005

Carrodeguas, R. G., De Aza, A. H., García-Páez, I., De Aza, S., & Pena, P. (2010). Revisiting the Phase-Equilibrium Diagram of the Ca3(PO4)2 -CaMg(SiO 3)2 System. *Journal of the American Ceramic Society*, *93*, 561–569. http://doi.org/10.1111/j.1551-2916.2009.03425.x

Carrodeguas, R. G., & De Aza, S. (2011). α-Tricalcium phosphate: Synthesis, properties and biomedical applications. *Acta Biomaterialia*, *7*(10), 3536–3546. http://doi.org/10.1016/j.actbio.2011.06.019

Caverzasio, J., Palmer, G., Suzuki, a, & Bonjour, J. P. (1997). Mechanism of the mitogenic effect of fluoride on osteoblast-like cells: evidences for a G protein-dependent tyrosine phosphorylation process. *Journal of Bone and Mineral Research : The Official Journal of the American Society for Bone and Mineral Research*, *12*(12), 1975–83. http://doi.org/10.1359/jbmr.1997.12.12.1975

Cheng, K., Weng, W., Wang, H., & Zhang, S. (2005). In vitro behavior of osteoblast-like cells on fluoridated hydroxyapatite coatings. *Biomaterials*, *26*(32), 6288–6295. http://doi.org/10.1016/j.biomaterials.2005.03.041

Clarke, B. (2008). Normal bone anatomy and physiology. *Clinical Journal of the American Society of Nephrology : CJASN*, *3 Suppl 3*, 131–139. http://doi.org/10.2215/CJN.04151206

Coulombe, J., Faure, H., Robin, B., & Ruat, M. (2004). In vitro effects of strontium

ranelate on the extracellular calcium-sensing receptor. *Biochemical and Biophysical Research Communications*, *323*(4), 1184–1190. http://doi.org/10.1016/j.bbrc.2004.08.209

Cowin, S., & Telega, J. (2003). *Bone Mechanics Handbook, 2nd Edition. - . Applied Mechanics Reviews* (Vol. 56). http://doi.org/10.1115/1.1579463

Cox, S. (2012). Synthesis method of hydroxyapaite. *Ceramics*, *2*, 1–10. Retrieved from http://www.ceram.com/uploads/resources/whitepapers/hydroxyapatite-white-paper.pdf

Cui, Y., Winton, M. I., Zhang, Z. F., Rainey, C., Marshall, J., De Kernion, J. B., & Eckhert, C. D. (2004). Dietary boron intake and prostate cancer risk. *Oncology Reports*, *11*(4), 887–892.

Cullity, B. D., & Stock, S. R. (2001). Elements of X-ray Diffraction, 3rd edition. *Prentice Hall*, Chapter 1.

Curran, D. J., Fleming, T. J., Towler, M. R., & Hampshire, S. (2011). Mechanical parameters of strontium doped hydroxyapatite sintered using microwave and conventional methods. *Journal of the Mechanical Behavior of Biomedical Materials*, *4*(8), 2063–2073. http://doi.org/10.1016/j.jmbbm.2011.07.005

Currey, J. D. (2002). Bone: Structure and Mechanics, *Princeton University Press*, 110–121.

Currey, J. D. (2012). The structure and mechanics of bone. *Journal of Materials Science*, *47*(1), 41–54. http://doi.org/10.1007/s10853-011-5914-9

Dahl, S. G., Allain, P., Marie, P. J., Mauras, Y., Boivin, G., Ammann, P., Christiansen, C. (2001). Incorporation and distribution of strontium in bone. *Bone*, *28*(4), 446–453. http://doi.org/10.1016/S8756-3282(01)00419-7

Devirian, T. A., & Volpe, S. L. (2003). The physiological effects of dietary boron. *Critical Reviews in Food Science and Nutrition*, *43*(2), 219–231. http://doi.org/10.1080/10408690390826491

Dickens, B., Schroeder, L. W., & Brown, W. E. (1974). Crystallographic studies of the role of Mg as a stabilizing impurity in β-Ca3(PO4)2. The crystal structure of pure β-Ca3(PO4)2. *Journal of Solid State Chemistry*, *10*(3), 232–248. http://doi.org/10.1016/0022-4596(74)90030-9

Dorozhkin, S. V. (2012). Calcium orthophosphates as biomaterials and bioceramics. In *Phosphates: Sources, Properties and Applications* (pp. 251–340). Retrieved from http://www.scopus.com/inward/record.url?eid=2-s2.0-84892301268&partnerID=tZOtx3y1

Dorozhkin, S. V., & Epple, M. (2002). Biological and medical significance of calcium phosphates. *Angewandte Chemie - International Edition*, *41*(17), 3130–3146. http://doi.org/10.1002/1521-3773(20020902)41:17<3130::AID-ANIE3130>3.0.CO;2-1

Ducheyne, P., & Qiu, Q. (1999). Bioactive ceramics: The effect of surface reactivity

on bone formation and bone cell function. *Biomaterials*, 20, 2287-2303. http://doi.org/10.1016/S0142-9612(99)00181-7

Edwards, P. D., & Ramulu, M. (2009). Investigation of microstructure, surface and subsurface characteristics in titanium alloy friction stir welds of varied thicknesses. *Science and Technology of Welding and Joining*, *14*(5), 476–483. http://doi.org/10.1179/136217109X425838

Elliott, J. C. (1994). Structure and chemistry of the apatites and other calcium orthophosphates. *Studies in Organic Chemistry*, 18, 34-50. http://doi.org/10.1016/B978-0-444-81582-8.50006-7

Elliott, J. C., Wilson, R. M., & Dowker, S. E. P. (2002). Apatite structures. *Advances in X-Ray Analysis*, *45*(c), 172–181. http://doi.org/10.1007/s10522-009-9234-2

Enderle, R., Götz-Neunhoeffer, F., Göbbels, M., Müller, F. A., & Greil, P. (2005). Influence of magnesium doping on the phase transformation temperature of β-TCP ceramics examined by Rietveld refinement. *Biomaterials*, *26*(17), 3379–3384. http://doi.org/10.1016/j.biomaterials.2004.09.017

Eslami, H., Solati-Hashjin, M., & Tahriri, M. (2009). The comparison of powder characteristics and physicochemical, mechanical and biological properties between nanostructure ceramics of hydroxyapatite and fluoridated hydroxyapatite. *Materials Science and Engineering C*, *29*(4), 1387–1398. http://doi.org/10.1016/j.msec.2008.10.033

Eslami, H., Solati-Hashjin, M., & Tahriri, M. (2010). Effect of fluorine ion addition on structural, thermal, mechanical, solubility and biocompatibility characteristics of hydroxyapatite nanopowders. *Advances in Applied Ceramics*, *109*(4), 200–212. http://doi.org/10.1179/174367509X12503626841550

Evis, Z. (2007). Reactions in hydroxylapatite-zirconia composites. *Ceramics International*, *33*(6), 987–991. http://doi.org/10.1016/j.ceramint.2006.02.012

Evis, Z., Basar, B., Sun, Z. P. (2010). Diametral strength testing of hydroxyapatites doped with yttrium and fluoride, *Advances in Applied Ceramics*, 109, 383-388. http://doi.org/10.1179/174367510X12677121374429

Evis, Z., Ergun, C., & Doremus, R. H. (2005). Hydroxylapatite-zirconia composites: Thermal stability of phases and sinterability as related to the CaO-ZrO2 phase diagram. *Journal of Materials Science*, *40*(5), 1127–1134. http://doi.org/10.1111/j.1151-2916.2000.tb01634.x

Exley, C. (2008). Aluminium and medicine. *Molecular and Supramolecular Bioinorganic Chemistry*, *6*, 1–24.

Fanghänel, J., Bayerlein, T., Gedrange, T., Kauschke, E., Rumpel, E., Gerike, W., Proff, P. (2006). Bone functions and the requirements for bone grafts and substitutes in the orofacial region. *Folia Morphologica*, *65*(1), 56–58.

Farzadi, a., Solati-Hashjin, M., Bakhshi, F., & Aminian, A. (2011). Synthesis and characterization of hydroxyapatite/β-tricalcium phosphate nanocomposites

using microwave irradiation. *Ceramics International*, *37*(1), 65–71. http://doi.org/10.1016/j.ceramint.2010.08.021

Fathi, M. H., & Mohammadi Zahrani, E. (2009). Mechanical alloying synthesis and bioactivity evaluation of nanocrystalline fluoridated hydroxyapatite. *Journal of Crystal Growth*, *311*(5), 1392–1403. http://doi.org/10.1016/j.jcrysgro.2008.11.100

Fernández, E., Gil, F. J., Ginebra, M. P., Driessens, F. C., Planell, J. a, & Best, S. M. (1999). Calcium phosphate bone cements for clinical applications. Part I: solution chemistry. *Journal of Materials Science. Materials in Medicine*, *10*(3), 169–176. http://doi.org/10.1023/A:1008937507714

França, R., Samani, T. D., Bayade, G., Yahia, L., & Sacher, E. (2014). Nanoscale surface characterization of biphasic calcium phosphate, with comparisons to calcium hydroxyapatite and β-tricalcium phosphate bioceramics. *Journal of Colloid and Interface Science*, *420*, 182–188. http://doi.org/10.1016/j.jcis.2013.12.055

Fratzl, P., Gupta, H. S., Paschalis, E. P., & Roschger, P. (2004). Structure and mechanical quality of the collagen-mineral nano-composite in bone. *Journal of Materials Chemistry*, *14*(14), 2115. http://doi.org/10.1039/b402005g

Frenken, J. W. F. H., Bouwman, W. F., Bravenboer, N., Zijderveld, S. A., Schulten, E. A. J. M., & Ten Bruggenkate, C. M. (2010). The use of Straumann Bone Ceramic in a maxillary sinus floor elevation procedure: A clinical, radiological, histological and histomorphometric evaluation with a 6-month healing period. *Clinical Oral Implants Research*, *21*(2), 201–208. http://doi.org/10.1111/j.1600-0501.2009.01821.x

Fu, Y.-F., & Chen, D.-M. (2008). The influence of Sr2+ on the cytotoxicity of strontium substituted hydroxyapatite (Sr-HA). *Gongneng Cailiao/Journal of Functional Materials*, *39*(4), 645–646+650. http://doi.org/1164 [pii]

Gbureck, U., Grolms, O., Barralet, J. E., Grover, L. M., & Thull, R. (2003). Mechanical activation and cement formation of β -tricalcium phosphate. *Biomaterials*, *24*(23), 4123–4131. http://doi.org/10.1016/S0142-9612(03)00283-7

Gibson, I. R., & Bonfield, W. (2002). Novel synthesis and characterization of an AB-type carbonate-substituted hydroxyapatite. *Journal of Biomedical Materials Research*, *59*(4), 697–708. http://doi.org/10.1002/jbm.10044

Gross, K., & Rodríguez-Lorenzo, L. M. (2004a). Sintered hydroxyfluorapatites. Part I: Sintering ability of precipitated solid solution powders. *Biomaterials*, *25*(7-8), 1375–1384. http://doi.org/10.1016/S0142-9612(03)00565-9

Gross, K., & Rodríguez-Lorenzo, L. M. (2004b). Sintered hydroxyfluorapatites. Part II: Mechanical properties of solid solutions determined by microindentation. *Biomaterials*, *25*(7-8), 1385–1394. http://doi.org/10.1016/S0142-9612(03)00636-7

Grynpas, M. D., Hamilton, E., Cheung, R., Tsouderos, Y., Deloffre, P., Hott, M., & Marie, P. J. (1996). Strontium increases vertebral bone volume in rats at a low dose that does not induce detectable mineralization defect. *Bone*, *18*(3), 253–259. http://doi.org/10.1016/8756-3282(95)00484-X

Hak, D. J. (2007). The use of osteoconductive bone graft substitutes in orthopaedic trauma. *The Journal of the American Academy of Orthopaedic Surgeons*, *15*(9), 525–536. http://doi.org/15/9/525 [pii]

He, L. H., Standard, O. C., Huang, T. T. Y., Latella, B. A., & Swain, M. V. (2008). Mechanical behaviour of porous hydroxyapatite. *Acta Biomaterialia*, *4*(3), 577–586. http://doi.org/10.1016/j.actbio.2007.11.002

Inoue, M., LeGeros, R. Z., Inoue, M., Tsujigiwa, H., Nagatsuka, H., Yamamoto, T., & Nagai, N. (2004). In vitro response of osteoblast-like and odontoblast-like cells to unsubstituted and substituted apatites. *Journal of Biomedical Materials Research. Part A*, *70*(4), 585–593. http://doi.org/10.1002/jbm.a.30116

Ito, A., Senda, K., Sogo, Y., Oyane, A., Yamazaki, A., & Legeros, R. Z. (2006). Dissolution rate of zinc-containing beta-tricalcium phosphate ceramics. *Biomedical Materials (Bristol, England)*, *1*, 134–139. http://doi.org/10.1088/1748-6041/1/3/007

Jensen, S. S., Yeo, A., Dard, M., Hunziker, E., Schenk, R., & Buser, D. (2007). Evaluation of a novel biphasic calcium phosphate in standardized bone defects. A histologic and histomorphometric study in the mandibles of minipigs. *Clinical Oral Implants Research*, *18*(6), 752–760. http://doi.org/10.1111/j.1600-0501.2007.01417.x

Ji, B., & Gao, H. (2004). Mechanical properties of nanostructure of biological materials. *Mechanics and Physics of Solids*, *52*(9), 1963–1990. http://doi.org/10.1016/j.jmps.2004.03.006

Jillavenkatesa, A., & Condrate, R. A. (1998). The Infrared and Raman Spectra of β- and α-Tricalcium Phosphate ($Ca_3(PO_4)_2$). *Spectroscopy Letters*, 31(8), 1619–1634. http://doi.org/10.1080/00387019808007439

Jinawath, S., Pongkao, D., Suchanek, W., & Yoshimura, M. (2001). Hydrothermal synthesis of monetite and hydroxyapatite from monocalcium phosphate monohydrate. *International Journal of Inorganic Materials*, *3*(7), 997–1001. http://doi.org/10.1016/S1466-6049(01)00199-4

Kalita, S. J., Bhardwaj, A., & Bhatt, H. A. (2007). Nanocrystalline calcium phosphate ceramics in biomedical engineering. *Materials Science and Engineering C*, *27*(3), 441–449. http://doi.org/10.1016/j.msec.2006.05.018

Kannan, S., & Ferreira, J. M. F. (2006). Synthesis and thermal stability of hydroxyapatite-β-tricalcium phosphate composites with cosubstituted sodium, magnesium, and fluorine. *Chemistry of Materials*, *18*(1), 198–203. http://doi.org/10.1021/cm051966i

Kannan, S., Lemos, I. A. F., Rocha, J. H. G., & Ferreira, J. M. F. (2005). Synthesis

and characterization of magnesium substituted biphasic mixtures of controlled hydroxyapatite/β-tricalcium phosphate ratios. *Journal of Solid State Chemistry*, *178*(10), 3190–3196. http://doi.org/10.1016/j.jssc.2005.08.003

Kannan, S., Rebelo, A., & Ferreira, J. M. F. (2006). Novel synthesis and structural characterization of fluorine and chlorine co-substituted hydroxyapatites. *Journal of Inorganic Biochemistry*, *100*(10), 1692–1697. http://doi.org/10.1016/j.jinorgbio.2006.06.005

Kannan, S., Ventura, J. M., & Ferreira, J. M. F. (2007). Aqueous precipitation method for the formation of Mg-stabilized β-tricalcium phosphate: An X-ray diffraction study. *Ceramics International*, *33*(4), 637–641. http://doi.org/10.1016/j.ceramint.2005.11.014

Kasten, P., Luginbühl, R., van Griensven, M., Barkhausen, T., Krettek, C., Bohner, M., & Bosch, U. (2003). Comparison of human bone marrow stromal cells seeded on calcium-deficient hydroxyapatite, beta-tricalcium phosphate and demineralized bone matrix. *Biomaterials*. http://doi.org/10.1016/S0142-9612(03)00062-0

Kim, H. W., Koh, Y. H., Kong, Y. M., Kang, J. G., & Kim, H. E. (2004). Strontium substituted calcium phosphate biphasic ceramics obtained by a powder precipitation method. *Journal of Materials Science: Materials in Medicine*, *15*(10), 1129–1134. http://doi.org/10.1023/B:JMSM.0000046395.76435.60

Kim, H. W., Lee, E. J., Kim, H. E., Salih, V., & Knowles, J. C. (2005). Effect of fluoridation of hydroxyapatite in hydroxyapatite-polycaprolactone composites on osteoblast activity. *Biomaterials*, *26*(21), 4395–4404. http://doi.org/10.1016/j.biomaterials.2004.11.008

Kim, H. W., Noh, Y. J., Koh, Y. H., & Kim, H. E. (2003). Enhanced performance of fluorine substituted hydroxyapatite composites for hard tissue engineering. *Journal of Materials Science: Materials in Medicine*, *14*, 899–904. http://doi.org/10.1023/A:1025638811361

Kim, T. G., & Park, B. (2005). Synthesis and growth mechanisms of one-dimensional strontium hydroxyapatite nanostructures. *Inorganic Chemistry*, *44*(26), 9895–9901. http://doi.org/10.1021/ic051013m

Koch, C. F., Johnson, S., Kumar, D., Jelinek, M., Chrisey, D. B., Doraiswamy, a., Mihailescu, I. N. (2007). Pulsed laser deposition of hydroxyapatite thin films. *Materials Science and Engineering C*, *27*(3), 484–494. http://doi.org/10.1016/j.msec.2006.05.025

Kockan, U., & Evis, Z. (2010). Prediction of hexagonal lattice parameters of various apatites by artificial neural networks. *Journal of Applied Crystallography*, *43*(4), 769–779. http://doi.org/10.1107/S0021889810018133

Koepp, H. E., Schorlemmer, S., Kessler, S., Brenner, R. E., Claes, L., Günther, K.-P., & Ignatius, A. a. (2004). Biocompatibility and osseointegration of beta-TCP: histomorphological and biomechanical studies in a weight-bearing sheep model.

Journal of Biomedical Materials Research. Part B, Applied Biomaterials, *70*, 209–217. http://doi.org/10.1002/jbm.b.30034

Koumoulidis, G. C., Katsoulidis, A. P., Ladavos, A. K., Pomonis, P. J., Trapalis, C. C., Sdoukos, A. T., & Vaimakis, T. C. (2003). Preparation of hydroxyapatite via microemulsion route. *Journal of Colloid and Interface Science*, *259*(2), 254–260. http://doi.org/10.1016/S0021-9797(02)00233-3

Kurashina, K., Kurita, H., Hirano, M., Kotani, A., Klein, C. P. A. T., & De Groot, K. (1997). In vivo study of calcium phosphate cements: Implantation of an α-tricalcium phosphate/dicalcium pbosphate dibasic/tetracalcium phosphate monoxide cement paste. *Biomaterials*, *18*(7), 539–543. http://doi.org/10.1016/S0142-9612(96)00162-7

Kuwahara, H., Mazaki, N., Takahashi, M., Watanabe, T., Yang, X., & Aizawa, T. (2001). Mechanical properties of bulk sintered titanium nitride ceramics. *Materials Science and Engineering A*, *319-321*, 687–691. http://doi.org/10.1016/S0921-5093(01)00936-4

Landi, E., Tampieri, A., Celotti, G., & Sprio, S. (2000). Densification behaviour and mechanisms of synthetic hydroxyapatites. *Journal of the European Ceramic Society*, *20*(14-15), 2377–2387. http://doi.org/10.1016/S0955-2219(00)00154-0

Landi, E., Tampieri, A., Mattioli-Belmonte, M., Celotti, G., Sandri, M., Gigante, A., Biagini, G. (2006). Biomimetic Mg- and Mg,CO3-substituted hydroxyapatites: synthesis characterization and in vitro behaviour. *Journal of the European Ceramic Society*, *26*(13), 2593–2601. http://doi.org/10.1016/j.jeurceramsoc.2005.06.040

Laurencin, D., Almora-Barrios, N., de Leeuw, N. H., Gervais, C., Bonhomme, C., Mauri, F., Smith, M. E. (2011). Magnesium incorporation into hydroxyapatite. *Biomaterials*, *32*(7), 1826–1837. http://doi.org/10.1016/j.biomaterials.2010.11.017

Le Huec, J. C., Clément, D., Aunoble, S., Tournier, C., & Harmand, M. F. (2009). A brief summary of 15 years of research on beta-tricalcium phosphates. *SAS Journal*, *3*(3), 112–113. http://doi.org/10.1016/j.esas.2009.09.007

Lee, B.-T., Youn, M.-H., Paul, R. K., Lee, K.-H., Song, H.-Y., Yang, J.-H., Kwon, T.-Y. (2011). Synthesis of spherical hydroxyapatite granules with interconnected pore channels using camphene emulsion. *Journal of Biomedical Materials Research. Part B, Applied Biomaterials*, *99*(1), 150–7. http://doi.org/10.1002/jbm.b.31882

Lee, E. J., Lee, S. H., Kim, H. W., Kong, Y. M., & Kim, H. E. (2005). Fluoridated apatite coatings on titanium obtained by electron-beam deposition. *Biomaterials*, *26*(18), 3843–3851. http://doi.org/10.1016/j.biomaterials.2004.10.019

Lee, J. M., Choi, B. B. R., Choi, J. H., Kim, G. C., Hwang, D. S., Chang, M. C., Kim, U. K. (2013). Osteoblastic response to the hydroxyapatite/gelatin

nanocomposite and bio-calcium phosphate cement. *Tissue Engineering and Regenerative Medicine*, *10*(2), 47–52. http://doi.org/10.1007/s13770-013-0344-1

Legeros, R. Z. (1991). Monographs in oral science Vol. 15. Calcium phosphates in oral biology and medicine. In *Legeros, R. Z. Monographs in Oral Science, Vol. 15. Calcium Phosphates in Oral Biology and Medicine. Ix+201p. S. Karger Ag: Basel, Switzerland; New York, New York, USA. Illus* (p. IX+201P). Retrieved from <Go to ISI>://BCI:BCI199141037174

Legeros, R. Z., Lin, S., Rohanizadeh, R., Mijares, D., & Legeros, J. P. (2003). Biphasic calcium phosphate bioceramics: Preparation, properties and applications. *Journal of Materials Science: Materials in Medicine*, *14*(3), 201–209. http://doi.org/10.1023/A:1022872421333

Leroux, L., & Lacout, J. L. (2001). Preparation of calcium strontium hydroxyapatites by a new route involving calcium phosphate cements. *Journal of Materials Research*, *16*, 171–178. http://doi.org/10.1557/jmr.2001.0028

Leventouri, T. (2006). Synthetic and biological hydroxyapatites: Crystal structure questions. *Biomaterials*, *27*(18), 3339–3342. http://doi.org/10.1016/j.biomaterials.2006.02.021

Li, X., Ito, A., Sogo, Y., Wang, X., & LeGeros, R. Z. (2009). Solubility of Mg-containing β-tricalcium phosphate at 25ºC. *Acta Biomaterialia*, *5*(1), 508–517. http://doi.org/10.1016/j.actbio.2008.06.010

Li, Y., Weng, W., & Tam, K. C. (2007a). Novel highly biodegradable biphasic tricalcium phosphates composed of a-tricalcium phosphate and β-tricalcium phosphate. *Acta Biomaterialia*, *3*(2), 251–254. http://doi.org/10.1016/j.actbio.2006.07.003

Li, Z. Y., Lam, W. M., Yang, C., Xu, B., Ni, G. X., Abbah, S. a., Lu, W. W. (2007b). Chemical composition, crystal size and lattice structural changes after incorporation of strontium into biomimetic apatite. *Biomaterials*, *28*(7), 1452–1460. http://doi.org/10.1016/j.biomaterials.2006.11.001

Liang, L., Rulis, P., & Ching, W. Y. (2010). Mechanical properties, electronic structure and bonding of a-and β-tricalcium phosphates with surface characterization. *Acta Biomaterialia*, *6*(9), 3763–3771. http://doi.org/10.1016/j.actbio.2010.03.033

Ma, G., & Liu, X. Y. (2009). Hydroxyapatite: Hexagonal or monoclinic? *Crystal Growth and Design*, *9*(7), 2991–2994. http://doi.org/10.1021/cg900156w

Ma, M. G., Zhu, Y. J., & Chang, J. (2006). Monetite formed in mixed solvents of water and ethylene glycol and its transformation to hydroxyapatite. *Journal of Physical Chemistry B*, *110*(29), 14226–14230. http://doi.org/10.1021/jp061738r

Mackie, P. E., Elliot, J. C., & Young, R. A. (1972). Monoclinic structure of synthetic Ca5(PO4)3Cl, chlorapatite. *Acta Crystallographica Section B Structural Crystallography and Crystal Chemistry*, *28*(6), 1840–1848.

http://doi.org/10.1107/S0567740872005114

Marchi, J., Dantas, A. C. S., Greil, P., Bressiani, J. C., Bressiani, A. H. A., & Müller, F. A. (2007). Influence of Mg-substitution on the physicochemical properties of calcium phosphate powders. *Materials Research Bulletin*, *42*(6), 1040–1050. http://doi.org/10.1016/j.materresbull.2006.09.015

Marchi, J., Greil, P., Bressiani, J. C., Bressiani, A., & Müller, F. (2009). Influence of synthesis conditions on the characteristics of biphasic calcium phosphate powders. *International Journal of Applied Ceramic Technology*, *6*(1), 60–71. http://doi.org/10.1111/j.1744-7402.2008.02254.x

Mardziah, C. M., Sopyan, I., & Ramesh, S. (2009). Strontium-doped hydroxyapatite nanopowder via sol-gel method: Effect of strontium concentration and calcination temperature on phase behavior. *Trends in Biomaterials and Artificial Organs*, 23(2), 105–113.

Marieb, E. N., & Hoehn, K. (2013). Human Anatomy & Physiology, *Ninth Edition, Pearson*, 7, 878-881

Marks, S. C., & Odgren, P. R. (2002). *Principles of Bone Biology*. *Principles of Bone Biology*. (book), 3-15. http://doi.org/10.1016/B978-012098652-1.50103-7

Marlow, F., Khalil, A. S. G., & Stempniewicz, M. (2007). Circular mesostructures: solids with novel symmetry properties. *Journal of Materials Chemistry*, *17*(21), 2168. http://doi.org/10.1039/b700532f

Martin, R. B. (2003). Bones: structure and mechanics. *Journal of Biomechanics*, 36(6), 893-901. http://doi.org/10.1016/S0021-9290(03)00033-2

Martini, F.H & Nath, J. (2009). *Fundamentals of Anatomy and Physiology*. *Learning Benjamin Cummings*, 7, 170-196. http://doi.org/612

Matsumoto, N., Yoshida, K., Hashimoto, K., & Toda, Y. (2009). Thermal stability of β-tricalcium phosphate doped with monovalent metal ions. *Materials Research Bulletin*, *44*(9), 1889–1894. http://doi.org/10.1016/j.materresbull.2009.05.012

Matsunaga, K., & Murata, H. (2009). Strontium substitution in bioactive calcium phosphates: A first-principles study. *Journal of Physical Chemistry B*, *113*(11), 3584–3589. http://doi.org/10.1021/jp808713m

Matsushita, N., Terai, H., Okada, T., Nozaki, K., Inoue, H., Miyamoto, S., & Takaoka, K. (2004). A new bone-inducing biodegradable porous beta-tricalcium phosphate. *Journal of Biomedical Materials Research. Part A*, *70*(3), 450–458. http://doi.org/10.1002/jbm.a.30102

McCormack, A. P., Anderson, P. A., & Tencer, A. F. (1993). Effect of controlled local release of sodium-fluoride on bone-formation- filling a defect in the proximal femoral cortex. *Journal of Orthopaedic Research*, *11*(4), 548–555. http://doi.org/10.1002/jor.1100110409

McLeod, K., Kumar, S., Dutta, N. K., Smart, R. S. C., Voelcker, N. H., & Anderson, G. I. (2010). X-ray photoelectron spectroscopy study of the growth kinetics of

biomimetically grown hydroxyapatite thin-film coatings. *Applied Surface Science*, *256*(23), 7178–7185. http://doi.org/10.1016/j.apsusc.2010.05.047

Mehmel, M. (1932). Über die Struktur des Apatits. L. *Z Für Kristallographie*, *323-331*(81), 323–331.

Metsger, D. S., Rieger, M. R., & Foreman, D. W. (1999). Mechanical properties of sintered hydroxyapatite and tricalcium phosphate ceramic. *Journal of Materials Science: Materials in Medicine*, *10*, 9–17. http://doi.org/10.1023/A:1008883809160

Meyers, M., Chen, P., Lin, A., & Seki, Y. (2008). Biological materials: Structure and mechanical properties. *Progress in Materials Science*, *53*(1), 1–206. http://doi.org/10.1016/j.pmatsci.2007.05.002

Mirhadi, B., Mehdikhani, B., & Askari, N. (2011). Synthesis of nano-sized β-tricalcium phosphate via wet precipitation. *Processing and Application of Ceramics*, 193–198. http://doi.org/10.2298/PAC1104193M

Mobasherpour, I., Heshajin, M. S., Kazemzadeh, a., & Zakeri, M. (2007). Synthesis of nanocrystalline hydroxyapatite by using precipitation method. *Journal of Alloys and Compounds*, *430*(1-2), 330–333. http://doi.org/10.1016/j.jallcom.2006.05.018

Moseke, C., & Gbureck, U. (2010). Tetracalcium phosphate: Synthesis, properties and biomedical applications. *Acta Biomaterialia*, *6*(10), 3815–3823. http://doi.org/10.1016/j.actbio.2010.04.020

Mousny, M., Omelon, S., Wise, L., Everett, E. T., Dumitriu, M., Holmyard, D. P., Grynpas, M. D. (2008). Fluoride effects on bone formation and mineralization are influenced by genetics. *Bone*, *43*(6), 1067–1074. http://doi.org/10.1016/j.bone.2008.07.248

O'Donnell, M. D., Fredholm, Y., de Rouffignac, A., & Hill, R. G. (2008). Structural analysis of a series of strontium-substituted apatites. *Acta Biomaterialia*, *4*(5), 1455–1464. http://doi.org/10.1016/j.actbio.2008.04.018

Öchsner, A., Silva, L. F. M. da, & Altenbach, H. (2013). Characterization and development of biosystems and biomaterials. *Advanced Structured Materials*, 29, 120-254. http://doi.org/10.1007/978-3-642-31470-4

Ogose, A., Hotta, T., Hatano, H., Kawashima, H., Tokunaga, K., Endo, N., & Umezu, H. (2002). Histological examination of beta-tricalcium phosphate graft in human femur. *Journal of Biomedical Materials Research*, *63*(5), 601–4. http://doi.org/10.1002/jbm.10380

Ogose, A., Hotta, T., Kawashima, H., Kondo, N., Gu, W., Kamura, T., & Endo, N. (2005). Comparison of hydroxyapatite and beta tricalcium phosphate as bone substitutes after excision of bone tumors. *Journal of Biomedical Materials Research - Part B Applied Biomaterials*, *72*(1), 94–101. http://doi.org/10.1002/jbm.b.30136

Pors Nielsen, S. (2004). The biological role of strontium. *Bone*, 35(3), 583–588. http://doi.org/10.1016/j.bone.2004.04.026

Pramanik, S., Agarwal, A. K., Rai, K. N. N., & Garg, A. (2007). Development of high strength hydroxyapatite by solid-state-sintering process. *Ceramics International*, *33*(3), 419–426. http://doi.org/10.1016/j.ceramint.2005.10.025

Qu, H., & Wei, M. (2006a). Effect of fluorine content on mechanical properties of sintered fluoridated hydroxyapatite. *Materials Science and Engineering C*, *26*(1), 46–53. http://doi.org/10.1016/j.msec.2005.06.005

Qu, H., & Wei, M. (2006b). The effect of fluoride contents in fluoridated hydroxyapatite on osteoblast behavior. *Acta Biomaterialia*, *2*(1), 113–119. http://doi.org/10.1016/j.actbio.2005.09.003

Rabiee, S. M., Moztarzadeh, F., Salimi-Kenari, H., Solati-Hashjin, M., & Mortazavi, S. M. J. (2008). Study of biodegradable ceramic bone graft substitute. *Advances in Applied Ceramics*, *107*(4), 199–202. http://doi.org/10.1179/174367607X227972

Radin, S. R., & Ducheyne, P. (1993). The effect of calcium phosphate ceramic composition and structure on in vitro behavior. II. Precipitation. *Journal of Biomedical Materials Research*, *27*(1), 35–45. http://doi.org/10.1002/jbm.820270106

Rameshbabu, N., Sampath Kumar, T. S., & Prasad Rao, K. (2006). Synthesis of nanocrystalline fluorinated hydroxyapatite by microwave processing and its in vitro dissolution study. *Bulletin of Materials Science*, 29, 611–615. http://doi.org/10.1007/s12034-006-0012-3

Rangavittal, N., Landa-Cánovas, A. R., González-Calbet, J. M., & Vallet-Regí, M. (2000). Structural study and stability of hydroxyapatite and beta-tricalcium phosphate: two important bioceramics. *Journal of Biomedical Materials Research*, *51*(4), 660–668. http://doi.org/10.1002/1097-4636(20000915)51:4<660::AID-JBM14>3.0.CO;2-B

Rauschmann, M. A., Wichelhaus, T. A., Stirnal, V., Dingeldein, E., Zichner, L., Schnettler, R., & Alt, V. (2005). Nanocrystalline hydroxyapatite and calcium sulphate as biodegradable composite carrier material for local delivery of antibiotics in bone infections. *Biomaterials*, *26*, 2677–2684. http://doi.org/10.1016/j.biomaterials.2004.06.045

Raynaud, S., Champion, E., Lafon, J. P., & Bernache-Assollant, D. (2002). Calcium phosphate apatites with variable Ca/P atomic ratio III. Mechanical properties and degradation in solution of hot pressed ceramics. *Biomaterials*, *23*(4), 1081–1089. http://doi.org/10.1016/S0142-9612(01)00220-4

Renaudin, G., Jallot, E., & Nedelec, J. M. (2009). Effect of strontium substitution on the composition and microstructure of sol-gel derived calcium phosphates. *Journal of Sol-Gel Science and Technology*, 51, 287–294. http://doi.org/10.1007/s10971-008-1854-5

Rho, J. Y., Kuhn-Spearing, L., & Zioupos, P. (1998). Mechanical properties and the hierarchical structure of bone. *Medical Engineering and Physics*, *20*(2), 92–102. http://doi.org/10.1016/S1350-4533(98)00007-1

Rivera-Muñoz, E. M. (2000). Hydroxyapatite-based materials: synthesis and characterization. *Biomedical Engineering - Frontier and Challenges*, 75–98. http://doi.org/10.5772/19123

Rodríguez-Lorenzo, L. M., Hart, J. N., & Gross, K. A. (2003). Influence of fluorine in the synthesis of apatites. Synthesis of solid solutions of hydroxy-fluorapatite. *Biomaterials*, *24*(21), 3777–3785. http://doi.org/10.1016/S0142-9612(03)00259-X

Romieu, G., Garric, X., Munier, S., Vert, M., & Boudeville, P. (2010). Calcium-strontium mixed phosphate as novel injectable and radio-opaque hydraulic cement. *Acta Biomaterialia*, *6*(8), 3208–3215. http://doi.org/10.1016/j.actbio.2010.02.008

Rude, R. K., Singer, F. R., & Gruber, H. E. (2009). Skeletal and hormonal effects of magnesium deficiency. *Journal of the American College of Nutrition*, *28*(2), 131–41. http://doi.org/10.1080/07315724.2009.10719764

Rumpel, E., Wolf, E., Kauschke, E., Bienengräber, V., Bayerlein, T., Gedrange, T., & Proff, P. (2006). The biodegradation of hydroxyapatite bone graft substitutes in vivo. *Folia Morphologica*, *65*(1), 43–48.

Ryu, H. S., Youn, H. J., Sun Hong, K., Chang, B. S., Lee, C. K., & Chung, S. S. (2002). An improvement in sintering property of β-tricalcium phosphate by addition of calcium pyrophosphate. *Biomaterials*, *23*(3), 909–914. http://doi.org/10.1016/S0142-9612(01)00201-0

Saint-Jean, S. J., Camiré, C. L., Nevsten, P., Hansen, S., & Ginebra, M. P. (2005). Study of the reactivity and in vitro bioactivity of Sr-substituted alpha-TCP cements. *Journal of Materials Science. Materials in Medicine*, *16*(11), 993–1001. http://doi.org/10.1007/s10856-005-4754-z

Sakakura, T., Kamoshita, M., Iguchi, H., Wang, J., & Ishizawa, N. (2010). Apatite-type SrPr4(SiO4)3O. *Acta Crystallographica Section E: Structure Reports Online*, *66*(9), E66–i68,sup–1–4. http://doi.org/10.1107/S1600536810033349

Samavedi, S., Whittington, A. R., & Goldstein, A. S. (2013). Calcium phosphate ceramics in bone tissue engineering: A review of properties and their influence on cell behavior. *Acta Biomaterialia*, 9(9), 8037-8045. http://doi.org/10.1016/j.actbio.2013.06.014

Sanosh, K. P., Chu, M. C., Balakrishnan, A., Kim, T. N., & Cho, S. J. (2010). Sol-gel synthesis of pure nano sized β-tricalcium phosphate crystalline powders. *Current Applied Physics*, *10*(1), 68–71. http://doi.org/10.1016/j.cap.2009.04.014

Shi, Z., Huang, X., Cai, Y., Tang, R., & Yang, D. (2009). Size effect of hydroxyapatite nanoparticles on proliferation and apoptosis of osteoblast-like cells. *Acta Biomaterialia*, *5*(1), 338–345.

http://doi.org/10.1016/j.actbio.2008.07.023

Shiota, T., Shibata, M., Yasuda, K., & Matsuo, Y. (2008). Influence of β-tricalcium phosphate dispersion on mechanical properties of hydroxyapatite ceramics. *Journal of the Ceramic Society of Japan*, *116*(1357), 1002–1005. http://doi.org/10.2109/jcersj2.116.1002

Spivak, J. M., & Hasharoni, A. (2001). Use of hydroxyapatite in spine surgery. *European Spine Journal*, *10*(SUPPL. 2). http://doi.org/10.1007/s005860100286

Sun, Z. P., Ercan, B., Evis, Z., & Webster, T. J. (2010). Microstructural, mechanical, and osteocompatibility properties of Mg2+/F--doped nanophase hydroxyapatite. *Journal of Biomedical Materials Research - Part A*, *94*(3), 806–815. http://doi.org/10.1002/jbm.a.32745

Tavares, D. D. S., Resende, C. X., Quitan, M. P., Castro, L. D. O., Granjeiro, J. M., & Soares, G. D. A. (2011). Incorporation of strontium up to 5 Mol. (%) to hydroxyapatite did not affect its cytocompatibility. *Materials Research*, *14*(4), 456–460. http://doi.org/10.1590/S1516-14392011005000073

Ten Cate, J. M., & Featherstone, J. D. B. (1991). Mechanistic aspects of the interactions between fluoride and dental enamel. *Critical Reviews in Oral Biology and Medicine*, 2(2), 283–296. http://doi.org/10.1177/10454411910020030101

Terra, J., Dourado, E. R., Eon, J.-G., Ellis, D. E., Gonzalez, G., & Rossi, A. M. (2009). The structure of strontium-doped hydroxyapatite: an experimental and theoretical study. *Physical Chemistry Chemical Physics : PCCP*, 11(3), 568–577. http://doi.org/10.1039/b802841a

Thamaraiselvi, T. V, & Rajeswari, S. (2004). Biological Evaluation of Bioceramic Materials - A Review. *Trends Biomater. Artif. Organs*, 18(1), 9–17. Retrieved from http://www.sbaoi.org

Toker, S. M., Tezcaner, A., & Evis, Z. (2011). Microstructure, microhardness, and biocompatibility characteristics of yttrium hydroxyapatite doped with fluoride. *Journal of Biomedical Materials Research - Part B Applied Biomaterials*, *96 B*(2), 207–217. http://doi.org/10.1002/jbm.b.31754

Tortet, L., Gavarri, J. R., Nihoul, G., & Dianoux, A. J. (1997). Study of protonic mobility in $CaHPO_4 \cdot 2H_2O$ (Brushite) and $CaHPO_4$(Monetite) by infrared spectroscopy and neutron scattering. *Journal of Solid State Chemistry*, *132*(1), 6–16. http://doi.org/10.1006/jssc.1997.7383

Vallet-Regí, M., & González-Calbet, J. M. (2004). Calcium phosphates as substitution of bone tissues. *Progress in Solid State Chemistry*, *32*(1-2), 1–31. http://doi.org/10.1016/j.progsolidstchem.2004.07.001

Wang, T., & Feng, Z. (2005). Dynamic mechanical properties of cortical bone - The effect of mineral content. *Materials Letters*, *59*(18), 2277–2280. http://doi.org/10.1016/j.matlet.2004.08.048

Wang, T., Zhang, J.-C., Chen, Y., Xiao, P.-G., & Yang, M.-S. (2007). Effect of zinc ion on the osteogenic and adipogenic differentiation of mouse primary bone marrow stromal cells and the adipocytic trans-differentiation of mouse primary osteoblasts. *Journal of Trace Elements in Medicine and Biology : Organ of the Society for Minerals and Trace Elements (GMS)*, *21*(2), 84–91. http://doi.org/10.1016/j.jtemb.2007.01.002

Webster, T. J., Ergun, C., Doremus, R. H., Siegel, R. W., & Bizios, R. (2001). Enhanced osteoclast-like cell functions on nanophase ceramics. *Biomaterials*, *22*(11), 1327–1333. http://doi.org/10.1016/S0142-9612(00)00285-4

Webster, T. J., Massa-Schlueter, E. a., Smith, J. L., & Slamovich, E. B. (2004). Osteoblast response to hydroxyapatite doped with divalent and trivalent cations. *Biomaterials*, *25*(11), 2111–2121. http://doi.org/10.1016/j.biomaterials.2003.09.001

Webster, T. J., Siegel, R. W., & Bizios, R. (1999). Osteoblast adhesion on nanophase ceramics. *Biomaterials*, *20*(13), 1221–1227. http://doi.org/10.1016/S0142-9612(99)00020-4

Wei, M., Evans, J. H., Bostrom, T., & GrØndahl, L. (2003). Synthesis and characterization of hydroxyapatite, fluoride-substituted hydroxyapatite and fluorapatite. *Journal of Materials Science: Materials in Medicine*, *14*(4), 311–320. http://doi.org/10.1023/A:1022975730730

Weiner, S., & Traub, W. (1992). Bone structure: From angstroms to microns. *Faseb Journal*, *6*(3), 879–885. Retrieved from <Go to ISI>://WOS:A1992HE39000011

Wen, F.-S., Zhao, X., Ding, H., Huo, H., & Chen, J.-S. (2002). Hydrothermal synthesis and photoluminesent properties of Sb3+-doped and (Sb3+,Mn2+)-co-doped calcium hydroxyapatite. *Journal of Materials Chemistry*, *12*(12), 3761–3765. http://doi.org/10.1039/B205807C

Xin, R., Leng, Y., Chen, J., & Zhang, Q. (2005). A comparative study of calcium phosphate formation on bioceramics in vitro and in vivo. *Biomaterials*, *26*(33), 6477–6486. http://doi.org/10.1016/j.biomaterials.2005.04.028

Xu, G., Aksay, I. A., & Groves, J. T. (2001). Continuous crystalline carbonate apatite thin films. A biomimetic approach. *Journal of the American Chemical Society*, *123*(10), 2196–2203. http://doi.org/10.1021/ja002537i

Yamada, S., Heymann, D., Bouler, J. M., & Daculsi, G. (1997). Osteoclastic resorption of calcium phosphate ceramics with different hydroxyapatite/β-tricalcium phosphate ratios. *Biomaterials*, *18*(15), 1037–1041. http://doi.org/10.1016/S0142-9612(97)00036-7

Yashima, M., Sakai, A., Kamiyama, T., & Hoshikawa, A. (2003). Crystal structure analysis of β-tricalcium phosphate Ca3(PO4)2 by neutron powder diffraction. *Journal of Solid State Chemistry*, *175*(2), 272–277. http://doi.org/10.1016/S0022-4596(03)00279-2

Yeong, K. C. B., Wang, J., & Ng, S. C. (1999). Fabricating densified hydroxyapatite ceramics from a precipitated precursor. *Materials Letters*, *38*, 208–213.

Yin, X., Stott, M. J., & Rubio, A. (2003). α - and β -tricalcium phosphate: A density functional study. *Physical Review B*, *68*(20), 205205. http://doi.org/10.1103/PhysRevB.68.205205

Yoshida, K., Hyuga, H., Kondo, N., Kita, H., Sasaki, M., Mitamura, M., Toda, Y. (2006). Substitution model of monovalent (Li, Na, and K), divalent (Mg), and trivalent (Al) metal ions for β-tricalcium phosphate. *Journal of the American Ceramic Society*, *89*(2), 688–690. http://doi.org/10.1111/j.1551-2916.2005.00727.x

Zhang, H., & Cooper, A. I. (2005). Synthesis and applications of emulsion-templated porous materials. *Soft Matter*, *1*(2), 107–113. http://doi.org/10.1039/b502551f

Zhang, S., Prabhakaran, M. P., Qin, X., & Ramakrishna, S. (2015). Biocomposite scaffolds for bone regeneration: Role of chitosan and hydroxyapatite within poly-3-hydroxybutyrate-co-3-hydroxyvalerate on mechanical properties and in vitro evaluation. *Journal of the Mechanical Behavior of Biomedical Materials*, *51*, 88–98. http://doi.org/10.1016/j.jmbbm.2015.06.032

Zhu, Z. L., Yu, H. Y., Zeng, Q., & He, H. W. (2008). Characterization and biocompatibility of fluoridated biphasic calcium phosphate ceramics. *Applied Surface Science*, *255*(2), 552–554. http://doi.org/DOI 10.1016/j.apsusc.2008.06.055

Zyman, Z. Z., Ivanov, I. G., & Glushko, V. I. (1999). Possibilities for strengthening hydroxyapatite ceramics. *Journal of Biomedical Materials Research*, *46*(1), 73–79. http://doi.org/10.1002/(SICI)1097-4636(199907)46:1<73::AID-JBM8>3.0.CO;2-4